Interference Modeling and Performance Analysis of 5G MmWave Networks

by

Solmaz Niknam

B.S., Shiraz University of Technology, Iran, 2010

M.S., Iran University of Science and Technology, Iran, 2012

AN ABSTRACT OF A DISSERTATION

submitted in partial fulfillment of the
requirements for the degree

DOCTOR OF PHILOSOPHY

Department of Electrical and Computer Engineering
College of Engineering

KANSAS STATE UNIVERSITY
Manhattan, Kansas

2019

Abstract

Triggered by the popularity of smart devices, wireless traffic volume and device connectivity have been growing exponentially during recent years. The next generation of wireless networks, i.e., 5G, is a promising solution to satisfy the increasing data demand through combination of key enabling technologies such as deployment of a high density of access points (APs), referred to as ultra-densification, and utilization of a large amount of bandwidth in millimeter wave (mmWave) bands. However, due to unfavorable propagation characteristics, this portion of spectrum has been under-utilized. As a solution, large antenna arrays that coherently direct the beams will help overcome the hostile characteristics of mmWave signals. Building networks of directional antennas has given rise to many challenges in wireless communication design. One of the main challenges is how to incorporate 5G technology into current networks and design uniform structures that bring about higher network performance and quality of service. In addition, the other factor that can be severely impacted is interference behavior. This is basically due to the fact that, narrow beams are highly vulnerable to obstacles in the environment.

Motivated by these factors, the present dissertation addresses some key challenges associated with the utilization of mmWave signals. As a first step towards this objective, we first propose a framework of how 5G mmWave access points can be integrated into the current wireless structures and offer higher data rates. The related resource sharing problem has been also proposed and solved, within such a framework.

Secondly, to better understand and quantify the interference behavior, we propose interference models for mmWave networks with directional beams for both large scale and finite-sized network dimension. The interference model is based on our proposed blockage model which captures the average number of obstacles that cause a complete link blockage,

given a specific signal beamwidth. The main insight from our analysis shows that considering the effect of blockages leads to a different interference profile.

Furthermore, we investigate how to model interference considering not only physical layer specifications but also upper layers constraints. In fact, upper network layers, such as medium access control (MAC) protocol controls the number of terminals transmitting simultaneously and how resources are shared among them, which in turn impacts the interference power level. An interesting result from this analysis is that, from the receiving terminal standpoint, even in mmWave networks with directional signals and high attenuation effects, we still need to maintain some sort of sensing where all terminals are not allowed to transmit their packets, simultaneously. The level of such sensing depends on the terminal density.

Lastly, we provide a framework to detect the network regime and its relation to various key deployment parameters, leveraging the proposed interference and blockage models. Such regime detection is important from a network management and design perspective. Based on our finding, mmWave networks can exhibit either an interference-limited regime or a noise-limited regime, depending on various factors such as access point density, blockage density, signal beamwidth, etc.

Interference Modeling and Performance Analysis of 5G MmWave Networks

by

Solmaz Niknam

B.S., Shiraz University of Technology, Iran, 2010

M.S., Iran University of Science and Technology, Iran, 2012

A DISSERTATION

submitted in partial fulfillment of the
requirements for the degree

DOCTOR OF PHILOSOPHY

Department of Electrical and Computer Engineering
College of Engineering

KANSAS STATE UNIVERSITY
Manhattan, Kansas

2019

Approved by:

Major Professor
Balasubramaniam Natarajan

Copyright

Abstract

Triggered by the popularity of smart devices, wireless traffic volume and device connectivity have been growing exponentially during recent years. The next generation of wireless networks, i.e., 5G, is a promising solution to satisfy the increasing data demand through combination of key enabling technologies such as deployment of a high density of access points (APs), referred to as ultra-densification, and utilization of a large amount of bandwidth in millimeter wave (mmWave) bands. However, due to unfavorable propagation characteristics, this portion of spectrum has been under-utilized. As a solution, large antenna arrays that coherently direct the beams will help overcome the hostile characteristics of mmWave signals. Building networks of directional antennas has given rise to many challenges in wireless communication design. One of the main challenges is how to incorporate 5G technology into current networks and design uniform structures that bring about higher network performance and quality of service. In addition, the other factor that can be severely impacted is interference behavior. This is basically due to the fact that, narrow beams are highly vulnerable to obstacles in the environment.

Motivated by these factors, the present dissertation addresses some key challenges associated with the utilization of mmWave signals. As a first step towards this objective, we first propose a framework of how 5G mmWave access points can be integrated into the current wireless structures and offer higher data rates. The related resource sharing problem has been also proposed and solved, within such a framework.

Secondly, to better understand and quantify the interference behavior, we propose interference models for mmWave networks with directional beams for both large scale and finite-sized network dimension. The interference model is based on our proposed blockage model which captures the average number of obstacles that cause a complete link blockage,

given a specific signal beamwidth. The main insight from our analysis shows that considering the effect of blockages leads to a different interference profile.

Furthermore, we investigate how to model interference considering not only physical layer specifications but also upper layers constraints. In fact, upper network layers, such as medium access control (MAC) protocol controls the number of terminals transmitting simultaneously and how resources are shared among them, which in turn impacts the interference power level. An interesting result from this analysis is that, from the receiving terminal standpoint, even in mmWave networks with directional signals and high attenuation effects, we still need to maintain some sort of sensing where all terminals are not allowed to transmit their packets, simultaneously. The level of such sensing depends on the terminal density.

Lastly, we provide a framework to detect the network regime and its relation to various key deployment parameters, leveraging the proposed interference and blockage models. Such regime detection is important from a network management and design perspective. Based on our finding, mmWave networks can exhibit either an interference-limited regime or a noise-limited regime, depending on various factors such as access point density, blockage density, signal beamwidth, etc.

Contents

List of Figures

List of Tables

Acknowledgments

I would like to thank my advisor, Prof. Balasubramaniam Natarajan, for his continuous support and encouragement. Thank you Dr. Bala, for giving me the opportunity to be a part of WiCom family. You supported me greatly and were always willing to help me not only during the course of my graduate research but also in many life' difficult moments over the past three years.

My sincere gratitude to my advisory committee members Dr. Caterina Scoglio, Dr. Punit Prakash, and Dr. Nathan Albin for their time and constructive comments and feedback that helped me improve my dissertation.

I would also like to thank Dr. Harpreet S. Dhillon for his great mentorship during my visit to Virginia Tech university. Thank you Dr. Harpreet, you thought me that success is not possible only through hardworking, rigor and paying attention to the details.

I am grateful for having the opportunity to work with great researchers of my area, during my Ph.D study. I would like to thank my collaborators Dr. Hani Mehrpouyan and Dr. Ali Arshad Nasir for their time and insightful comments that helped me improve my works.

I would also like to thank my officemates at WiCom research Lab Alaleh Alivar, Hazhar S. Karimi, Kumar S. Jhala, and Wenji Zhang who brought lots of joy and pleasure to the office and made it feels like home.

I am also grateful to have my parents for their never ending love, kindness and support. There are not enough words to describe how thankful I am to have both of you. Thank you for always being there for me. I would also like to thank my siblings whose voices over the phone make me forget everything and just smile.

I am immensely thankful to have Reza, my love and my life partner by my side. You are the most amazing person in my life. Thank you for taking care of me beyond my dreams and expectations. Thank you for always being there for me through thick and thin.

Dedication

To my love, Reza, who never gave up on me, for his endless support.

And to my family and friends.

Abbreviation

2G	second generation
3G	third generation
3GPP	third Generation Partnership Project
4G	forth generation
5G	fifth generation
AP	access point
AWGN	additive white Gaussian noise
BER	bit error rate
BPP	binomial point process
BPSK	binary phase shift keying
CCDF	complement cumulative density function
CDF	cumulative density function
CDMA	code division multiple access
CPP	cox point process
CSMA	carrier sense multiple access
CSMA/CA	carrier sense multiple access/collision avoidance
D-CSMA	directional-carrier sense multiple access
FDMA	frequency division multiple access
GHz	gigahertz
GSM	global system for mobile
H-PPP	homogeneous poisson point process
IH-PPP	inhomogeneous poisson point process
IoT	Internet of things
KKT	Karush-kuhn-Tucker
LRT	likelihood ratio test
LT	Laplace transform
LTE	long term evolution
LoS	line of sight
MAC	medium access control
ME	maximum entropy
MGF	moment generating function
MIMO	multiple-input multiple-output
MPP	Matern point process
MmWAVE	millimeter wave

NLoS	non-line of sight
NP	Neyman-Pearson
OFDMA	orthogonal frequency division multiple access
PDF	probability density function
PGF	probability generating function
PGFL	probability generating functional
PLC	power line communication
PPP	Poisson point process
PSD	power spectral density
QoS	quality of service
RAP	radio access point
RBS	radio base station
RC	raised-cosine
ROC	receiver operating curve
RX	receiver
SC	small cell
SDMA	space division multiple access
SINR	signal to interference plus noise ratio
SNR	signal to noise ratio
TDMA	time division multiple access
TX	transmitter
UWA	under water acoustic
V2G	vehicle to grid

Chapter 1

Introduction

1.1 Overview and Motivation

Wireless communication refers to a form of communication technology where information can be transmitted through the air without requiring any cable or wires. During the last couple of decades, there have been rapid changes in wireless communication technologies from the Global system for mobiles (GSM), namely second generation (2G) to Long Term Evolution (LTE), known as fourth generation (4G)(see Fig. 1.1). The fundamental motivation behind such an evolution is higher data-rate, higher capacity and lower latency. In addition to throughput enhancement, there are other requirements including higher energy-efficiency, quality of service improvement, device connectivity, and network compatibility with current technologies that need to be considered when migrating to a new mobile technology generation. Exponential increase in wireless data rate demand, large number of connected devices and real-time control of many connected devices is a burden to legacy technologies. Fifth generation (5G) of wireless communication technology is expected to be the cure-all wonder solution to the current wireless networks' deficiencies. Table 1.1 provides the major requirements of 5G networks that are expected to be satisfied through combination of modifications deployed in network layer design, network architecture and spectrum regulation and standardization. Among the requirements outlined in Table 1.1, the need for higher

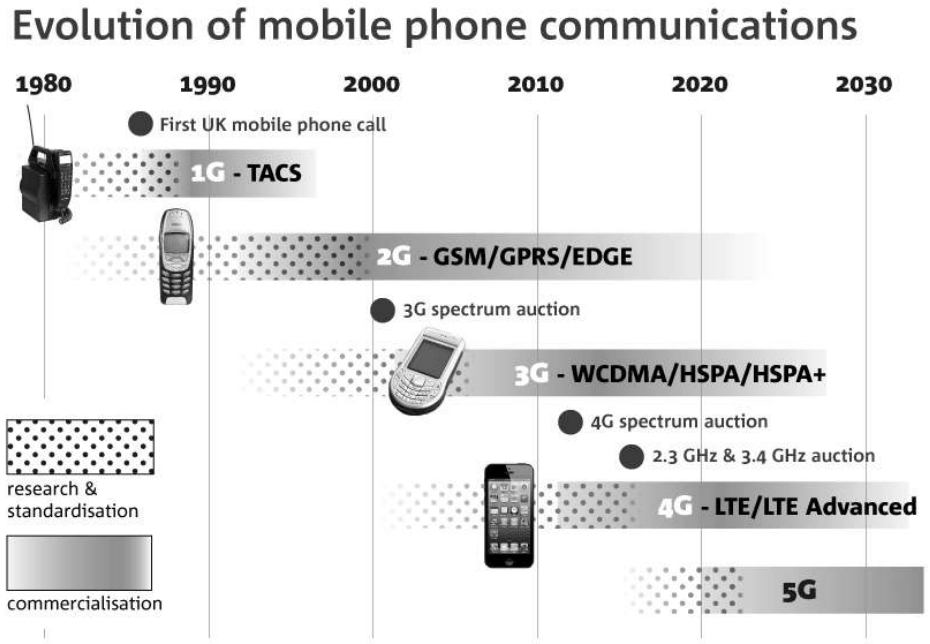

Fig. 1.1: Evolution of mobile phone communications from both research and commercialization standpoint [1].

data rate has attracted the most attention and can be achieved through combination of enabling technologies, namely *ultra densification*, *millimeter Wave (mmWave)* and *massive multiple-input multiple-output (MaMIMO)*, also known as "big three" [5]. A straightforward way to increase the capacity is to deploy much more radio base stations (RBSs) and admit higher number of users under radio coverage (ultra densification solution). Another solution is to equip the RBSs with a number of antennas much larger than the number of active users (MaMIMO solution). Moreover, given the overcrowded sub-6 GHz frequency band and immense amount of relatively under-utilized spectrum in the mmWave frequency range, i.e., 30-300 GHz, going up in frequency and utilizing the mmWave spectrum is another promising key option (mmWave solution). However, due to challenging propagation characteristics

[1] **Internet of Things** is the inter-networking of physical devices, vehicles, buildings, and other items embedded with electronics, software, sensors, actuators, and network connectivity which enable these objects to collect and exchange data [6].

Table 1.1: Major requirements of next generation 5G networks[4]

Higher data rate (1∼10 Gbps, 10 times increase compared to LTE networks)
Lower latency (1ms round trip latency, 10 times reduction compared to LTE networks)
Higher bandwidth efficiency
Increase in the number of connected device (1000s of connected devices to realize IoT [1])
Increase in network availability (99.999%, network should be always available)
Higher coverage (100% coverage for 'anytime anywhere' connectivity)
Reduction in energy usage (reduction by almost 90% to develop a green technology)
Higher battery life (reduction in power consumption by devices)

of mmWave signals, such as severe pathloss, atmospheric absorption and low penetration through obstacles, this portion of spectrum has been almost idle, thus far[3]. Having large antenna arrays that coherently direct the beam energy will help overcome the hostile characteristics of mmWave signals[7]. However, utilization of the highly directional beams in a very crowded environment of obstacles and transmitting nodes changes many aspects of the wireless system design. In this regard, there are couple of key research questions that need to be address properly.

Question 1: How can a network with narrow beam transmission be integrated with current wireless networks (such as 3G, LTE, etc.) in a uniform framework, resulting in higher network capacity?

Question 2: Considering narrow mmWave beams with high sensitivity to even small-sized obstacles (like human body, car, etc.), what would be a proper model to incorporate the effect of the obstacles in the environment?

Question 3: Including the effect of obstacles and also base stations densification in 5G mmWave networks, how does the interference profile change in such networks? What would be proper interference models that takes mmWave specifications and node densification into account?

Question 4: Given the fact that the interference signal and its undesired effects are impacted by features of the interfering nodes at different network layers, what would

be a proper interference model that accounts for not only physical layer specifications but also upper network layers (medium access control (MAC), etc.) constraints?

Question 5: Given a proper interference model, how does the user experience change in mmWave networks? Do users experience a lower interference power level? (or) due to the increase in density of interfering nodes, will there be higher interference power?

1.2 Contributions

In order to address the aforementioned questions, in chapter 3, we develop a network scheme under which both mmWave small cells and current networks technologies can be integrated into a single uniform framework and provide users with higher throughput. In addition, we study the interference behavior by modeling the statistical characteristics of the received aggregated interference considering mmWave specifications and beam directionality in the presence of random blockages in the environment. We evaluate interference behavior in both large scale and finite-sized networks. The detailed results are provided in chapters 4 and 5. Using the proposed interference model, we determine the network regime, in the sense that whether the network performance is degraded by interference (interference-limited regime) or thermal noise is the only major factor that is dominant (noise-limited regime), in chapter 6. In fact, network regime impacts MAC layer design and resource allocation strategies. Furthermore, it is also critical in terms of providing further interference coordination in case of being in interference-limited regime. However, when the network is in a noise-limited regime, a simple interference management mechanism suffices in order to provide the required quality of service (QoS). Moreover, in order to provide a more realistic model, we include not only physical layer constraints but also MAC layer characteristics in modeling the aggregated interference footprint. A cross-layer interference analysis is presented in chapter 7. In fact, network operation and traffic behavior that describe the transmitters activity and the interrelation among terminals are established by MAC protocols. Therefore, an efficient and comprehensive interference model for mmWave applications should ideally include

both physical layer specifications and MAC layers constraints. In summary, this dissertation addresses the state of the art across multiple dimensions as listed below:

Contribution 1: Develop a scheme to integrate both current LTE and narrow beam mmWave RBSs and utilize both mmWave frequency bands together with the beachfront spectrum [2] towards achieving higher network throughput. This contribution is discussed in detail in chapter 3 and also appears in the following article:

[8] **S. Niknam**, A. A. Nasir, H. Mehrpouyan and B. Natarajan,"A Multiband OFDMA Heterogeneous Network for Millimeter Wave 5G Wireless Applications" in *IEEE Access*, vol. 4, pp. 5640-5648, 2016.

Contribution 2,3: Model the aggregated [3] interference power in the network of narrow beams with low penetration through obstacles in both large scale and finite-sized networks (only physical layer consideration). These contributions are discussed in detail in chapters 4 and 5, respectively and also appear in the following articles:

[9] **S. Niknam**, B. Natarajan and H. Mehrpouyan, "A Spatial-Spectral Interference Model for Millimeter Wave 5G Applications," *IEEE Veh. Tech. Conf.*, 2017, pp. 1-5.

[10] **S. Niknam**, B. Natarajan and R. Barazideh, "Interference Analysis for Finite-Area 5G mmWave Networks Considering Blockage Effect," in *IEEE Access*, vol. 6, pp. 23470-23479, 2018.

Contribution 4: Study the network regime and evaluate whether the performance of the mmWave network is limited by interference (due to the dense deployment of nodes) or (given the very narrow beamwidth and high sensitivity of mmWave signals to blockages) noise will be dominant. This contribution is discussed in detail in chapter 6 and also appears in the following article:

[2]Range of microwave frequencies that extends from several hundred MHz to a few GHz and corresponds to wavelengths in the range of a few centimeters up to about a meter [5].

[3]The entire amount of interference power, from all interfering devices, received at a location.

[11] **S. Niknam** and B. Natarajan, "On the Regimes in Millimeter Wave Networks: Noise-Limited or Interference-Limited?," *IEEE Int. Conf. on Commun. Workshops*, 2018, pp. 1-6.

Contribution 5: Model the received interference considering both physical and MAC layers constraints. This contribution is discussed in detail in chapter 7 and also appears in the following article:

[12] **S. Niknam**, R. Barazideh and B. Natarajan, "Cross-layer Interference Modeling for 5G MmWave Networks in the Presence of Blockage," *IEEE Veh. Tech. Conf.*, 2018, pp. 1-5.

[13] **S. Niknam**, H. Dhillon and B. Natarajan, "A Joint PHY/MAC Interference Analysis with Blockage Effect for 5G MmWave Networks," to be submitted to *IEEE Trans. on Veh. Tech.*, 2018.

1.3 Dissertation Outline

The remainder of this dissertation is organized as follows. Chapter 2 provides the background on stochastic geometry, point processes and some fundamental concepts widely used in wireless communication. We develop a multi-band heterogeneous framework, in chapter 3, where mmWave small cells can be intergraded in current LTE networks and provide higher data rate. In chapters 4 and 5, a spatial-spectral interference model has been proposed for large scale and finite-sized mmWave networks considering the effect of blockages in the environment, respectively. In chapter 6, a binary hypothesis test is suggested in order to determine whether mmWave network performance is limited by noise or we have an interference-limited behavior in such networks. In chapter 7, a cross-layer interference analysis is provided for mmWave network to determine how the higher layer characteristics impact the interference behavior. Finally, concluding remarks are provided in chapter 8.

Chapter 2

Background

In this chapter, we provide key background information on stochastic geometry [1], point processes, and some general concepts that are widely used in wireless communication and also in this dissertation so that readers can follow the discussions and calculations in the following chapters. Therefore, this chapter can be fully or partially skipped if readers have enough background information on the related topics.

2.1 Stochastic Geometry

In order to study the network performance and perform interference analysis, we use stochastic geometry as a strong mathematical tool which is the basis for numerous applications. It is well known that the performance of any wireless system depends on the geometry of the locations of the transmitting and receiving terminals. This is due to the fact that received signal power and interference depend critically on the distances between numerous transmitters and receivers. In addition, in wireless networks, there is considerable uncertainty and randomness in node arrangement arising from factors such as node mobility and the unplanned user-installed radio access points (RAPs). Therefore, stochastic geometry, or in particular point processes which is a rigorous mathematical tool to model the spatial location of points, provides a natural way of defining the properties of wireless networks. Since,

[1] This tool has been widely used through this dissertation

we extensively use this tool as a leverage to analyze the interference behaviour and network performance, some of the key and fundamental concepts underlying this powerful tool are discussed in this chapter. This basic concepts will enable the readers to develop a better understanding of the analysis in the subsequent chapters. For a more thorough exposition, readers are referred to [14–17].

A deterministic point sequence can be represented by $\psi = (x_k)_{k\in\mathbb{N}}$. We denoted by $\mathcal{N}$ the space of all sequences. If $\mathcal{N}$ is the outcome space of a random process, then this random process is called a *point process*. A formal definition can be found in [16]. Generally speaking, "a point process is a random collection of points that resides in some space, where in our applications, the points represents the locations of wireless nodes in the real world" [17]. A convenient way to represent a point process is to use the random counting measure, which mathematically is defined as

$$\Psi(B) = \sum_{X_i \in \Phi} \mathbb{1}(X_i \in B). \tag{2.1}$$

Here, Φ is the point process. In addition, X_i is used to represent the points in the point process. Furthermore, B is a subset of the Euclidean space $\mathbb{R}^d$.

In the following subsections, we concisely introduce some of basic concepts from the point processes. We start with explaining some of the important measures of point processes that are quite useful in derivations of the important performance metrics related to wireless communications. Subsequently, we proceed with introducing several important point processes and the characteristics that make them suitable to model various type of wireless networks.

2.1.1 Statistical Measures

Here, we present two important measures for a general point process that are widely used in this dissertation. For more discussion on each measure and also further detailed measures, interested readers are referred to [17].

Mean Measure

The mean or expectation measure maps the set of points in the point process to the mean number of the point in it. Mean measure can be calculated for a smaller subsets of the point process. For instance, if B is a subset of the given point process, then

$$\mu(B) = \mathbb{E}[\Psi(B)]. \tag{2.2}$$

Probability Generating Functional (PGFL)

The probability generating function is defined as the mean of the product of values of a specific function at any point in the point process. Therefore, the PGFL of the point process Φ with respect to function g, denoted by $M_\Phi(g)$, is defined by

$$M_\Phi\left(g\right) = \mathbb{E}\left[\prod_{X_i \in \Phi} g\left(X_i\right)\right]. \tag{2.3}$$

If the function $g(X_i)$ is defined as $g(X_i) = \mathrm{e}^{-\mathrm{s}f(X_i)}$ where $f\left(X_i\right)$ is also a function value at each point, then the PGFL of the function $g(X_i)$ gives the Laplace transform of the function $g(.)$. Note that s is the Laplace transform variable. This special function is quite important, since it is used in characterization of the signal to interference plus noise ratio (SINR) metric in many wireless applications. In fact, SINR metric is mathematically defined based on the Laplace transform of the aggregated interference.

Now, we proceed with introducing some of the useful point processes in modeling various wireless network scenarios. Basically, there are many varieties of point processes, including Poisson point process (PPP), Binomial point process (BPP), Matern point process (MPP), Cox point process (CPP) and etc. [2]. Based on their mathematical characteristics, these point processes are suitable for modeling a certain type of wireless networks. Among them PPP is the simplest and widely used example of a point process. This is due to the specific characteristics of this point process which makes the analysis tractable and less complex,

[2] A more complete list of point process can be found in [18].

while providing useful insights with acceptable accuracy.

2.1.2 General Poisson Point Process

Definition 2.1.1. ***General Poisson point process***[17]

The PPP on Eucledian space $\mathbb{R}^d$ with mean intensity measure Λ is a point process such that

- *for every compact set $B \subset \mathbb{R}^d$, number of points in set B, denoted as $N(B)$ has a poisson distribution with mean $\Lambda(B)$. If Λ admits a density λ, we have*

$$\mathbb{P}\{N(B) = k\} = exp\left(-\int_B \lambda(x)\mathrm{d}x\right).\frac{\left(\int_B \lambda(x)\mathrm{d}x\right)^k}{k!} \tag{2.4}$$

- *if B_1, B_2, ..., B_m are disjoint compact sets, then $N(B_1)$, $N(B_2)$, ..., $N(B_m)$ are independent.*

The homogeneous PPP is a special case where $\Lambda(B) = \lambda|B|$. In addition, PPP is a member of the two general classes of point process which are *stationary* and *motion-invariant* point processes. Informally speaking, a stationary point process is a point process whose distribution is invariant to translation. Moreover, if the distribution of the point process is also invariant to rotations about the origin, the point process is said to be motion-invariant[16]. These characteristics of PPP, along with independence of the disjoint sets make it a tractable point process.

2.1.3 Binomial Point Process

In BPP, a fixed number of nodes is identically and independently distributed on a compact set $W \subset \mathbb{R}^d$. In addition, the number of points in a subset $A \subset W$ is binomially distributed with parameters $n = \Psi(W)$ and $p = \frac{|A|}{|W|}$. The intensity of the points is given by

$$\Lambda(A) = n\frac{|A \bigcap W|}{|W|} \tag{2.5}$$

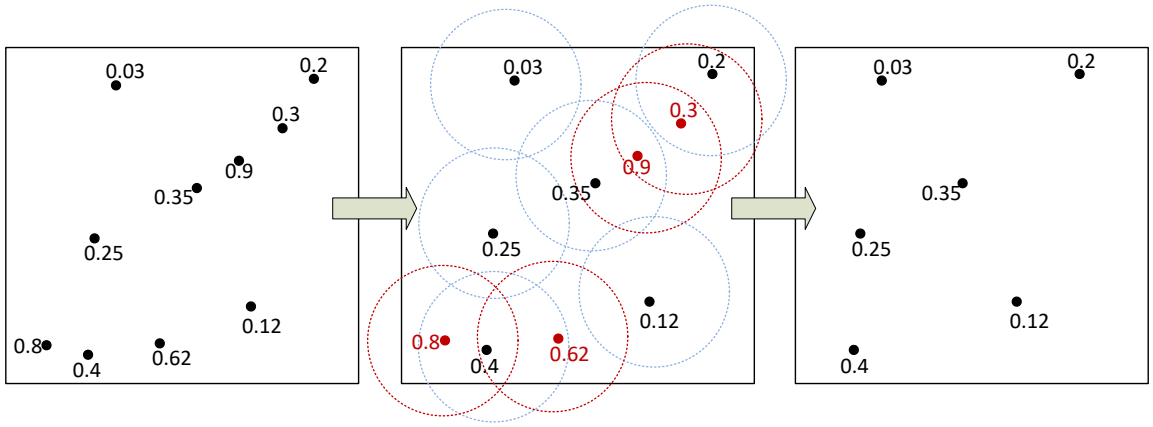

Fig. 2.1: Generating a Matern type II point process from its parent PPP.

The fact that the total number of points is fixed makes the number of points in disjoint subsets to be dependent, unlike PPP. However, BPP is still a rotation-invariant point process.

2.1.4 Matern Point Process

MPP is a type of Hard-core point process where points are not closer than a certain distance to each other. In fact, MPP can be viewed as a thinned version of PPP. Generally speaking, there are two types of MPP, i.e., MPP-type I and MPP-type II. Basically, in type-I MPP, we start with a parent PPP and then for each point in the point process, we remove all points closer than a specific distance. However, in MPP-type II, we tag each point of the primary PPP with a uniformly distributed random mark in $[0, 1]$. Then, for each point, only those neighbors closer than a certain distance with smaller marks are removed from the point process (see Fig. 2.1). Later, in chapter 7, we see that this type of point process is a reasonable option to model the CSMA/CA networks, where not all the transmitters are allowed to transmit based on the MAC protocol, and some close by transmitters postpone their transmission in order to avoid collision of the data packets.

2.2 Fading in Wireless Communication

In wireless communication, while propagating from the transmitter to the receiver, the signal may experience various types of impairments such as path loss, multipath attenuation, and so on. The actual attenuation depends on many different factors including, radio frequency, time, mobility and distance between the transmitter and the receiver, atmospheric condition, and presence of any object in the path between the transmitting and the receiving pair (TX-RX pair). The time variation of the received signal power in transmission medium (wireless channel), due to the aforementioned or any other factors, is referred to as fading. Fading, in general, is categorized as small scale and large scale. The average attenuation of the received signal power which depends on the geographical distance between the TX-RX pair defines the large scale fading. In fact, the transmitted signal power attenuates over distance as the signal travels from the transmitter to the receiver. Shadowing which is the result of the presence of objects in the path is also considered a large scale fading effect. Therefore, large scale fading captures the signal attenuation due to both pathloss and shadowing.

There are three common pathloss models that are widely used, and defined as follows[15]:

- $\mathrm{PL}(r) = \max(r_0, r)^{\beta}$
- $\mathrm{PL}(r) = (1 + r)^{\beta}$
- $\mathrm{PL}(r) = r^{\beta}$

where, r represent the distance and β is called the pathloss exponent which depends mainly on the frequency of operation and also the atmospheric condition, determined using field measurements. The common pathloss model (the one that we also use in our calculation) includes a simple power law function which is the last model.

On the other side, small scale fading is concerned with the rapid fluctuation of the received signal over a short time period or short travel distance. A general way to include the effect of small scale fading is to represent the signal amplitude by a random variable, usually a Nakagami-m (Nakagami distribution with parameter m) distributed random variable. Therefore, the corresponding instantaneous power is gamma distributed. In the special

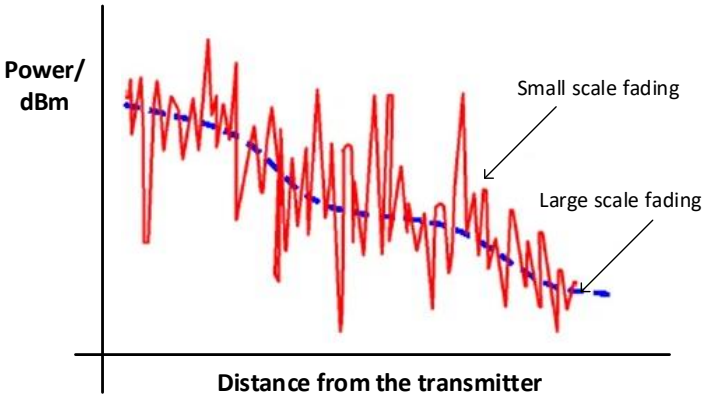

Fig. 2.2: Representation of the effect of small and large scale fading on signal power[2].

case $m = 1$, we have Rayleigh fading with an exponentially distributed instantaneous power, which is a very common channel model in wireless communication. For $m > 1$, the signal amplitude fluctuates less compared to the Rayleigh distribution. There is another familiar type of fading, called Rician fading, which is similar to Rayleigh fading, except the fact that a strong dominant signal component exists in Rician model. The presence of this strong component makes Rician a better channel model, when there is a strong signal component received from the line-of-sight path between the TX-RX pair (For instance, in case of mmWave signal where the presence of line of sight (LoS) should be guaranteed due to the strong signal attenuation in non line of sight (NLoS) paths). Rician and Nakagami models behave approximately the same, in the average sense. However, due to the fact that Nakagami model is less complex and more tractable, it is widely used as an acceptable approximation of Rician fading when the LoS component exists[19].

2.3 Relay Communication

Generally speaking, relays are terminals that receive the signal from the transmitters and forward it to the receivers. The general purpose of this retransmission is to increase the throughput (by decoding and re-encoding the signal) or extend the radio coverage (by amplifying the signal). In addition, some times the goal of the relay terminals is to perform

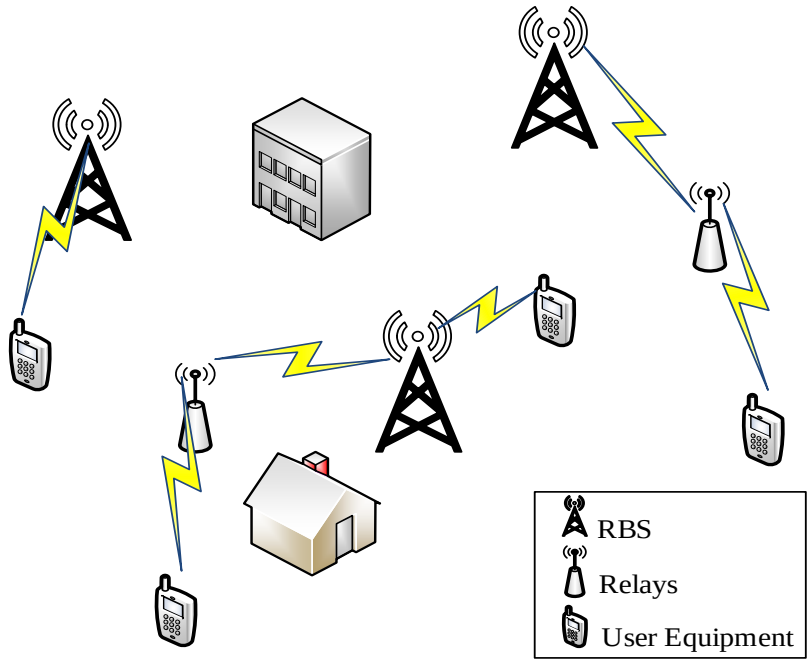

Fig. 2.3: Representation of relay communication and how relays can be used for coverage extension and macro-diversity in the presence of obstacles.

macrodiversity and overcome signal blockage due to the presence of objects in the path between the transmitters and the receivers[20].

2.4 Multiple Access and Random Access

In a multi-user communication setup, the signaling dimension (frequency, time, space and coding), or simply wireless resources, need to be shared between the transmitters (for instance mobile users) in order to overcome the resource shortage and increase the capacity (which simply can be providing service to higher number of users). Basically, resource sharing techniques are used to allow a large number of mobile users to share the resource blocks and this can be performed in a dedicated or random manner. The choice of whether to use multiple access or random access will depend on the system application, the traffic characteristics of the users in the system, the performance requirements, and the characteristics of the channel and other interfering systems operating in the same bandwidth[20]. For instance, for the users with bursty traffic, sharing the signaling dimension in a random manner is

preferable. Since, dedicated channel allocation to the users which generate data only at a specific time instances is inefficient.

The main categories of deterministic channel access techniques include:

- Frequency division multiple-access (FDMA)
- Time division multiple-access (TDMA)
- Code division multiple-access (CDMA)
- Space Division Multiple access (SDMA)

Moreover, the random access techniques can be generally divided as:

- Pure ALOHA
- Slotted ALOHA
- Carrier Sense Multiple Access (CSMA)

Generally speaking, with the ALOHA protocol if a terminal has data to send, it proceed with the transmission and while it is transmitting, it may receive data from another terminals. With this protocol, there will be packet collision and terminals need to try retransmission later. In the slotted version of the ALOHA, transmitters are permitted to send their packets only at the beginning of some discrete timeslots. This will reduce the probability of collision to some extent.

On the other hand, in CSMA protocol, the transmitting terminals need to listen to the medium (radio channel) before sending their packets. If the channel is clear, they will transmit their packets; otherwise, the transmission is postponed to a clear timeslot.

Chapter 3

Multiband Heterogeneous Framework

As it has been mentioned in previous chapters, it is expected that utilization of the large bandwidth in the mmWave band and deployment of heterogeneous networks (HetNets) will help address the data rate requirements of 5G networks. However, high pathloss and shadowing in the mmWave frequency band, strong interference in the HetNets due to massive network densification, and coordination of various air interfaces are challenges that must be addressed. In this chapter, we consider a relay-based multiband orthogonal frequency division multiple access [1] (OFDMA) HetNet in which mmWave small cells [2] are deployed within the service area of larger cells (also known as macro cells). Specifically, we attempt to exploit the distinct propagation characteristics of mmWave bands (i.e., 60 GHz –the *V-band*– and 70–80 GHz –the *E-band*–) and the LTE band to maximize overall data rate of the network via efficient resource allocation. The problem is solved using a modified dual decomposition approach and then a low complexity greedy solution based on iterative activity selection algorithm is presented. Simulation results show that the proposed approach outperforms conventional schemes.

[1] OFDMA is a multiuser version of the popular OFDM modulation scheme that is widely utilized in many applications ranging from wired communication such as power-line communication (PLC) [21;22] and Home-Plug Green PHY standard for vehicle to grid (V2G) communications to wireless communications based on 4G, 5G, 802.11p wireless access standards, cognitive radio [23], and underwater acoustic (UWA) communication [24;25].

[2] Basically, a cell is a smaller area of a cellular network where it is covered under the radio propagation of a single RBS.

3.1 Introduction

The ubiquity of cloud-based applications, ultra-high resolution video streaming, entertainment and many new emerging applications have created an increasing demand for higher data rate in wireless networks. Fifth generation wireless networks are a solution to that demand because of their promising ability to handle sheer amount of data. In order to satisfy the data rate demand, the large available bandwidth in mmWave bands is a promising candidate[3]. Specifically, the 60 GHz unlicensed frequency band is a valuable frequency resource for offloading traffic from licensed bands. Therefore, 5G networks must be designed to utilize the new frequency bands as well as coexisting and integrating with other radio access technologies[5].

Extreme densification is another key enabling technology for increasing capacity that can be realized by deploying heterogeneous networks (HetNets). HetNets with low-power, low-complexity BSs such as pico and femto, referred to as small cells (SCs), coupled with conventional macro BSs can potentially improve the overall throughput of cellular networks[26]. Based on Nokia estimates, integrating mmWave SC with 2 GHz carrier bandwidth with macro BS that utilizes current technology such as LTE-advanced not only can provide a 2 [Tb/km^{2}s] area capacity, but can also lower the required density for SC deployment[27].

One way to enhance system throughput is to incorporate SCs that operate in licensed and unlicensed mmWave band in the coverage area of conventional macrocells. Base stations of SCs can perform a switching procedure between licensed and unlicensed mmWave bands using the transceiver structure in[28]. Such a utilization of cells that support licensed and unlicensed mmWave bands and LTE frequencies allow maximum throughput through switching and aggregation and alleviate traffic congestion via offloading.

Advantageous utilization of the two aforementioned enabling technologies necessitates a proper model of network elements and radio resource incorporation within the advanced architecture of HetNets. Specifically, development of a scheme that efficiently utilizes radio resource, including bandwidth and transmission power, and allows switching between different technologies while mitigating intercell and interuser interference is a critical issue[27].

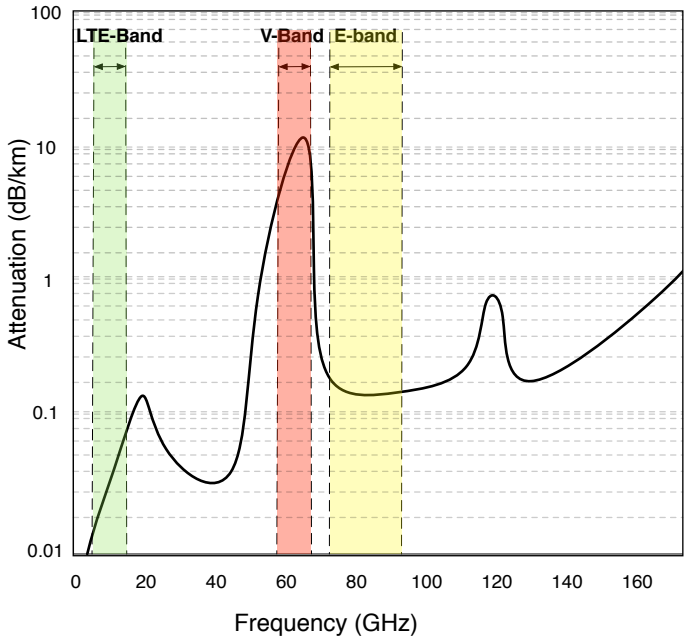

Fig. 3.1: Atmospheric attenuation versus operating frequency [3].

Hence, many works have been carried out in this regard. However, the problem of considering frequency bands with *completely different propagation* characteristics to enhance throughput and reduce interference, a huge limiting factor in current wireless cellular networks, is a novel concept. This is especially the case for mmWave frequencies, where the V-band has completely different propagation characteristics compared to E-band and they both differ greatly with respect to lower LTE frequency band (see Fig. 3.1). In this chapter, we demonstrate this concept in the context of relay-based multiband OFDMA network. Prior efforts related to resource allocation in OFDMA HetNets have mainly focused on single frequency band operations. This limits their applicability to the proposed model as detailed in the next subsection.

3.1.1 Related works

A resource allocation scheme for heterogeneous OFDMA systems with relays has been proposed in [29]. However, the problems of relay selection, subcarrier and power allocation are solved separately through disjoint steps which may not be a suitable solution; since, subcar-

rier allocation is greatly affected by power allocation.[30] considers a joint resource allocation for HetNets but the total power budget is equally shared among all allocated channels. This can be a limitation for mmWave systems because channel conditions for users can differ considerably as a result of significant human shadowing and pathloss[3]. A resource allocation scheme for OFDMA HetNets is presented in[31] to maximize network throughput. However, the users are assigned to specific cells without freedom to select the appropriate serving cell.[32] investigates a game-theoretic resource allocation hierarchy for heterogeneous relay networks, but relay selection is not considered even though it can potentially provide additional degrees of freedom to overcome pathloss and shadowing. In addition to the above approaches and while not considering HetNets, many research articles have considered the important scenario of joint resource allocation in OFDM relay systems[33–35] but these approaches do not take into account propagation characteristics at mmWave frequencies and are designed to utilize only a single frequency band for communication.[33] considers a relay system consisting of one source, one relay, and one destination using a single microwave frequency band, which does not take the benefits of relays and band selection into account. In addition, a minimum rate requirement for each user is not taken into account. Therefore, the work in[33] may not be well-suited for applications in mmWave systems that must overcome significant propagation issues. A downlink point-to-multipoint wireless network in which the network consists of one source or BS, one relay, and multiple users has been taken into account in[34]. However, since pathloss and shadowing significantly affect mmWave networks, a single relay may not be able to support multiple users. In addition, the algorithm proposed in[34] only supports a single band, does not consider subcarrier pairing, and sets no constraints on ensuring a minimum rate for a given user. These omissions may result in loss of communication links, inefficient use of bandwidth, and poor quality of service. Reference[35] considers an uplink multi-user transmission scenario in which multiple mobile users communicate with a BS through various relay stations. However in[35], the direct link, or the valuable communication link in the mmWave band is not considered and the authors adopt a high signal-to-noise ratio (SNR) regime to convert the resource allocation problem into a concave optimization problem. The resulting solution is only precise at high SNRs,

which may be rarely the case in mmWave systems that suffer from significant pathloss and shadowing. It is worth reiterating that none of the mentioned works utilize multiple frequency bands with very different propagation characteristics and they are all designed to operate in a single frequency band.

3.1.2 Contributions

In this chapter, we propose a new mmWave HetNet model that uses the mmWave and LTE bands to maximize the overall throughput of the network while meeting power constraints and QoS of each user. Incorporating the LTE band in the model is especially important since mmWave signals are significantly attenuated by atmospheric absorbtion, as shown in Fig. 3.1. In this model, each macro cell contains a macro BS that operates in mmWave and LTE frequency bands and several small BS that operate only in mmWave frequency band serving the outdoor and indoor users, respectively (see Fig. 3.2). Confining the small BSs to solely operate in mmWave frequency bands helps reduce interference without sophisticated intercell and interuser interference cancellation techniques. In fact, the strong attenuation and penetration loss of mmWave signals decreases the probability that an outdoor user will be covered by a small BS[36]. This phenomenon also results in negligible interference between a macro BS and small cell users and vice versa. Therefore, this model allows the use of the frequencies in the LTE band with favorable propagation characteristics to meet the users' QoS requirements, while the frequencies in the mmWave band are used to reduce the overall level of interference in the network and achieve higher throughputs. The other important advantages of the proposed model can be summarized as follows:

- By allowing users to adaptively switch between different frequency bands, the model enables the combination of dual air interfaces (i.e., small BSs with licensed and unlicensed mmWave air interface are coupled with macro BS utilizing mmWave and LTE air interface), leading to increased throughput.

- To support dense networks in a reliable fashion, 5G wireless networks will more extensively use relays[37]. Therefore, we incorporate relays into our model and consider a

two-hop (from the BS to the relays and from relays to the users) transmission scheme. Moreover, relays can overcome the severe pathloss and shadowing issue in the mmWave band, especially at 60 GHz, as shown in Fig. 3.1.

- A new degree of freedom in which a subcarrier applied in the second hop may differ from the one in the first hop, is also considered. This technique, called subcarrier pairing, improves the system sum-rate[38] and can be combined with frequency band selection to enhance coverage, especially at mmWave frequencies. For example, if a relay-to-user link distance is longer than the BS-to-relay link and cannot be adequately supported by the V-band (see Fig. 3.1), subcarrier pairing allows for the use of an E-band subcarrier (in the case of a macro-cell base station, the proposed approach can select subcarriers in the E-band or LTE frequency band) with more suitable propagation characteristics to support this link. Our results show that this approach increases the overall sum rate of the network.

In this new relay-based multiband OFDMA model, we analytically formulate the optimal resource allocation strategy that maximizes the overall throughput subject to a power constraint and users' QoS requirements. The resulting optimization problem is solved using the dual decomposition approach. Finally, by using the sub-gradient method and an iterative algorithm, the joint resource allocation problem is solved and a suboptimal low complexity greedy solution is presented, as well. Simulations show that the use of smaller cells, relays, and distinct *propagation* characteristics at LTE, V-band and E-band allows the proposed model to overcome large pathloss and shadowing at mmWave frequencies and achieve significantly high data rates.

3.2 Proposed Model

Comprehensive deployment of 5G networks operating in the V-band face substantial obstacles including high pathloss and significant signal attenuation due to shadowing[3]. Unlike the V-band that suffers from strong gaseous attenuation, the E-band has a large available

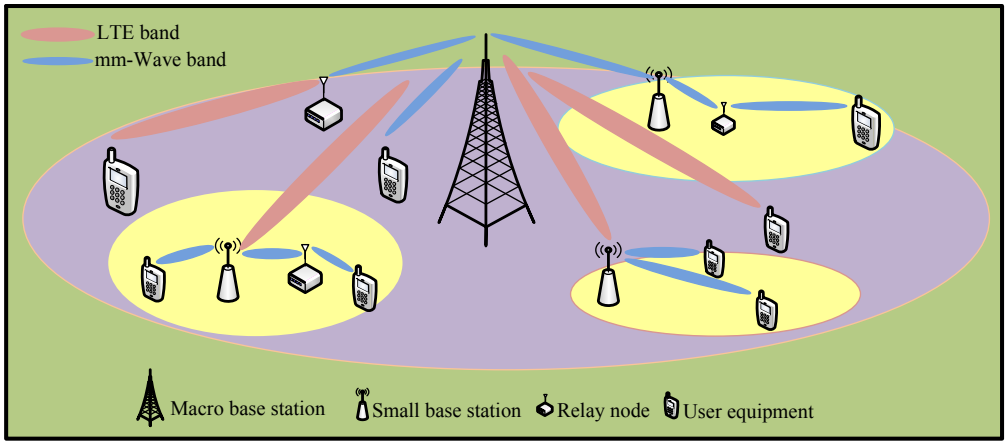

Fig. 3.2: Single cell of the HetNet.

spectrum in order to support transmissions over longer distances. Our model is an OFDMA HetNet that operates in LTE, V-band and E-band, as shown in Fig. 3.2. It consists of several service areas, including a macro BS coupled with $\mathcal{L}$ small BSs $\{f_0, f_1, ..., f_l, ..., f_{\mathcal{L}}\}$, where f_0 is the macro BS that is connected to the small BSs through backhaul links. The BSs mainly attempt to communicate over V-band frequencies but to maintain an acceptable quality of service at low SNR, E-band frequencies can be also used. The macro BS employs the LTE frequency band in addition to mmWave frequency bands in order to serve distant outdoor users for whom mmWave signaling is inefficient due to its strong attenuation. Significant penetration loss at mmWave frequencies ensures that the interference introduced from macro BS to indoor users and from small BS to outdoor users is negligible. In addition, strong channel attenuation and deployment of a highly directional antenna in mmWave systems diminish the effect of interference in the HetNet.

The proposed model assumes that several relay terminals assist in carrying information from BS to the users in order to overcome shadowing by establishing a long-distance connection. Based on channel conditions at different frequency bands, there are two modes of operation: *relay link mode* and *direct link mode*. The BS decides to either utilize the relays or transmit the information through the direct link. If the BS-to-relay and relay-to-user links are favorable compared to the BS-to-user link, then the relay link is used. Otherwise, BS-to-user link is employed. In the first hop, the BS broadcast data to the users and relays

over a given subcarrier. Then, in the relay link mode, the relays decode and forward the received data to the users in the second hop over a subcarrier, which may differ from the subcarrier in the first hop. This subcarrier pairing is performed based on the sum-weighted rate maximization criterion. In fact, the subcarriers in the first and second hops can be in the LTE, E-band and V-band, depending on channel conditions. If the direct link mode is selected, the relays do not forward the received information to the users, and the BSs transmit the data solely through the direct link in the first hop and keep silent in the second hop. A particular relay node can serve more than one user, and a user can receive data from different relays.

Similar to[33–35], we assume the network operates in time-division duplex mode, so channel reciprocity is used to estimate all channel parameters at the macro BS. The macro BS is also assumed to perform the resource allocation centrally and provide information to the small BSs using backhaul links that interconnect them to the entire network. This allows simple hardware structures at the small BSs, thereby reducing their cost of deployment. Subsequently, users and relays are informed of the resource allocation parameters during the signaling process that precedes data transmission (i.e., the hand-shaking stage). Due to the fact that subcarriers may carry different types of services, various weights are applied to individual users in the system, determined based on requested service priority, to meet the QoS requirements for each user. The respective resource allocation scheme for this model is provided in the following section.

3.3 Resource Allocation in the Proposed Model

In cell l for a user k_l that receives data through the BS and a relay m_l in the first and second hops over subcarrier pair $(i_b, j_{b'})$, the weighted normalized rate can be expressed as[39]

$$\mathbb{R}_l = \sum_{\mathcal{S}_l} \zeta_{m_l,k_l}^{i_b,j_{b'}} \frac{w_{k_l}}{2} \log_2 \left(1 + \alpha_{m_l,k_l}^{i_b,j_{b'}} p_{m_l,k_l}^{i_b,j_{b'}}\right), (\text{bits/s/Hz}) \tag{3.1}$$

where the notations are given in Table 5.1. Additionally,

- $p_{m_l,k_l}^{i_b,j_{b'}} = p_{m_l,k_l}^{f_l,(i_b,j_{b'})} + p_{m_l,k_l}^{R_l,(i_b,j_{b'})}$ is the aggregate power of user k_l and relay m_l over subcarrier pair $(i_b, j_{b'})$ in the first and second hops,

- w_{k_l} represents the weight of QoS requirements for user k_l,

- $p_{m_l,k_l}^{f_l,(i_b,j_{b'})}$ denotes the transmit power of the BS f_l to a given user-relay pair (k_l, m_l) over subcarrier i_b paired with subcarrier $j_{b'}$ in the second hop,

- $p_{m_l,k_l}^{R_l,(i_b,j_{b'})}$ shows the transmit power of relay m_l to user k_l, over subcarrier $j_{b'}$ paired with subcarrier i_b in the first hop, and

- $\alpha_{m_l,k_l}^{i_b,j_{b'}}$ is the equivalent channel gain for a given subcarrier pair $(i_b, j_{b'})$ allocated to user-relay pair (k_l, m_l), which is determined as

$$\alpha_{k_l,m_l}^{i_b,j_{b'}} \triangleq \begin{cases} \frac{\alpha_{f_l m_l}^{i_b} \alpha_{f_l k_l}^{j_{b'}}}{\alpha_{f_l m_l}^{i_b} + \alpha_{m_l k_l}^{j_{b'}} - \alpha_{f_l k_l}^{i_b}}, & \text{relay link mode} \\ \alpha_{f_l k_l}^{i_b} & \text{direct link mode.} \end{cases} \tag{3.2}$$

In the direct link mode, the BS and relay powers are given by $p_{m_l,k_l}^{f_l,(i_b,j_{b'})} \triangleq p_{m_l,k_l}^{i_b,j_{b'}}$ and $p_{m_l,k_l}^{R_l,(i_b,j_{b'})} \triangleq 0$, respectively. $\zeta_{m_l,k_l}^{i_b,j_{b'}}, \forall (i_b, j_{b'}, k_l, m_l)$ is defined as a binary factor in order to assist mathematical discussion of the resource allocation problem. $\zeta_{m_l,k_l}^{i_b,j_{b'}} = 1$ demonstrates that subcarrier pair $(i_b, j_{b'})$ is allocated to the user-relay pair (k_l, m_l).

3.3.1 Problem Formulation

The resource allocation problem under a minimum rate requirement for each user and a total power constraint can be formalized as

$$\mathbb{P}1: \quad \max_{(\boldsymbol{p},\boldsymbol{\zeta})} \sum_{l} \sum_{\mathcal{S}_l} \zeta_{m_l,k_l}^{i_b,j_{b'}} \frac{w_{k_l}}{2} \log_2 \left(1 + \alpha_{m_l,k_l}^{i_b,j_{b'}} p_{m_l,k_l}^{i_b,j_{b'}}\right) \tag{3.3a}$$

Table 3.1: Notations

$\mathcal{L} = \{1, ..., L\}$	Set of cells
$\mathcal{B} = \{1, ..., B\}$	Set of frequency bands
$\mathcal{N} = \{1, ..., N\}$	Set of subcarriers in each frequency bands
$\mathcal{M}_l = \{1, ..., M_l\}$	Set of relays in cell l
$\mathcal{K}_l = \{1, ..., K_l\}$	Set of users in cell l
i_b	Subcarrier in the first hop over frequency bands b
$j_{b'}$	Subcarrier in the second hop over frequency bands b'
m_l	Relay m in cell l
k_l	User k in cell l
$\alpha^a_{cc'}$	Fading gain of channel between transmitter c and receiver c' over subcarrier a
$\mathcal{S}_l$	$\mathcal{S}_l = \{(b, b', i, j, m_l, k_l) \mid l \in \mathcal{L}; b, b' \in \mathcal{B}; i, j \in \mathcal{N}; m_l \in \mathcal{M}_l; k_l \in \mathcal{K}_l\}$

subject to

$$\sum_{j,b,b',m_l,k_l} \zeta^{i_b,j_{b'}}_{m_l,k_l} = 1, \quad \forall i, l \tag{3.3b}$$

$$\sum_{i,b,b',m_l,k_l} \zeta^{i_b,j_{b'}}_{m_l,k_l} = 1, \quad \forall j, l \tag{3.3c}$$

$$\sum_{b,b',i,j,m_l} \frac{w_{k_l}}{2} \zeta^{i_b,j_{b'}}_{m_l,k_l} \log_2(1 + \alpha^{i_b,j_{b'}}_{m_l,k_l} p^{i_b,j_{b'}}_{m_l,k_l}) \geq R_{\min} \ \forall k_l, l \tag{3.3d}$$

$$\sum_{\mathcal{S}_l} \zeta^{i_b,j_{b'}}_{m_l,k_l} p^{i_b,j_{b'}}_{m_l,k_l} \leq P_l \quad \forall l \tag{3.3e}$$

$$p^{i_b,j_{b'}}_{m_l,k_l} \geq 0, \tag{3.3f}$$

$$\zeta^{i_b,j_{b'}}_{m_l,k_l} \in \{0, 1\} \ . \tag{3.3g}$$

$\sum_{a,b,...,z}$ is used to denote $\sum_a \sum_b \dots \sum_z$ for simpler representation of the mathematical notations. For each l, $\boldsymbol{p}$ and $\boldsymbol{\zeta}$ denote the sets of nonnegative real numbers $p^{i_b,j_{b'}}_{m_l,k_l}$ and $\zeta^{i_b,j_{b'}}_{m_l,k_l}$, respectively. Constraints (3.3b) and (3.3c) correspond to constraints associated with *exclusive* pairing of the subcarriers in the first and second hops. In other words, only one unique subcarrier i_b in the first time hop is paired with subcarrier $j_{b'}$ in the second hop. Furthermore, (3.3e) represents the total power constraint for each BS. Practically, each user

in the network also has a minimum rate requirement. We consider (3.3d) as a constraint in the resource allocation problem in order to provide each user a minimum rate of R_{min}. Aggregate power is obtained by solving the optimization problem and then the power of each small BSs, macro BS, and relay nodes for a specific user over the corresponding subcarrier is calculated using the following equations [39]

$$p_{m_l,k_l}^{f_l,(i_b,j_{b'})} = \frac{\alpha_{m_l k_l}^{j_{b'}}}{\alpha_{f_l m_l}^{i_b} + \alpha_{m_l k_l}^{j_{b'}} - \alpha_{f_l k_l}^{i_b}} p_{m_l,k_l}^{i_b,j_{b'}}, \tag{3.4}$$

$$p_{m_l,k_l}^{R_l,(i_b,j_{b'})} = \frac{\alpha_{f_l m_l}^{i_b} - \alpha_{f_l k_l}^{j_{b'}}}{\alpha_{f_l m_l}^{i_b} + \alpha_{m_l k_l}^{j_{b'}} - \alpha_{f_l k_l}^{i_b}} p_{m_l,k_l}^{i_b,j_{b'}}. \tag{3.5}$$

Since the optimization problem in (3.3) consists of a binary parameter $\zeta_{m_l,k_l}^{i_b,j_{b'}}$, solving it requires application of integer programming, which has excessive computational complexity [40]. In order to make the problem tractable, we relax the integer factor such that it can be real values equal or greater than zero. After relaxing the constraint in (3.3g), the optimization problem in (3.3) can be rewritten as

$$\mathbb{P}2: \quad \max_{(\boldsymbol{p},\boldsymbol{\zeta})} \sum_{l} \sum_{\mathcal{S}_l} \zeta_{m_l,k_l}^{i_b,j_{b'}} \frac{w_{k_l}}{2} \log_2 \left(1 + \frac{\alpha_{m_l,k_l}^{i_b,j_{b'}} p_{m_l,k_l}^{i_b,j_{b'}}}{\zeta_{m_l,k_l}^{i_b,j_{b'}}}\right) \tag{3.6}$$

$$\text{s.t.} \qquad (3.3b), (3.3c), (3.3e), (3.3f),$$

$$\sum_{b,b',i,j,m_l} \frac{w_{k_l}}{2} \zeta_{m_l,k_l}^{i_b,j_{b'}} \log_2 \left(1 + \frac{\alpha_{m_l,k_l}^{i_b,j_{b'}} p_{m_l,k_l}^{i_b,j_{b'}}}{\zeta_{m_l,k_l}^{i_b,j_{b'}}}\right) \geq R_{\min} \quad \forall k_l, l, \tag{3.7}$$

$$\text{and} \quad \zeta_{m_l,k_l}^{i_b,j_{b'}} \geq 0, \ \forall (i_b, j_{b'}, m_l, k_l). \tag{3.8}$$

Lemma 1. *The objective function in* $\mathbb{P}2$ *is concave in* p *and* ζ.

Proof. Let $q(x) = x \log(1 + y/x)\,|_{y=ax+b} = x \log\left(1 + a + \frac{b}{x}\right)$. Then, for $x > 0$, $q(x)$ is a concave function (This can be demonstrated by taking its second derivative). Consequently, $x \log(1 + y/x)$ is concave, since its restriction to any line, i.e. $q(x)$, is concave [40]. Therefore, the objective function in $\mathbb{P}2$ is a concave function in that it is a nonnegative weighted sum of concave functions in the form of $x \log(1 + y/x)$. ■

Since $\mathbb{P}2$, is a convex optimization problem, it can be solved by any standard method of solving convex problems. However, the value of $\zeta_{m_l,k_l}^{i_b,j_{b'}}$ may not be integer. Therefore, we proceed with the modified two-stage dual decomposition method as we discuss in the following. It is worth mentioning that if the number of subcarriers is adequately large, then the *duality gap* of a non-convex optimization problem reduces to zero[41]. The dual problem is given by

$$\begin{aligned} \mathbb{P}3: \quad & \min_{\boldsymbol{\tau},\boldsymbol{\delta}} D\left(\boldsymbol{\delta},\boldsymbol{\tau}\right) = \min_{\boldsymbol{\tau},\boldsymbol{\delta}} \max_{\boldsymbol{p},\boldsymbol{\zeta}} \; L\left(\boldsymbol{p},\boldsymbol{\zeta},\boldsymbol{\delta},\boldsymbol{\tau}\right) \\ & \text{s.t.} \quad (3.3b) \quad \text{and} \quad (3.3c), \end{aligned} \tag{3.9}$$

where the Lagrangian is given by

$$\begin{aligned} L(\boldsymbol{p},\boldsymbol{\zeta},\boldsymbol{\tau},\boldsymbol{\delta}) = & \sum_{l}\sum_{\mathcal{S}_l} \zeta_{m_l,k_l}^{i_b,j_{b'}} \frac{w_{k_l}}{2} \log_2\Big(1+\frac{\alpha_{m_l,k_l}^{i_b,j_{b'}} p_{m_l,k_l}^{i_b,j_{b'}}}{\zeta_{m_l,k_l}^{i_b,j_{b'}}}\Big) + \sum_{l}\tau_l\Big(P_l - \sum_{\mathcal{S}_l} p_{m_l,k_l}^{i_b,j_{b'}}\Big) \\ & + \sum_{l,k_l}\delta_l^{k_l}\Bigg(\sum_{b,b',i_b,j_{b'},m} \frac{w_k}{2}\zeta_{m_l,k_l}^{i_b,j_{b'}} \log_2\Big(1+\frac{\alpha_{m_l,k_l}^{i_b,j_{b'}} p_{m_l,k_l}^{i_b,j_{b'}}}{\zeta_{m_l,k_l}^{i_b,j_{b'}}}\Big) - R_{\min}\Bigg). \end{aligned} \tag{3.10}$$

In (3.10), $\delta_l^{k_l}$ and τ_l are Lagrangian multipliers.

Lemma 2. *For a given $\zeta_{m_l,k_l}^{i_b,j_{b'}}$, the optimal power allocation that maximizes $L(\boldsymbol{p},\boldsymbol{\zeta},\boldsymbol{\tau},\boldsymbol{\delta})$ is given by*

$$\Big(p_{m_l,k_l}^{i_b,j_{b'}}\Big)^* = \zeta_{m_l,k_l}^{i_b,j_{b'}} \underbrace{\left[\frac{\left(1+\delta_l^{k_l}\right)w_{k_l}}{2\tau_l} - \frac{1}{\alpha_{m_l,k_l}^{i_b,j_{b'}}}\right]^+}_{g_{m_l,k_l}^{i_b,j_{b'}}}, \tag{3.11}$$

where $[x]^+$ indicates $\max(0,x)$.

Proof. By applying *Karush-Kuhn-Tucker* (KKT) condition to the Lagrangian function, we

have

$$\frac{\partial L}{\partial p_{m_l,k_l}^{i_b,j_{b'}}} = \sum_l \sum_{S_l} \left(\left(1+\delta_l^{k_l}\right) \zeta_{m_l,k_l}^{i_b,j_{b'}} \frac{w_{k_l}}{2} \frac{\frac{\alpha_{m_l,k_l}^{i_b,j_{b'}}}{\zeta_{m_l,k_l}^{i_b,j_{b'}}}}{1+\frac{\alpha_{m_l,k_l}^{i_b,j_{b'}} p_{m_l,k_l}^{i_b,j_{b'}}}{\zeta_{m_l,k_l}^{i_b,j_{b'}}}} - \tau_l \right) = 0$$

$$\implies \left(1+\delta_l^{k_l}\right) \frac{w_{k_l}}{2} \frac{\alpha_{m_l,k_l}^{i_b,j_{b'}}}{1+\frac{\alpha_{m_l,k_l}^{i_b,j_{b'}} p_{m_l,k_l}^{i_b,j_{b'}}}{\zeta_{m_l,k_l}^{i_b,j_{b'}}}} = \tau_l$$

$$\implies \left(1+\delta_l^{k_l}\right) \frac{w_{k_l}}{2} \frac{\alpha_{m_l,k_l}^{i_b,j_{b'}}}{\tau_l} - 1 = \frac{\alpha_{m_l,k_l}^{i_b,j_{b'}} p_{m_l,k_l}^{i_b,j_{b'}}}{\zeta_{m_l,k_l}^{i_b,j_{b'}}}$$

$$\implies p_{m_l,k_l}^{i_b,j_{b'}} = \zeta_{m_l,k_l}^{i_b,j_{b'}} \left(\frac{\left(1+\delta_l^{k_l}\right) w_{k_l}}{2\tau_l} - \frac{1}{\alpha_{m_l,k_l}^{i_b,j_{b'}}} \right)$$

Considering constraint (3.3f), the power values must be positive. Therefore, (3.11) gives the optimal power expression. ■

Lemma 3. *The integer valued* $\zeta_{m_l,k_l}^{i_b,j_{b'}}$ *that maximizes* $L(\boldsymbol{p},\boldsymbol{\zeta},\boldsymbol{\tau},\boldsymbol{\delta})$ *corresponds to*

$$\zeta^{*}{}_{m_l,k_l}^{i_b,j_{b'}} = \begin{cases} 1 & (i_b,j_{b'},m_l,k_l) = \arg \max\limits_{k_l,m_l,i_b,j_{b'}} Z_{m_l,k_l}^{i_b,j_{b'}} \\ 0 & \textit{otherwise.} \end{cases} \tag{3.12}$$

Proof. In order to find the optimal value of the binary factor $\zeta_{m_l,k_l}^{i_b,j_{b'}}$, we substitute (3.11) into (3.9) and obtain

$$\begin{aligned} D\left(\boldsymbol{\delta},\boldsymbol{\tau}\right) = & \max_{\boldsymbol{\zeta}} \; L\left(\boldsymbol{p}^{*},\boldsymbol{\zeta},\boldsymbol{\delta},\boldsymbol{\tau}\right) \\ & \text{s.t.} \quad (3.3\text{b}) \;\text{and}\; (3.3\text{c}). \end{aligned} \tag{3.13}$$

Subsequently, it can be rewritten as

$$\max_{\boldsymbol{\zeta}} L\left(\boldsymbol{p}^{*},\boldsymbol{\zeta},\boldsymbol{\tau},\boldsymbol{\delta}\right) = \max_{\boldsymbol{\zeta}} \left(\sum_l \sum_{\mathcal{S}_l} \zeta_{m_l,k_l}^{i_b,j_{b'}} Z_{m_l,k_l}^{i_b,j_{b'}} + C\left(\tau_l,\delta_l^{k_l}\right) \right), \tag{3.14}$$

Table 3.2: Resource Allocation Algorithm

Algorithm of the joint resource allocation
1*: Initialize the Lagrangian multipliers (first iteration) and generate the channel fading gains (Alpha parameters).*
2*: Find the* $(i_b, j_{b'}, m_l, k_l)$ *that maximize* Z*, and set the corresponding* $\zeta_{m_l,k_l}^{i_b,j_{b'}} = 1$.
3*: Find the optimal value of the power* ${p^*}_{m_l,k_l}^{i_b,j_{b'}}$ *by (3.11).*
4*: Update Lagrangian multipliers.*
5*: Iterate the above steps until all Lagrangian multipliers converge. Iteration will stop when* $\frac{\left\|\delta^{(l+1)}-\delta^{(l)}\right\|}{\left\|\delta^{(l+1)}\right\|} < \varepsilon_\delta, \frac{\left\|\tau^{(l+1)}-\tau^{(l)}\right\|}{\left\|\tau^{(l+1)}\right\|} < \varepsilon_\tau$.
6*: End*

where

$$Z_{m_l,k_l}^{i_b,j_{b'}} = \frac{\left(1+\delta_l^{k_l}\right) w_{k_l}}{2} \log_2(1+\alpha_{m_l,k_l}^{i_b,j_{b'}} g_{m_l,k_l}^{i_b,j_{b'}}) - \tau_l g_{m_l,k_l}^{i_b,j_{b'}}, \tag{3.15}$$

$$C(\tau,\delta) = \sum_{l=0}^{L} \tau_l P_l - \sum_{k_l=1}^{K_l} \delta_l^{k_l} R_{\min}. \tag{3.16}$$

Since, (3.16) is constant with respect to $\zeta_{m_l,k_l}^{i_b,j_{b'}}$, the maximum value of the Lagrangian is achieved by adopting the maximum values of $Z_{m_l,k_l}^{i_b,j_{b'}}$. ■

The Lagrangian multipliers are updated via (3.17) and (3.18).

$$(\tau_l)^{n+1} = (\tau_l)^n - \varepsilon_\tau \left(P_l - \sum_{\mathcal{S}_l} \zeta_{m_l,k_l}^{i_b,j_{b'}} \, g_{m_l,k_l}^{i_b,j_{b'}} \right) \forall l, \tag{3.17}$$

$$\left(\delta_l^{k_l}\right)^{n+1} = \left(\delta_l^{k_l}\right)^n - \varepsilon_\delta \left(\sum_{b,b',i_b,j_{b'},m_l} \frac{w_{k_l}}{2} \, \zeta_{m_l,k_l}^{i_b,j_{b'}} \log_2(1+\alpha_{m_l,k_l}^{i_b,j_{b'}} \, g_{m_l,k_l}^{i_b,j_{b'}}) - R_{\min} \right) \forall k_l, l. \tag{3.18}$$

A brief algorithm of the joint resource allocation problem is summarized in Table 3.2.

3.3.2 Suboptimal Solution

The solution discussed in the previous subsection is a near-optimal solution; since, the integer factor ζ is relaxed. As mentioned, the duality gap decreases by increasing the number of subcarriers. However, the computational complexity of the problem increases as the number of subcarriers, relays, users, and the SCs increase, i.e., $O\left(KM(L+1)BN!\right)$. The computational complexity is mainly due to the search for the optimal value of the factor ζ. Therefore, we provide a suboptimal greedy solution to find ζ, based on the "Greedy Iterative Activity Selection" algorithm[42]. Generally, given a set of activities, this algorithm enables the selection of a subset of non-conflicting activities to perform within a time frame, which leads to maximizing the objective function. In this case, we treat resources as non-conflicting activities due to the unique allocation property. Subsequently, by sorting their corresponding Z values, we try to add the resource indices with the highest Z values to the subset of selected activities. The steps involved in the greedy algorithm are outlined in Table 3.3.

Table 3.3: Suboptimal Solution

Greedy Algorithm
Sort $\mathcal{S}_l$ by corresponding Z values, for every l
$\mathcal{S}_l^* = \mathcal{S}_l(1)$
$r = 1$
$n = length(\mathcal{S}_l)$
for $q = r+1 : n$
if $(b,b')_q \neq (b,b')_r$ || $(b,b')_q = (b,b')_r$ and $(i,j)_q \neq (i,j)_r$
$\mathcal{S}_l^* = \mathcal{S}_l^* \cup \mathcal{S}_l^*(q)$
$Z_{\mathcal{S}_l} = 0$ for $(b,b',i,j)_q$
end
Sort $\mathcal{S}_l$
$r = q$
end

3.4 Simulation Results

In this section, we present simulation results that demonstrate the advantage of the proposed scheme in enhancing the overall sum-weighted rate of HetNets by deploying the E-band and V-band SCs and considering their specific propagation characteristics within the service area of macro BSs. The presence of LoS of links is assumed given the high antenna directivity in the mmWave band. We also consider the extended large-scale path-loss model, which is dependent on the distance and frequency of operation[3], expressed as

$$\mathrm{PL}\,(d,f)\,(\mathrm{dB}) = \gamma.10\log_{10}\left(\frac{f}{f_0}\right) + \beta.10\log_{10}\left(\frac{d}{d_0}\right) + \chi_{\mathrm{dB}}, \tag{3.19}$$

where f/f_0 and d/d_0 are the ratio of the frequency and distance deviation about the center carrier frequency and reference distance, respectively. β and γ are path-loss exponent and frequency-dependency factor, respectively. χ_{dB} is the shadowing factor which is a zero mean Gaussian random variable with standard deviation ψ_{dB}. In order to model large-scale fading, the reference distance is set to be $d_0 = 5$ meter (resp. $d_0 = 10$ meter) for the small cells (resp. macro cell). The distance between transmitters and receivers, in the small cells (resp. macro cell), are random in interval [10 50] and [10 30] (resp. [50 500] and [100 300]) meters in the direct and relay links, respectively. Although, we use a generic deployment scenario, the results here can be extended to any specific scenario for example, the ones in 3rd Generation Partnership Project (3GPP). We set the other large scale parameter, i.e., pathloss exponent to 2.5 and 2 for the 60 GHz and 70—80 GHz bands, in the small cells (resp. macro cell), respectively[3] p. 106. Moreover, the shadowing effect of the channels is modeled by a zero mean Gaussian random variable with standard deviation 5.4 dB and 4.7 dB (resp. 5 dB and

Table 3.4: Pathloss Model Parameters

	V-band		E-band		LTE
	indoor	outdoor	indoor	outdoor	
β	2.5	2.2	2	2.1	2
ψ_{dB}	$5.4dB$	$5dB$	$4.7dB$	$2.1dB$	$4dB$
γ	9.4		2		2

2.1 dB) for the 60 GHz and 70–80 GHz bands, respectively[3]. For the LTE band, pathloss exponent and shadowing standard deviation are set to 2 and 4 dB, respectively[43]. In the proposed scheme, initial Lagrangian multipliers are randomly set and the step size for the subgradient method is set to $0.5/\sqrt{n}$, where n denotes the iteration index. ε_δ and ε_τ are set to be 10^{-4}. The weights w_{k_l} are considered to be $w_{k_l} = 1 + (k_l - 1)/(K_l - 1), \forall k_l, l$ which is used only as an example. The minimum rate requirement for the users is set to 3 (bits/sec/Hz) and the total transmit power is set to 3 dB (resp. 16 dB) for the small BSs (resp. macro BS). For clarity purposes, a list of the parameters set in the simulation are provided in Table 3.4 and 3.5. As for the performance comparison, some other comparable and related approaches of resource allocation as well as the optimal solution as the upper bound with maximum throughput and highest complexity are considered:

- ***EP***: The conventional equal power scheme in which power is equally allocated to all subcarriers.
- ***SubOpt no-pairing***: Scheme in which subcarrier pairing technique is not taken into account.
- ***LTE only***: Scheme where only LTE frequency band is considered.
- ***E only***: Scheme where only mmWave E-band is considered.
- ***SubOpt***: The greedy solution presented in this chapter.

The sum-weighted rate of the network versus the number of subcarriers with, $M_l = 2$ relays and $K_l = 4$ in each cell is shown in Fig. 3.3. As anticipated, it can be observed that

Table 3.5: Simulation Parameters

	Small cells		Macro cell	
P_l	$3dB$		$16dB$	
R_{min}	3 bits/s/Hz		3 bits/s/Hz	
	Relay link	Direct link	Relay link	Direct link
$d_0(m)$	[10 30]	[10 50]	[100 300]	[50 500]
ε_δ, ε_τ	10^{-4}			
step size	$0.5/\sqrt{n}$, n denotes the iteration index			

by increasing the number of subcarriers, the sum-weighted rate of the network increases for all three schemes. However, the proposed joint resource allocation outperforms the other two schemes. Moreover, the largest gain is obtained by applying power allocation; while subcarrier pairing also provides reasonable gains.

Fig. 3.4 shows the sum-weighted rate versus the number of users in the network, with $M_l = 5$ relays in each cell and $N = 15$ subcarriers in each frequency band. We observe a similar pattern to Fig. 3.3, where power allocation provides the largest gain, followed by subcarrier pairing. This can primarily be attributed to the nature of mmWave channels, which are significantly affected by shadowing and pathloss. Subcarrier pairing also provides the resource allocation algorithm with flexibility to switch between frequency bands based on channel conditions. This is the main reason that the proposed algorithm outperforms the approach with no subcarrier pairing, as shown in Figs. 3.3 and 3.4.

Fig. 3.5 demonstrates the sum-weighted rate of the network in three cases: one case in which the network utilizes the proposed scheme while applying the mentioned resource allocation and two cases in which either LTE band or E-band is used. It shows that the E-band can be effectively used to overcome significant path loss at V-band frequencies. In fact, because of the strong signal attenuation in the V-band, communication over this band is only possible over short-range distances, so, users that are far from BSs and/or relays experience poorer received SNRs, causing a reduction in data rate. By including the E-band in the resource allocation problem, however a HetNet can take advantage of lower pathloss in the E-band in order to enhance the overall sum-weighted rate of the network. Fig. 3.5 indicates the importance of utilizing various bands within the mmWave band for future HetNets. It can also be seen in Fig. 3.6, that for the longer distances when V-band cannot provide the desired quality of service, the E-band and LTE subcarriers can be used instead. As expected, adding more resources leads to an increase in sum-weighted rate. However, this proposed scheme opportunistically utilizes an unlicensed frequency band that was previously underutilized.

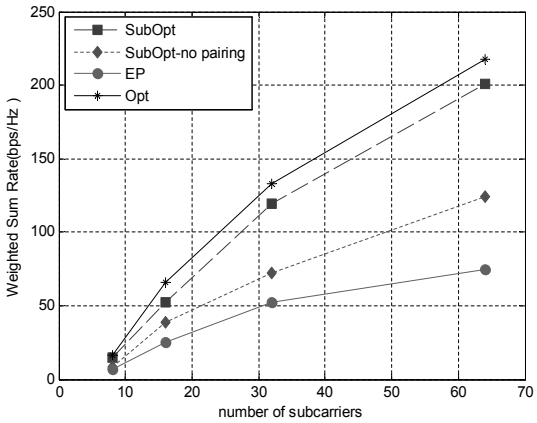

Fig. 3.3: Sum-weighted rate versus number of subcarrier for $K_l = 4$ and $M_l = 2$ in each cell, $L = 3$ cell.

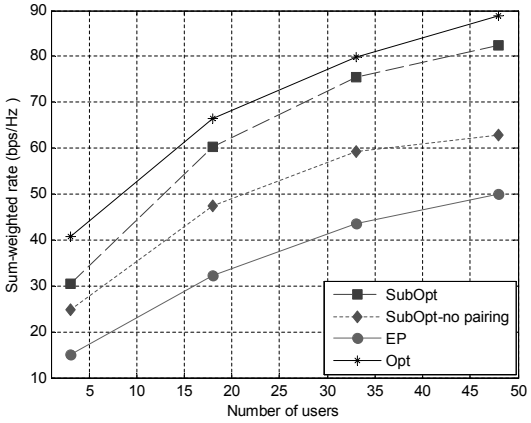

Fig. 3.4: Sum-weighted rate versus number of user for $N = 15$ in each band, $M_l = 5$ in each cell, $L = 3$ cell.

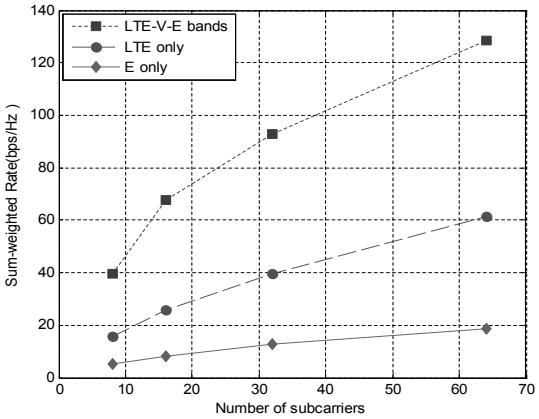

Fig. 3.5: Sum-weighted rate versus number of subcarrier for $M_l = 2$, $K_l = 2$ in each cell, $L = 3$ cell.

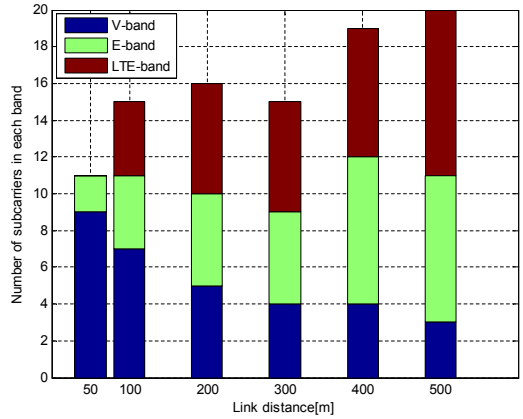

Fig. 3.6: Number of subcarriers in each band versus link distance for $M_l = 2$, $K_l = 2$ and $N = 8$ in each cell, $L = 3$ cell.

3.5 Summary and Conclusion

This chapter proposed a new scheme for utilizing mmWave frequency bands with distinct propagation characteristics in a HetNet structure. A resource allocation problem that considers utilization of E-band and V-band along with LTE band, subcarrier allocation, subcarrier pairing, and relay selection was formulated. The proposed scheme was applied to the downlink scenario of a HetNet with a macro BS coupled with small mmWave BSs. Our objective was to maximize the sum-weighted rate of the network while considering a minimum rate

requirement for each user. The resulting optimization problem was solved by considering its dual form. Subsequently, a suboptimal solution was presented. Simulation results showed that our scheme outperformed conventional schemes and demonstrated that utilization of E- and V-bands can play a major role in addressing the propagation challenges at mmWave frequencies.

Chapter 4

Spatial-Spectral Interference model (Large scale Networks)

The potential of the mmWave band in meeting the ever growing demand for high data rate and capacity in emerging 5G wireless networks is well-established. Since mmWave systems are expected to use highly directional antennas with very focused beams to overcome severe pathloss and shadowing in this band, the nature of signal propagation in mmWave wireless networks may differ from current networks. One factor that is influenced by such propagation characteristics is the interference behavior, which is also impacted by simultaneous use of the unlicensed portion of the spectrum by multiple users. Therefore, considering the propagation characteristics in the mmWave band, this chapter proposes a spatial-spectral interference model for 5G mmWave applications, in the presence of Poisson field of blockages and interferers operating in licensed and unlicensed mmWave spectrum. Consequently, the average bit error rate of the network is calculated. Simulation is also carried out to verify the outcomes of the chapter.

4.1 Introduction

As it has been mentioned in previous chapters, one of the key enabling technologies of emerging 5G wireless networks is the use of bandwidth in the mmWave frequencies, i.e, 30–300 GHz[5]. However, due to undesirable propagation characteristics of mmWave signals such as severe pathloss, strong gaseous attenuation, low diffraction (due to short wavelength) around objects and large phase noise, this section of the spectrum has been underutilized. Having large antenna arrays that coherently direct the beam energy will help overcome the hostile characteristics of mmWave channels[3]. However, utilization of the highly directional beams changes many aspects of the wireless system design. Such directional links (that are susceptible to blockages by obstacles along with the distinct mmWave propagation characteristics), will considerably affect the interference model. In fact, interference in the mmWave band may exhibit an on-off behavior[5].

As new applications and standards compete to exploit open access frequencies, coexistence of licensed and unlicensed bands in 5G cellular networks is a critical consideration[7]. In addition, unlicensed frequencies provide a viable option for offloading traffic[5;8]. With such mixed use of licensed and unlicensed bands, interference in the mmWave band may have a more unpredictable behavior that needs to be taken into consideration. In general, users may be randomly distributed in space and could be using a random subset of frequency bands. There are multiple prior efforts that have focused on modeling the interference behavior. An uplink interference model for small cells of heterogeneous networks has been proposed in[44]. However, mmWave specifications in modeling the interference, i.e., the effect of the highly directional links and considerable sensitivity of mmWave beams to blockages are not taken into account. An interference model for wearable mmWave networks considering the effect of blockages has been suggested in [45]. However, the location of the interferers and the blockages are assumed to be deterministic. The authors in[46] have suggested an interference model for randomly distributed interferers, using a stochastic geometry based analysis. However, similar to[44] and[45], in[46], interferers are considered only in spatial domain. Such a consideration may not be adequate to model the interference in networks operating in both

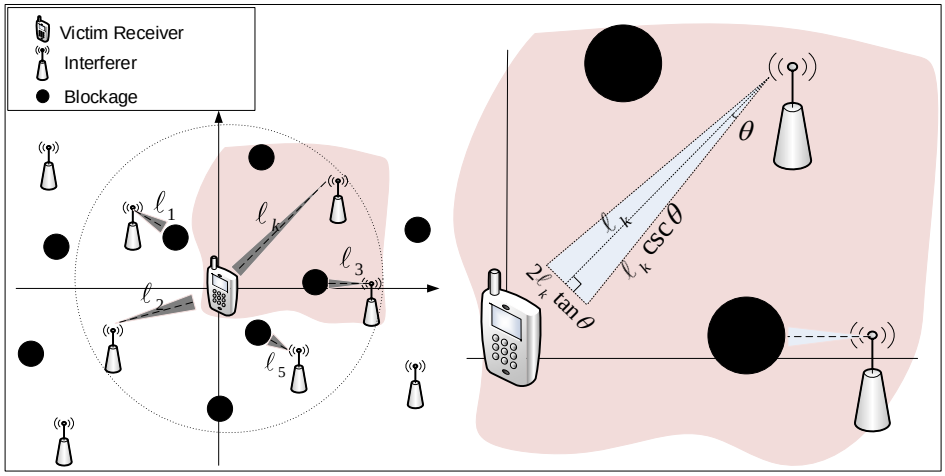

Fig. 4.1: The impact of interferers on the victim receiver in the presence of obstacles.

licensed and unlicensed frequency bands, due to the randomness in utilizing the frequencies by terminals that share the same spectrum. Authors in [47] have suggested a spectral-spatial model for interference analysis in networks considering the unlicensed frequency bands. However, the effect of the presence of the blockages in the environment is not taken into account in the model. In summary, current literature in interference modeling for 5G mmWave networks lacks the consideration for the propagation characteristics in the mmWave band, i.e., severe shadowing caused by highly directional links and the presence of blockages and simultaneous use of both licensed and unlicensed spectrums in the mmWave band.

4.1.1 Contributions

In this chapter, we propose a spatial-spectral model for interference analysis in 5G mmWave wireless networks while considering the impact of random number of blockages in the environment. We derive the closed-form expression of the moment generation function (MGF) of the aggregate interference to a victim receiver, considering blockages in the environment. Then, we use this MGF to derive the bit error rate (BER) expression at the victim receiver and validate it using Monte Carlo simulations of the network.

4.2 System Model

We consider a transmitter-receiver pair in the presence of random number of interferers with the receiver at the origin of $\mathbb{R}^2$ plane communicating with the transmitter over a desired communication link. The number of interferers follows a Poisson point process with parameter λ in the space-frequency domain[48]. We also model the spatial distribution of blockages as a Poisson point process with parameter ρ[49]. Considering the large scale signal attenuation, specially in case of mmWave signals that suffer greatly from gaseous attenuation and atmospheric absorbtion, only interference within a limited area around the victim receiver is significant[44;50]. A circular area of radius D around the victim receiver is assumed and the number of interferes inside the interfering circle is Poisson distributed with parameter $\lambda\pi D^2$[51]. Moreover, in this network, we are primarily concerned with active interferers that are in the LoS of the victim receiver. It is important to note that there could be other interferers that do not impact the victim receiver as their signals are blocked by obstacles. Similar to[45], we assume that there is no blockages in the desired communication link. The interferers and their distances to the victim receiver are denoted by I_k and ℓ_k, for $k = 1, 2, ..., U$, respectively. For the k^{th} individual interferer, we consider a radiation cone, denoted by S_k, where the edges are determined by the beamwidth of the signal. From Fig. 5.1, it is evident that for the k^{th} interferer, the radiation cone area, A_{S_k}, is given by

$$A_{S_k} = \frac{2\ell_k \tan(\theta) \,.\, \ell_k}{2} = \ell_k^2 \tan(\theta) \,. \tag{4.1}$$

Similar to[45;49] and[52], we assume that the beamwidth of mmWave signals, 2θ, is narrow enough that the signal from an interferer is blocked if at least one blockage is presented in the radiation cone of the given interferer. That is, the beamwidth, 2θ, is such that the base of the radiation cone of the interferer is smaller than the dimension of the blockage. This considerable sensitivity to blockages results from the high directionality of mmWave signals[3;5]. For instance, measurement results from[53], for a transmitter-receiver pair separated by 5 m, indicate that an average sized body of depth of 0.28 m causes 30-40 dB power

loss using directional antennas. Therefore, the probability of the k^{th} interferer not being blocked, p_k, is obtained by

$$p_k = \mathrm{e}^{-\rho A_{S_k}} = \mathrm{e}^{-\rho \ell_k^2 \tan(\theta)}, \tag{4.2}$$

which is consistent with the 3GPP[54] and potential indoor 5G 3GPP-like models[55] as well, where the probability of having LoS decreases exponentially as the length of the link increases. Based on the above assumption and system configuration, the received signal at the victim receiver, $R(t)$, is given by

$$R(t) = i_0(t) + \sum_{k=1}^{K} i_k(t) + n(t), \tag{4.3}$$

where K is the number of active interferers, $i_k(t)$ is the signal received from the k^{th} interferer, $i_0(t)$ is the desired signal, and $n(t)$ is the additive white Gaussian noise (AWGN) with zero mean and variance $N_0/2$. The received interference signal from the k^{th} interferer, can be represented as[20]

$$i_k(t) = \sqrt{q_k h_k \ell_k^{-\alpha}}\; v_k(t)\, \mathrm{e}^{-j2\pi f_k t + \psi_k}, \tag{4.4}$$

where $v_k(t)$ and q_k are the baseband equivalent and transmitted power of the k^{th} interferer, respectively, α is the pathloss exponent, and h_k is a Gamma distributed random variable that represents the squared fading gains of the Nakagami-m channel model (a generic model that can characterize different fading environments[20]). f_k and ψ_k denote the frequency and phase of the k^{th} interferer, respectively, which are assumed to be random[48].

4.3 Interference Analysis and System Performance

In this section, the MGF of the accumulated interference is derived and used to quantify the average BER at the victim receiver. Using (4.3) and (4.4), the SINR at the victim receiver

can be determined as

$$\mathrm{SINR} = \frac{q_0 h_0 \ell_0^{-\alpha}}{\sum_{k=1}^{K} \mathcal{P}_{I_k} + \sigma_n^2}, \tag{4.5}$$

where, σ_n^2 is the power of the additive noise bandlimited to the signal bandwidth $[-\frac{W}{2}.\frac{W}{2}]$. q_0, h_0, and ℓ_0 are the transmitted power, the squared channel fading gain, and the distance between desired transmitter and the receiver, respectively. $\mathcal{P}_{I_k}$ is the effective received interference power from the k^{th} interferer at the output of the matched filter which is obtained by

$$\mathcal{P}_{I_k} = q_k h_k \ell_k^{-\alpha} \int_{-W/2}^{+W/2} \Phi(f - f_k)|H(f)|^2 \mathrm{d}f. \tag{4.6}$$

Here, $H(f)$ is the transfer function of the matched filter on the receiver side, and $\Phi(f)$ is the power spectral density of the baseband equivalent of the interferers' signals. In order to evaluate the performance of the network, we assume that given the distribution of f_k, l_k, and ψ_k, the received interference signal at the output of the matched filter is a complex Gaussian distributed signal. This is a valid assumption as shown in [56]. Subsequently, we can relate the BER to SINR as BER=$\frac{1}{2}\mathrm{erfc}\sqrt{c\mathrm{SINR}}$, where c is a constant that depends on modulation used [20]. In order to find the average BER, we invoke the result in [57], in which it is shown that the expected value of functions in the form of $g(\frac{x}{y+b})$ can be written as

$$E_x\left[g\left(\frac{x}{y+b}\right)\right] = g(0) + \int_0^{\infty} g_m(\mathrm{s})\, M_y(m\mathrm{s})\mathrm{e}^{-\mathrm{s}mb}\mathrm{ds}. \tag{4.7}$$

Here, x is a Gamma distributed random variable, $M_y(m\mathrm{s})$ represents the MGF of y in a Nakagami-m fading environment, b is an arbitrary constant, and $g_m(\mathrm{s}) = -\frac{\sqrt{c}}{\pi}\frac{\Gamma(m+\frac{1}{2})}{\Gamma(m)}\frac{e^{-c\mathrm{s}}}{\sqrt{\mathrm{s}}}{}_1F_1(1-m;\frac{3}{2};c\mathrm{s})$, where ${}_1F_1(a;b;\mathrm{s})$ is the confluent hypergeometric function. In order to utilize (4.7)

to find the average BER, (4.5) can be rewritten as

$$\mathrm{SINR} = \frac{h_0}{\frac{1}{q_0 \ell_0^{-\alpha}} \sum_{k=1}^{K} \mathcal{P}_{I_k} + \sigma_n^2 / q_0 \ell_0^{-\alpha}}, \tag{4.8}$$

where, h_0 is a Gamma distributed random variable and $\sigma_n^2 / q_0 \ell_0^{-\alpha}$ is a constant. Therefore, using (4.7), the average BER can be written based on the MGF of the accumulated interference as

$$E_{h_0}\left[\mathrm{BER}\right] = \frac{1}{2} - \frac{\sqrt{c}}{\pi} \frac{\Gamma(m+\frac{1}{2})}{\Gamma(m)} \int_0^{\infty} \frac{{}_1F_1\left(1-m; \frac{3}{2}; c\mathrm{s}\right)}{\sqrt{\mathrm{s}}} M_I\left(m\mathrm{s}\right) e^{-(mb+c)\mathrm{s}} \mathrm{ds}, \tag{4.9}$$

where

$$M_I\left(\mathrm{s}\right) = E\left[\mathrm{e}^{\frac{\mathrm{s}}{q_0 \ell_0^{-\alpha}} \sum_{k=1}^{K} q_k h_k \ell_k^{-\alpha} \Omega(f_k)}\right], \tag{4.10}$$

$$\Omega(f_k) = \int_{-W/2}^{+W/2} \Phi(f - f_k) |H(f)|^2 \mathrm{d}f. \tag{4.11}$$

Since (4.10) is the MGF of sum of a random number of random variables, the distribution of the random variable K, i.e., the number of active interferers, is needed.

Lemma 4. *The number of active interferers, K, within the circular area of radius D (around the victim receiver) and the signal bandwidth W, is a Poisson random variable with parameter* $\frac{\lambda \pi W \left(1 - \mathrm{e}^{-D^2 \rho \tan\theta}\right)}{\rho \tan\theta}$.

Proof. Let $K = X_{I_1} + X_{I_2} + ... + X_{I_U}$, where X_{I_k} is the indicator that the k^{th} interferer is not blocked with probability p_k, given by (4.2). In order to make the analysis tractable, we assume that the blockages affect each link independently, i.e., the number of the blockages on different links are independent. The assumption of two links share no common blockages has negligible effect on accuracy [49]. Consequently, X_{I_k} can be modeled as an i.i.d Bernoulli distributed random variable with success probability p_k and I_k is assumed to take on Poisson distribution as presented in section 6.2. Therefore, given the distance ℓ_k, the probability

generating function (PGF) of X is obtained by [1]

$$\begin{aligned} G_{X|\ell_k}(\mathrm{z}) &= p_k \mathrm{z} + (1 - p_k) \\ &= \mathrm{e}^{-\rho \ell_k^2 \tan(\theta)} \mathrm{z} + (1 - \mathrm{e}^{-\rho \ell_k^2 \tan(\theta)}). \end{aligned} \tag{4.12}$$

In networks with Poisson field of interferers, the probability density function (PDF) of ℓ_k, i.e., the distance of the k^{th} interferer to the victim receiver, is given by [48],

$$\mathbb{P}(\ell) = \begin{cases} \frac{2\ell}{D^2} & 0 < \ell < D \\ 0 & \text{elsewhere.} \end{cases} \tag{4.13}$$

Based on (4.13), we can average out ℓ in (4.12) leading to

$$G_X(\mathrm{z}) = \frac{(1 - \mathrm{z}) \left(\mathrm{e}^{-\rho D^2 \tan\theta} - 1 \right)}{\rho D^2 \tan\theta} + 1. \tag{4.14}$$

Subsequently, the PGF of K is given by

$$\begin{aligned} G_K(\mathrm{z}) &= \mathrm{E}\left[\mathrm{z}^{\sum_{k=1}^{U} X_{I_k}} \right] = \sum_{k \geq 0} \left(\mathrm{E}\left[\mathrm{z}^X \right] \right)^k p(U = k) \\ &= G_U(G_X(\mathrm{z})) = \mathrm{e}^{\lambda \pi W \left(\frac{1 - \mathrm{e}^{-D^2 \rho \tan\theta}}{\rho \tan\theta} \right) (\mathrm{z} - 1)}, \end{aligned} \tag{4.15}$$

which is the PGF of a Poisson random variable with parameter $\frac{\lambda \pi W \left(1 - \mathrm{e}^{-D^2 \rho \tan\theta}\right)}{\rho \tan\theta}$. ■

Theorem 1. *The closed-form expression for the MGF of the accumulated interference corresponds to* (4.16).

[1] The subscript of X_{I_k} is dropped for notational simplicity.

$$M_I(s) = \exp\left\{\lambda\pi W\left(\frac{1-\mathrm{e}^{-D^2\rho\tan\theta}}{\rho\tan\theta}\right)\right.$$
$$\left.\times\left(\frac{2}{\alpha W}\sum_{n=0}^{\infty}\sum_{j=0}^{\infty}\prod_{i=0}^{n}\frac{(i+j-\frac{2}{\alpha})\kappa(j)}{\Gamma(n)\,\Gamma(j-1)}\left(\frac{\mathrm{s}\,q}{D^{\alpha}q_0\ell_0^{-\alpha}}\right)^{j}\frac{\Gamma(j+m)}{m^j\Gamma(m)}-1\right)\right\}. \tag{4.16}$$

Proof. Similar to[47] and[45], for simplicity, homogeneous interferers are assumed, i.e., all interferers transmit at the same power. Therefore, given the distribution of h, the MGF of the received signal from an arbitrary interferer, $M_{I_k|h}(\mathrm{s})$, is given by

$$\begin{aligned}M_{I_k|h}(\mathrm{s}) &= \mathrm{E}\left[\mathrm{e}^{\frac{\mathrm{s}}{q_0\ell_0^{-\alpha}}qh\ell^{-\alpha}\Omega(f)}|h\right]\\ &= \int_{-\frac{W}{2}}^{\frac{W}{2}}\int_0^D \mathrm{e}^{\frac{\mathrm{s}}{q_0\ell_0^{-\alpha}}qh\ell^{-\alpha}\Omega(f)}\frac{2\ell}{D^2}.\frac{1}{W}\mathrm{d}\ell\mathrm{d}f\\ &= \left(\frac{2}{D^2W\alpha}\right)\left(-\frac{\mathrm{s}qh}{q_0\ell_0^{-\alpha}}\right)^{\frac{2}{\alpha}}\int_{-\frac{W}{2}}^{\frac{W}{2}}\Gamma\left(-\frac{2}{\alpha},-\frac{\mathrm{s}qh\Omega(f)}{D^{\alpha}q_0\ell_0^{-\alpha}}\right)\Omega(f)^{\frac{2}{\alpha}}\mathrm{d}f.\end{aligned} \tag{4.17}$$

Here, f_k is a random variable that is uniformly distributed over $[\frac{-W}{2}\,\frac{W}{2}]$ which is a valid assumption in networks with Poisson field of interferers[48], and $\Gamma(a,x) \triangleq \int_x^{\infty} t^{a-1}\mathrm{e}^{-t}dt$ represents the Incomplete Gamma function. Using the Laguerre polynomials expansion of the Incomplete Gamma function[58], (4.17) is simplified to

$$M_{I_k|h}(\mathrm{s})=\frac{2}{\alpha W}\sum_{n=0}^{\infty}\sum_{j=0}^{\infty}\prod_{i=0}^{n}\frac{(i+j-\frac{2}{\alpha})\,\kappa(j)}{\Gamma(n)\,\Gamma(j-1)}\left(\frac{\mathrm{s}qh}{D^{\alpha}q_0\ell_0^{-\alpha}}\right)^{j}, \tag{4.18}$$

where $\kappa(j) = \int_{-W/2}^{W/2}\Omega(f)^j\mathrm{d}f$. Based on the assumption of general Nakagami-m fading channel, h is a Gamma distributed random variable representing the squared fading gain of the channel. Therefore, the MGF of the interference from the k^{th} interferer can be expressed

as

$$M_{I_k}(\mathrm{s}) = \frac{2}{\alpha W} \sum_{n=0}^{\infty} \sum_{j=0}^{\infty} \prod_{i=0}^{n} \frac{(i+j-\frac{2}{\alpha})\kappa(j)}{\Gamma(n)\,\Gamma(j-1)} \left(\frac{\mathrm{s}\,q}{D^{\alpha} q_0 \ell_0^{-\alpha}} \right)^{j} \frac{\Gamma(j+m)}{m^{j}\Gamma(m)}. \tag{4.19}$$

Assuming i.i.d. interference signals, justified by the fact that the sources of the interference are independent from one another[48], we have

$$\begin{aligned} M_I(\mathrm{s}) &= \mathrm{E}\Big[\mathrm{e}^{\mathrm{s}\sum_{k=1}^{K} I_k}\Big] = \sum_{k\geq 0} \left(\mathrm{E}\left[\mathrm{e}^{\mathrm{s}I_k}\right]\right)^{k} p(K=k) \\ &= G_K\left(M_{I_k}(\mathrm{s})\right) = \mathrm{e}^{\lambda\pi W\left(\frac{1-\mathrm{e}^{-D^2\rho\tan\theta}}{\rho\tan\theta}\right)\left(M_{I_k}(\mathrm{s})-1\right)}. \end{aligned} \tag{4.20}$$

Substituting (4.19) in (4.20), the closed-form expression for the accumulated interference is determined as in (4.16). ■

4.4 Simulation Results

In this section, we present numerical results to evaluate the performance of the network based on the proposed interference model and validate the results with Monte Carlo simulation. A network region of an area of $100\,\mathrm{m}^2$ is considered. The normalized distance between the desired transmitter and receiver is set to 1 m. We assume the pathloss exponent, α, and the shape factor of Nakagami distribution, m, are set to 2.5 and 3, respectively. Here, similar to[45], the power of all interferers assumed to be the same and set to 0 dB. The beamwidth of the mmWave signals, i.e. 2θ, is set to 20 degrees. An ideal raised cosine (RC) filter is assumed at the receiver's side with roll-off factor of 0. In addition, we consider a raised cosine shaped power spectral density for the interfering signals, as well. It is worth mentioning that the proposed model is not limited to specific power spectral densities of the desired and interferers' signals.

In Fig. 4.2, BER versus SNR is shown for different values of λ. Here, the density of the number of blockages, ρ, is set to 10^{-4}. As expected, as the density of the number of interferers

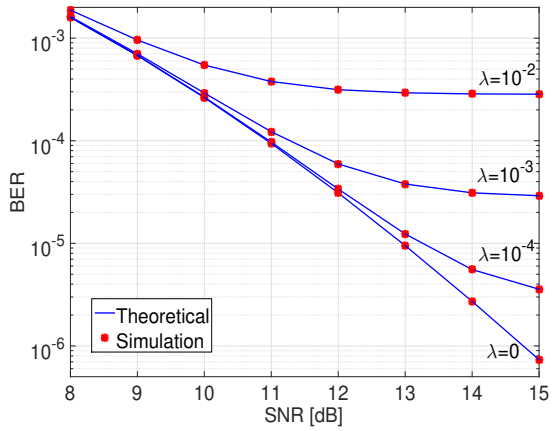

Fig. 4.2: Bit error rate versus SNR for different λ values, ρ=10^{-4}.

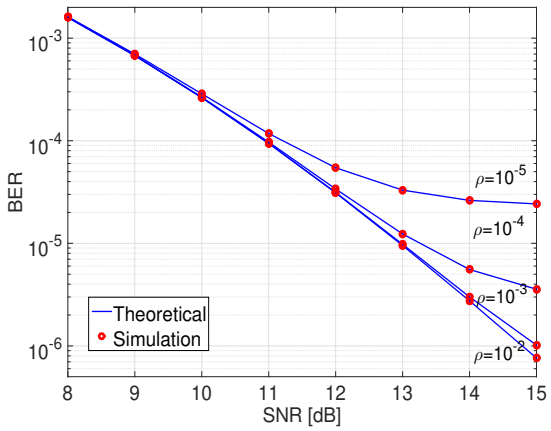

Fig. 4.3: Bit error rate versus SNR for different ρ values, λ=10^{-4}.

decreases, the performance of the system improves. For higher SNR values, the level of the error floor depends on the different λ values. Fig. 5.7 illustrates the performance of the system for different values of ρ, considering a fixed density of the number of interferers, i.e., λ=10^{-4}. As it is evident from Fig. 5.7, as the number of blockages increases, the probability of the interferers being blocked increases and consequently the performance of the network improves. Here, having higher blockage density in the network enhances the level of the error floor. This is an important result that indicates mmWave signals sensitivity to blockages can be advantageous in densely deployed networks, where objects and users that serve as obstacles reduces the level of the interference. It is important to note that, in both Fig. 4.2 and 5.7, the simulated average BER plots aligns well with the theoretical result from the derived interference model. Fig. 4.4 shows the BER versus SNR of the victim receiver with and without consideration of the blockages. As it is illustrated, when the presence of the obstacles is considered in the interference model, there is less interference signal introduced to the desired communication link. Unlike traditional wireless environment, the sensitivity of directional mmWave signals to the obstacles in the environment leads to a different interference profile that is effectively captured in the proposed model.

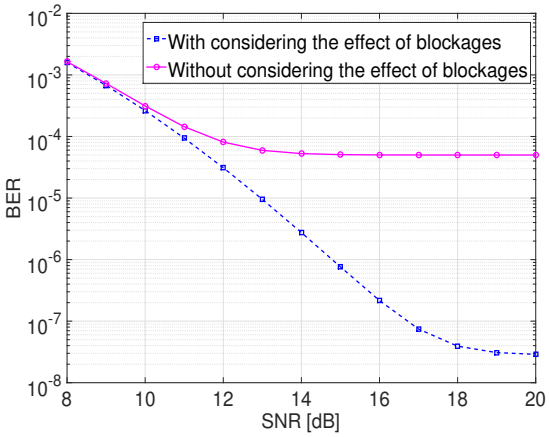

Fig. 4.4: Bit error rate versus SNR for λ=10^{-4} and ρ=10^{-2}.

4.5 Summary and Conclusion

In this chapter, we analyzed the performance of mmWave communication networks in the presence of Poisson field of interferers and blockages. Due to the use of the unlicensed mmWave frequency band, i.e. the 60 GHz band, user terminals that share the same spectrum in the network could introduce unpredictable interference to the desired communication links and possible interference could exist in both frequency and space. Considering randomness in the presence of interference in both spectral and spatial domains, we proposed a spatial-spectral model for interference in the network. In the proposed model, MGF of the accumulated interference was derived and based on the closed-form expression of MGF, the average BER at the victim receiver was calculated.

Chapter 5

Spatial-Spectral Interference model (Finite-sized Networks)

Previously in chapter 4, we derived the interference statistics of the aggregated interference at a reference node in the Poisson field of interferers. This is a valid assumption in large scale networks. However, in finite-sized networks with fixed number of nodes, BPP would be a more accurate model[59]. In this chapter, we first propose a blockage model considering mmWave specifications and correlated blockage effect. Subsequently, using the proposed blockage model, we derive a spatial-spectral interference model for dense finite-area 5G mmWave networks. The proposed interference model considers randomness of node configuration in both spatial and spectral domains. Finally, the error performance of the network from an arbitrarily located user perspective is calculated in terms of BER and outage probability metrics. The analytical results are validated via Monte-Carlo simulations. It is shown that considering mmWave specifications and also randomness in both spectral and spatial node configurations leads to a noticeably different interference profile.

5.1 Introduction

In previous chapter, we understand that it is important to consider random spatial models of the network configuration to accurately model the interference[60]. In addition to the spatial distance between nodes, the distance between their allocated frequencies also affects the amount of accumulated interference in a multi-user environment due to possible partial band overlap and out-of-band radiation. Therefore, uncertainty in network configuration may be observed in the spectral domain impacting the interference model. Moreover, with the notions of adaptive frequency selection and dynamic channel allocation strategies instead of static assignments[61], considering the uncertainty in spectral domain while modeling the accumulated interference provides a more accurate model. A precise interference model in turn impacts the design of interference coordination and management schemes.

There have been prior efforts on interference modeling considering random node distributions. Due to its analytical tractability, PPP is one of the popular random model assumed for node distribution[59]. A 2D-PPP has been suggested in[47] in order to consider the presence of interferers in both spectral and spatial domains in the interference model. However, an infinite-sized network area and an unlimited frequency band of operation are assumed in order to simplify the calculations. In addition, the effect of blockages and mmWave specifications such as high signal attenuation and beam directivity are not taken into account. Therefore, it may not be applicable to 5G mmWave networks. Assuming a PPP model, an interference model for finite-sized highly dense mmWave networks has been proposed in[45]. However, uncertainty in the configuration is only considered in the spatial domain. Moreover, BPP is a more appropriate choice for modeling finite-sized networks with a given number of access points (APs). In fact, in practical scenarios, the network area and also the number of nodes are finite which means that the point process formed by node arrangement is nonstationary[59]. Therefore, the network characteristics, such as interference statistics, differs in different locations and the performance becomes location dependent. In addition, unlike PPP, the number of nodes in disjoint areas becomes dependent. These features are not captured by the Poisson model. Authors in[44] have recommended a mobility-aware up-

link interference model for 5G networks with Binomial node distribution. However, only the interference from macro users to the small cell users is considered due to their higher power levels. Such an assumption may not be appropriate in a dense environment where the interference levels from individual interferers become less distinguishable as they are located in close proximity. In fact, in dense networks, the variance of interference levels from individual users decays with the node density [62]. In addition, mmWave specifications and hence the sensitivity of the beams to the blockages in the environment is not taken into account in [44]. There have been several prior works that model the effect of blockages [49;63–66]. However, in order to make the calculations tractable, [49;63–66] assume that the presence of one obstacle in the path between the transmitters and the receivers completely blocks the LoS link. Such an assumption may be justifiable in case of relatively long-distance links. However, in many practical applications such as indoor environments, outdoor small cells where coverage range is limited or even cases where terminals are equipped with larger number of antennas with wider beamwidths, more than one obstacle may be needed to impact the power level, causing link blockage (for instance, one to five persons in measurement conducted in [67] for indoor mmWave environments). Authors in [68] have suggested a blockage model, built with tools from stochastic geometry and renewal processes, for mmWave cellular communications considering the receiver dimension. However, the model in [68] is based on an unrealistic assumption of very large-sized receiver (i.e., receiver dimension $\rightarrow\infty$).

5.1.1 Contributions

In this chapter, we propose a spatial-spectral interference model for dense finite area 5G mmWave networks while considering realistic blockage effects. The important features of the proposed model can be summarized as follows:

- In order to capture the effect of blockages properly, we first propose a blockage model that calculates the effective number of the obstacles that results in complete link blockage. Then, we calculate the probability of the presence of that number of obstacles in the path from the interfering APs to the receiver which is the probability of the

complete blockage of the interference link. Therefore, unlike prior efforts that consider *binary blockage effect*, here we consider the partial blockage effect of every single obstacle that intersects (partially or completely, depending on the blockage size) the signal beamwidth.

- Binary effect of the blockages is the resultant of the assumption of 0° signal beamwidth in previous blockage modeling works, which is not realistic. In fact, considering such an assumption, a single obstacle that occurs within a given area (depends on the size of the obstacles) close to the LoS link (assumed to be with 0° beamwidth) causes complete link blockage. However, considering non-zero signal beamwidth, there might be cases where a single obstacle creates partial signal blockage. Therefore, we consider non-zero signal beamwidth in order to model the effect of blockages and the interference behavior.

- Using the proposed blockage model, we derive the MGF of the aggregated interference power in a finite-sized mmWave network while considering the configuration uncertainty of the nodes in the spectral domain as well as in spatial domain. Unlike prior works that consider configuration randomness only in spatial domain, we derive the spectral distance distribution and include the configuration randomness in the spectral domain, as well.

Subsequently, using the proposed interference model, we evaluate the performance and reliability of the desired communication link based on the average BER and signal outage probability metrics. It is important to note that average BER and the outage probabilities are the two metrics that can be used in order to evaluate the network performance in fast and slow varying spatial-spectral configuration scenario, respectively. In fact, when the spatial-spectral configuration changes rapidly, it is meaningful to average the interference analysis over all possible realization of the spatial-spectral configurations motivating the use of the average BER metric. However, in the slow varying scenario, the configuration changes slowly and it is more reasonable to calculate the interference for the given configuration and utilize the outage probability metric.

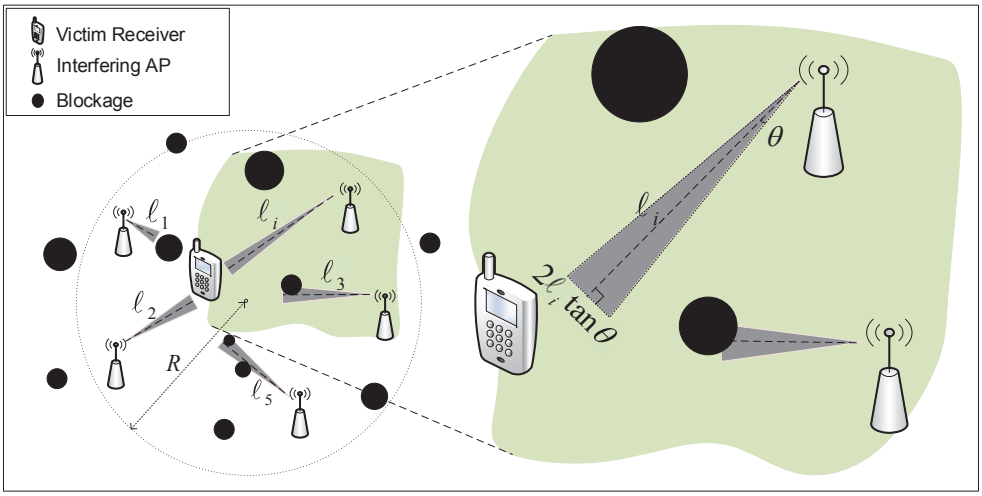

Fig. 5.1: The impact of interfering APs on the victim receiver in the presence of obstacles.

5.2 System Model

Fig. 5.1 represents the system model of interest in the present work. Here, we consider a reference pair of transmitter-receiver communicating over a desired communication link in the presence of N number of interfering APs in a circular area [1] with radius R and frequency range $[f_s, f_e]$. Interfering APs are distributed based on a BPP in the space-frequency domain with success probability p. In other words, we consider a grid structure where the total N interfering APs are randomly located at space-frequency locations based on Binomial point process [2]. The overall received interference signal at a certain point in the network is sum of the received signal from each element at random space-frequency location. We also assume that the reference receiver is at an arbitrary location $v_0 \in B(O,R) = \{x \in \mathbb{R}^2 \mid \|x\|_2 < R\}$ operating over an arbitrary frequency $f_0 \in [f_s, f_e]$. It has also been assumed that the reference transmitter-receiver pair is not a part of the point process. In fact, our model captures the introduced interference from other interfering APs, with random frequencies and physical locations, at an arbitrary frequency f_0 with physical location of the receiving unit at v_0. There are also random number of random-sized blockages in the environment.

[1] However out of the scope, our work can be extended to a polygon-shaped network by using the provided methodology in [69].

[2] This means that each AP has a physical location in the network and operates over a certain frequency, where the nodal arrangement in space-frequency space forms a BPP.

Table 5.1: Summary of System Model Parameters

Notation	Description
R	Radius of the area
N	Total number of interfering APs in the area of interest
p	Success probability of the BPP model (model of interfering APs locations)
ρ	Parameter of the PPP model (model of blockages locations)
v_0 (resp. f_0)	Location (resp. frequency) of the reference receiver
v_i (resp. f_i)	Location (resp. frequency) of the ith interfering AP
f_s (resp. f_e)	Minimum (resp. maximum) of the operational bandwidth
d_s (resp. d_e)	Minimum (resp. maximum) of the radius of the blockages (modeled as circles)
W	Bandwidth of the desired signal
2θ	Signal beamwidth

Similar to[49;64;66;70], we assume that blockages are PPP distributed with parameter ρ. It is worth reiterating that, the finite circular area of radius R represents the area where APs are located. However, blockages (objects in the environment such as humans, cars, trees and so on) are located even outside of the finite network area and can be modeled as PPP, distributed over 2D-plane. Therefore, the PPP assumption for capturing the blockage effect is quite justifiable. Due to the presence of the arbitrary blockages in the environment, the transmitted signal of interfering APs may be blocked and not all of the interfering APs contribute to the total received interference signal. Therefore, we are primarily concerned with the interferers that are in the LoS of the reference receiver. It is worth mentioning that, since at mmWave frequencies, the LoS component dominates and the strongest non-line-of-sight (NLoS) is not often strong in comparison[3]; it is important to maintain the LoS link [3] to have a reliable communication between the reference transmitter-receiver pair. Therefore, we assume that the desired communication link is not blocked. In Section 5.3, we provide the proposed blockage model and calculate the probability of each interfering APs being blocked. Subsequently, using the derived probability of the blockage, we obtain the distribution of the number of active (non-blocked) interfering APs. For a quick reference, we provide the system model parameters in Table 5.1.

[3]especially in delay-sensitive applications such as HDTV.

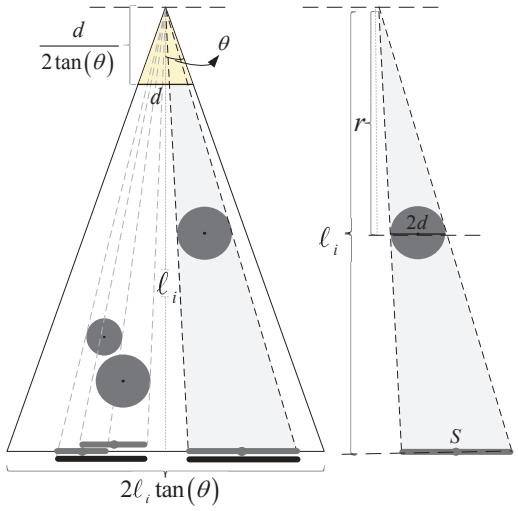

Fig. 5.2: Effective shadow of the blockages on the base of the radiation area.

5.3 Blockage Model

In order to calculate the probability of $i^{\text{th}} \in \{1, 2, ..., N\}$ interfering AP being blocked, as shown in Fig. 5.1, we consider a triangular-shaped radiation area [4], denoted by C_i, where the edges are determined by the beamwidth of the antenna (2θ). There are random number of blockages, modeled as circles with uniformly distributed radius d in $[d_s, d_e]$, within the path from the interfering APs to the reference receiver. It is worth mentioning that, our model is not confined to a specific obstacle size (small or large) and radius d can be any random value to abstract the effect of the mass of both small or large-sized obstacles. However, due to directionality of mmWave signals, the partial blockage concept, that we discuss in detail in this section, makes more sense in the context of small to medium-size obstacles (such as humans, trees and so on). Considering Fig. 5.2, blockages can be at any perpendicular distance r from interfering APs (see Fig. 5.2). Therefore, similar to [68], we assume that r is uniformly distributed in $[0, \ell_i]$. Here, ℓ_i is a random variable that represents the distances

[4] Radiation pattern of directional antennas (ignoring small side-lobes and back-lobes for mathematical tractability) can be modeled as $G(\phi)=cos^n(\phi)$ $\phi \in [0, \pi]$, where n is a positive number corresponding to the antenna pattern directivity [71]. In case of mmWave signals with very narrow beamwidth (large n), with a close approximation, this cosine elliptical radiation pattern can be approximated by a conic pattern with flat wavefront, due to being in the far-field (i.e., triangular-shaped pattern). Maintaining a reasonable accuracy, this assumption provides mathematical simplicity and tractability [72].

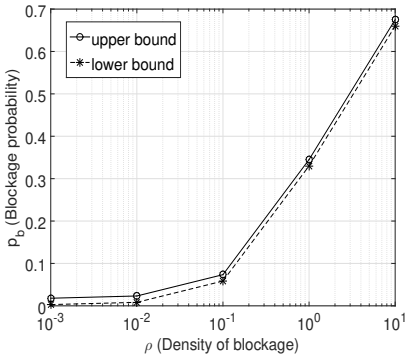

Fig. 5.3: p_b vs. ρ. Here, R=20m, v_0=10m, d_s=0.2m, d_e=0.8m and θ=20°.

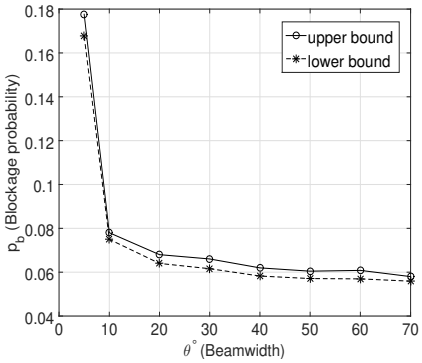

Fig. 5.4: p_b vs. θ. Here, R=20m, v_0=10m, d_s=0.2m, d_e=0.8m and ρ=10^{-1}.

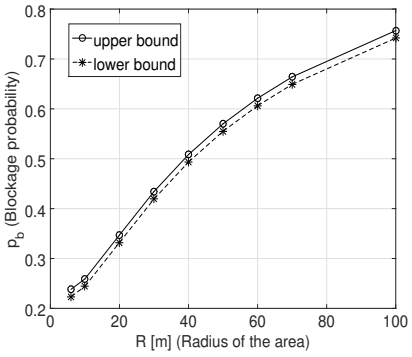

Fig. 5.5: p_b vs. R. Here, v_0=5m, d_s=0.2m, d_e=0.8m and ρ=10^{-2}.

from the i^{th} interfering AP to the reference receiver. Given the BPP assumption for the locations of the interfering APs, the distribution of ℓ_i is given by[5] [73]

$$f_L(\ell) = \begin{cases} \frac{2\ell}{R^2} & 0 < \ell \leq R - \|v_0\| \\ \frac{2\ell \cos^{-1}\left(\frac{\|v_0\|^2 - R^2 + \ell^2}{2\ell\|v_0\|}\right)}{\pi R^2} & R - \|v_0\| < \ell \leq R + \|v_0\| \,. \end{cases} \tag{5.1}$$

To calculate the blockage probability, we divide the distance r (perpendicular distance from the interfering AP to the obstacles in its corresponding radiation area) into two intervals, (i) $r \leq \frac{d}{2\tan(\theta)}$ and (ii) $r > \frac{d}{2\tan(\theta)}$. In the former interval, only one obstacle blocks the radiation area [6], while in the latter more than one blockage is needed to lose the LoS link from the interfering AP to the reference receiver. We calculate the blockage probabilities in both cases (denoted as p_{b1} and p_{b2}, respectively) and average over all realizations of r. Since in the first interval, only one obstacle blocks the entire radiation area, the probability of blockage is the probability of at least one Poisson-distributed blockage located in the upper

[5] We drop the subscript i for notational simplicity.

[6] To be more precise, the upper triangle (the yellow shaded area in Fig. 5.2) is blocked if the *center* of at least one obstacle is located inside the upper triangle. There will be a case where the blockage center is outside the triangle but close to the edges and part of the blockage resides within the area. However, for the sake of simplicity of the model, we ignore this case which can be included later as future work.

triangle in Fig. 5.2 which is given by

$$p_{\mathrm{b1}} | \, d = 1 - \mathrm{e}^{-\rho \frac{d^2}{4\tan(\theta)}}, \tag{5.2}$$

and given the uniform distribution of d, we have

$$\begin{aligned} p_{\mathrm{b1}} &= \int_{d_s}^{d_e} \left(1 - \mathrm{e}^{-\rho \frac{d^2}{4\tan(\theta)}}\right) \frac{1}{d_e - d_s} \mathrm{d}d \\ &= 1 - \frac{\sqrt{\frac{\pi \tan(\theta)}{\rho}}}{(d_e - d_s)} \left[\mathrm{erf}\left(d_e \sqrt{\frac{\rho}{4\tan(\theta)}}\right) - \mathrm{erf}\left(d_s \sqrt{\frac{\rho}{4\tan(\theta)}}\right) \right]. \end{aligned} \tag{5.3}$$

In order to calculate the blockage probability in the second interval ($r > \frac{d}{2\tan(\theta)}$), we borrow the concepts from point process projection along with results from queuing theory. As shown in Fig. 5.2, by projecting blockages onto the base of the radiation area, each blockage in the radiation area causes a shadow (blocked interval) with length $S{=}\frac{2d\ell_i}{r}$ on the base. Based on[74], the point process obtained by the projection of the points of a PPP from a random subset of a higher dimension onto a lower dimension subspace forms a PPP. Therefore, the number of the shadows of the blockages on the base follows a PPP. As shown in Fig. 5.2, the resulting blockages' shadows (gray lines on the base of the radiation area) may overlap with one another. We consider the overall overlapped shadow until the next upcoming non-blocked interval as a single resultant shadow (black lines on the base of the radiation area) with length S_{res}. It is worth mentioning that the number of the resultant shadows is a thinned version of the original PPP obtained from the projection of the blockages in the radiation area onto its base. In order to calculate the the density of the thinned PPP and also the resultant shadows' length, S_{res}, we model the overall projection process by an M/G/∞ queuing system [7], in which the initiation and the length of the shadows corresponds to the customer arrival (with poisson distribution) and their service times in the queue system, respectively. In fact, upon mapping the base of the radiation

[7] M/G/∞ is a queuing system with Poisson arrival of customers, infinite servers and general service time distribution.

area to the time duration $[0, 2\ell_i \tan(\theta)]$, we can model the initiation of the blockages' shadows (customers arrivals) as the Poisson point arrivals in that time duration. Furthermore, they are served immediately upon their arrival (infinite servers in the system) for a time that follows a general distribution (shadow lengths). The assumption of infinite number of servers accounts for the overlapped service times (overlapped shadows). By such correspondence, the interval $[0, 2\ell_i \tan(\theta)]$ consists of alternate busy (partial blocked segment) and idle (non-blocked segment) periods in the queue system. Therefore, the average length and number of the resultant blocked intervals (busy periods of the queue system), denoted as $\mathbb{E}[S_{\text{res}}]$ and $N_{S_{\text{res}}}$, is obtained via

$$\mathbb{E}[S_{\text{res}}] = \frac{\mathrm{e}^{\rho \mathbb{E}[S]} - 1}{\rho}, \tag{5.4}$$

and

$$e^{-\rho \mathbb{E}[S]} \left(1 + 2\rho \ell_i \tan\left(\theta\right)\right) \leq N_{S_{\text{res}}} \leq 1 + 2\rho \ell_i \tan\left(\theta\right), \tag{5.5}$$

respectively[75], where $\mathbb{E}\left[S\right]$ is given by

$$\begin{aligned} \mathbb{E}\left[S\right] &= \mathbb{E}\left[\frac{2d\ell}{r} \left| d, r, \ell \right.\right] \\ &= \int_{d_s}^{d_e} \int_{\frac{d}{2\tan(\theta)}}^{R+\|v_0\|} \int_{\frac{d}{2\tan(\theta)}}^{\ell} \frac{2d\ell}{r} f_D\left(d\right) f\left(r, \ell\right) \mathrm{d}d \, \mathrm{d}r \, \mathrm{d}\ell. \end{aligned} \tag{5.6}$$

Here,

$$f\left(r, \ell\right) = f_L\left(\ell\right) f\left(r \middle| \ell\right) = \begin{cases} f_L\left(\ell\right) \frac{1}{\ell} & 0 \leq r \leq \ell \\ 0 & \text{otherwise.} \end{cases} \tag{5.7}$$

Given the distribution of ℓ_i in (6.4) and the fact that both upper and lower bounds of $N_{S_{\text{res}}}$ are affine functions of ℓ_i, we can apply Jensen's inequality. Therefore, the average number

of the the resultant shadows can be bounded by

$$\mathrm{e}^{-\rho\mathbb{E}[S]}\left(1+2\rho\mathbb{E}[\ell]\tan\left(\theta\right)\right)\leq N_{S_{\mathrm{res}}}\leq 1+2\rho\mathbb{E}[\ell]\tan\left(\theta\right). \tag{5.8}$$

In order to have a complete blockage of the base with average length $2\mathbb{E}[\ell]\tan\left(\theta\right)$, $\left\lceil \frac{2\mathbb{E}[\ell]\tan(\theta)}{\frac{\mathrm{e}^{\rho\mathbb{E}[S]}-1}{\rho}}\right\rceil$ number of resultant shadows with average length $\mathbb{E}[S_{\mathrm{res}}]$ are needed. It is worth reiterating that the resultant equivalent shadows do not overlap with one another. Therefore, following the fact that resultant shadows are Poisson distributed with density $N_{S_{\mathrm{res}}}$, the probability of having $\left\lceil \frac{2\mathbb{E}[\ell]\tan(\theta)}{\frac{\mathrm{e}^{\rho\mathbb{E}[S]}-1}{\rho}}\right\rceil$ number of resultant shadows on the base of the radiation area, i.e., the probability of each interfering AP being completely blocked is given by

$$p_{\mathrm{b2}}=\frac{N_{S_{\mathrm{eff}}}^{\left\lceil \frac{2\mathbb{E}[\ell]\tan(\theta)}{\frac{\mathrm{e}^{\rho\mathbb{E}[S]}-1}{\rho}}\right\rceil}\mathrm{e}^{-N_{S_{\mathrm{eff}}}}}{\left\lceil \frac{2\mathbb{E}[\ell]\tan(\theta)}{\frac{\mathrm{e}^{\rho\mathbb{E}[S]}-1}{\rho}}\right\rceil !}. \tag{5.9}$$

Consequently, the overall blockage probability of each interfering AP, in the average sense, is obtained by

$$\begin{aligned} p_{\mathrm{b}} &= \Pr\left(r\leq\frac{\mathbb{E}\left[d\right]}{2\tan(\theta)}\right)p_{\mathrm{b1}}+\Pr\left(r>\frac{\mathbb{E}\left[d\right]}{2\tan(\theta)}\right)p_{\mathrm{b2}} \\ &= \frac{1}{\frac{\mathbb{E}[d]}{2\tan(\theta)}}p_{\mathrm{b1}}+\frac{1}{\mathbb{E}\left[\ell\right]-\frac{\mathbb{E}[d]}{2\tan(\theta)}}p_{\mathrm{b2}}. \end{aligned} \tag{5.10}$$

Given the upper and lower bounds of the number of resultant shadows in (5.8), the blockage probability in (6.1) is shown for different network parameters in Fig. 5.3, 5.4 and 5.5. As we can see, the gap between the upper and lower bounds is small. It is worth mentioning that, in this blockage model, we assume the receiver dimension spans the base of the radiation area. As we can see in Fig. 5.3, the blockage probability increases with increasing density of the obstacles, as expected. By increasing the beamwidth, in one hand the chance of signals intersecting with more obstacles in the environment increases. On the other hand, since the beam is wider, even after partial blockage due to an obstacle, the signal can be

partially received by the receiver. Both effects are captured in the proposed blockage model by considering the blockage density and the beamwidth. However, as shown in Fig. 5.4, the overall effect is in a way that the probability of blockage decreases as the beam gets wider. Moreover, by increasing the cell radius (which implies an increase in the average distance between the interfering APs and reference receiver) the probability of blockage increases. This is due to the fact that, considering the effective beamwidth of the signal being confined to the receiver's dimension, by increasing the average distance, the effective signal beamwidth becomes narrower with respect to the obstacles' dimension. Therefore, the chance of getting blocked and losing the LoS link increases, which is consistent with the 3GPP [76] and potential 5G models [55;63–66] as well, where the probability of having LoS decreases exponentially as the length of the link increases.

Considering the blockage probability in (6.1), the distribution of the total number of non-blocked interfering APs is calculated using the following lemma:

Lemma 5. *The total number of non-blocked interfering APs, denoted as K, is a Binomial random variable with success probability $p\,(1-p_{\mathrm{b}})$.*

Proof. Let $K = K_1 + K_2 + ... + K_N$, where K_i is a Bernoulli random variable and equals 1, if the i^{th} interfering AP is not blocked, and 0, otherwise. Therefore, the PGF of K_i is given by

$$G_{K_i}(\mathrm{z}) = (1-p_{\mathrm{b}})\mathrm{z} + p_{\mathrm{b}}. \tag{5.11}$$

Subsequently, we have

$$\begin{aligned} G_K(\mathrm{z}) &= \mathbb{E}\left[\mathrm{z}^{\sum_{i=1}^{N} K_i}\right] = \sum_{k\geq 0} \left(\mathbb{E}\left[\mathrm{z}^{K_i}\right]\right)^k p\,(N=k) \\ &= G_N\left(G_{K_i}(\mathrm{z})\right) = \left[(1-p) + p\left((1-p_{\mathrm{b}})\mathrm{z} + p_{\mathrm{b}}\right)\right]^N \\ &= \left[1 - p\,(1-p_{\mathrm{b}}) + p\,(1-p_{\mathrm{b}})\,\mathrm{z}\right]^N. \end{aligned} \tag{5.12}$$

which is the PGF of a Binomial random variable with success probability $p\,(1-p_{\mathrm{b}})$. ■

Now, given the distribution of the number of active interfering APs, in Section 5.4 we

derive the distribution of the aggregated interference power at the reference receiver. Using the derived distribution, we provide expressions for the error performance of the desired communication link in terms of average BER and outage probabilities.

5.4 Interference Statistics and System Performance

In this section, the MGF of the received aggregated interference power at the reference receiver is derived considering the configuration randomness of the interfering APs in both spectral and spatial domains. Given the distribution of the active interfering APs, denoted as K in lemma 6, the aggregated interference power at an arbitrarily located reference receiver is

$$I_{\text{agg}} = \sum_{i=1}^{K} \mathcal{P}_{I_i} \tag{5.13}$$

where, $\mathcal{P}_{I_i}$ is the effective received interference power from the i^{th} interfering AP at the output of the matched filter which is obtained by[47]

$$\mathcal{P}_{I_i} = q_i h_i \|\ell_i\|^{-\alpha} \Upsilon\left(\omega_i\right). \tag{5.14}$$

Here, q_i is the transmitted power of the i^{th} interfering AP. In addition, h_i and $\|.\|^{-\alpha}$ capture the Nakagami-m small scale fading and pathloss effects, respectively. $\ell_i = v_0 - v_i$ and $\omega_i = f_i - f_0$ denote the spatial and spectral distance between the i^{th} interfering AP (located at arbitrary spatial-spectral location $\{v_i, f_i\}$) and the reference receiver, respectively. Moreover, $\Upsilon\left(\omega_i\right)$ is defined as

$$\Upsilon(\omega_i) = \int_{f_0 - \frac{W}{2}}^{f_0 + \frac{W}{2}} \Phi\left(f - f_i\right) \left|H\left(f - f_0\right)\right|^2 \mathrm{d}f, \tag{5.15}$$

where, $H(f-f_0)$ is the transfer function of the matched filter at the reference receiver with arbitrary center frequency f_0 and bandwidth $[-\frac{W}{2}, \frac{W}{2}]$, and $\Phi(f-f_i)$ is the power spectral density of the baseband equivalent of the i^{th} interfering APs signals with frequency f_i. Considering (6.13), as $\|\ell_i\|^{-\alpha}$ captures the impact of spatial distances (and thereby random spatial configuration), $\Upsilon(\omega_i)$ accounts for the effect of frequency separation (and thereby random spectral configuration) in the interference power. The distribution of the aggregated interference power is obtained using the following theorem:

Theorem 2. *The MGF of the aggregated interference power at the arbitrarily located receiver, is given by*

$$M_{I_{\text{agg}}}(\mathrm{s}) = \left[1 - p\left(1-p_{\text{b}}\right) + p\left(1-p_{\text{b}}\right) M_{\mathcal{P}_{I_i}}(\mathrm{s})\right]^N, \tag{5.16}$$

where

$$M_{\mathcal{P}_{I_i}}(\mathrm{s}) \;= \sum_{n=0}^{\infty} \frac{(q\,\mathrm{s})^n}{n!} \frac{m^{-n}\Gamma\left(n+m\right)}{\Gamma\left(m\right)} \frac{2\gamma_n\left(f_s, f_e\right)\kappa_n\left(R, v_0\right)}{R^2\left(f_e - f_s\right)}. \tag{5.17}$$

Here, $M_{\mathcal{P}_{I_i}}(\mathrm{s})$ is the MGF of the i^{th} interfering AP power, where

$$\gamma_n\left(f_s, f_e\right) = \int_0^{\min(|\omega_e|,|\omega_s|)} \Upsilon(\omega)^n \mathrm{d}\omega + \int_0^{\max(|\omega_e|,|\omega_s|)} \Upsilon(\omega)^n \mathrm{d}\omega,$$

$$\kappa_n\left(R, v_0\right) = \int_0^{R-\|v_0\|} \ell^{-n\alpha+1}\,\mathrm{d}\ell \;+ \int_{R-\|v_0\|}^{R+\|v_0\|} \frac{\ell^{-n\alpha+1}}{\pi} \cos^{-1}\left(\frac{\|v_0\|^2 - R^2 + \ell^2}{2\ell\,\|v_0\|}\right) \mathrm{d}\ell. \tag{5.18}$$

and $\omega_e = f_e - f_0$, $\omega_s = f_s - f_0$.

Proof. In order to calculate the MGF of the received aggregated interference power, we have

$$\begin{aligned} M_{I_{\text{agg}}}(\mathrm{s}) &= \mathbb{E}\left[\mathrm{e}^{\mathrm{s}\sum_{i=1}^{K}\mathcal{P}_{I_i}}\right] = \sum_{k\geq 0}\left(\mathbb{E}\left[\mathrm{e}^{\mathrm{s}\mathcal{P}_{I_i}}\right]\right)^k p\left(K=k\right) \\ &= G_K\left(M_{\mathcal{P}_{I_i}}(\mathrm{s})\right) \\ &= \left[1-p\left(1-p_{\mathrm{b}}\right)+p\left(1-p_{\mathrm{b}}\right)M_{\mathcal{P}_{I_i}}(\mathrm{s})\right]^N, \end{aligned} \tag{5.19}$$

where, $M_{\mathcal{P}_{I_i}}(\mathrm{s})$ is the MGF of the i^{th} interfering AP power and calculated by [8]

$$\begin{aligned} M_{\mathcal{P}_{I_i}}(\mathrm{s}) &= \mathbb{E}\left[\mathrm{e}^{\mathrm{s}\,q\,h\,\ell^{-\alpha}\Upsilon(\omega)}\right] \\ &= \int_0^{\infty}\int_0^{R+\|v_0\|\max(|\omega_e|,|\omega_s|)}\int_0^{} \mathrm{e}^{\mathrm{s}\,q\,h\,\ell^{-\alpha}\Upsilon(\omega)} f_\Omega(\omega)\, f_L(\ell)\, f(h)\,\mathrm{d}\omega\,\mathrm{d}\ell\,\mathrm{d}h. \end{aligned} \tag{5.20}$$

Given the BPP assumption of the location of interferer in the space-frequency domain, the distributions of spectral distance [9] is derived as

$$f_\Omega(\omega) = \begin{cases} \frac{2}{f_e-f_s} & 0<\omega\leq \min\left(|\omega_e|,|\omega_s|\right) \\ \frac{1}{f_e-f_s} & \min\left(|\omega_e|,|\omega_s|\right)<\omega\leq \max\left(|\omega_s|,|\omega_s|\right) \end{cases} \tag{5.21}$$

where, $\omega_e = f_e - f_0$ and $\omega_s = f_s - f_0$. Having the spatial and spectral distance distributions given in (6.4) and (6.21), respectively, Nakagami-m assumption of the small scale fading component, i.e., h, and using the polynomial expansion of the exponential function, the integral in (6.20) reduces to that in (6.16). Subsequently, by substituting (6.16) in (6.19) the result in Theorem 3 is obtained. ■

In order to evaluate the system performance using the derived interference model in Theorem 3, we invoke the result in [9], in which using the MGF of the aggregated interference

[8] We drop the subscript i for notational simplicity.
[9] Detailed derivation of the distribution can be found in the Appendix A.

power, the average BER is calculated by the following expression,

$$\mathrm{BER}_{\mathrm{ave}} = \frac{1}{2} - \frac{\sqrt{c}}{\pi}\frac{\Gamma(m+\frac{1}{2})}{\Gamma(m)}\int_0^{\infty} \frac{{}_1F_1(m+\frac{1}{2};\frac{3}{2};-c\mathrm{s})}{\sqrt{\mathrm{s}}} M_{I_{\mathrm{agg}}}\left(-\frac{m}{q_0\ell_0^{-\alpha}}\mathrm{s}\right) \mathrm{e}^{-\frac{m\sigma_n^2}{q_0\ell_0^{-\alpha}}\mathrm{s}}\mathrm{ds}, \quad (5.22)$$

where, q_0 and ℓ_0 denote the power of the reference transmitter and the distance between the reference transmitter-receiver pair. Moreover, m is the shape factor of Nakagami distributed channel and c is a constant that depends on the modulation type. In addition, σ_n^2 represents the power of the additive noise bandlimited to the signal bandwidth $[-\frac{W}{2}, \frac{W}{2}]$.

The outage probability $P_{outage}(\eta)$ is defined as the cumulative distribution function (CDF) of the SINR evaluated at a threshold η which is

$$P_{outage} = \Pr\left(\mathrm{SINR} \leq \eta\right) = \Pr\left(\frac{q_0 h_0 \ell_0^{-\alpha}}{\sum_{i=1}^{K} \mathcal{P}_{I_i} + \sigma_n^2} \leq \eta\right). \quad (5.23)$$

In order to calculate the above probability we first rearrange the argument in (5.23) and obtain the following expression

$$P_{outage} = \Pr\left(\overbrace{-\frac{\eta\sum_{i=1}^{U}\mathcal{P}_{I_i}}{\sigma_n^2} + \frac{q_0 h_0 \ell_0^{-\alpha}}{\sigma_n^2}}^{\Lambda} \leq \eta\right) = F_{\Lambda}\left(\eta\right), \quad (5.24)$$

where, F_{Λ} denotes the CDF of random variable Λ. Now, using Gil-Pelaez inversion formula

$$F_{\Lambda}\left(\lambda\right) = \frac{1}{2} - \frac{1}{\pi}\int_0^{\infty} \mathrm{Im}\left\{M_{\Lambda}\left(j\mathrm{s}\right) e^{-j\mathrm{s}\lambda}\right\}\frac{\mathrm{ds}}{\mathrm{s}}, \quad (5.25)$$

and making the following substitution

$$M_{\Lambda}\left(\mathrm{s}\right) = \left(1 - \frac{q_0\ell_0^{-\alpha}\mathrm{s}}{m\sigma_n^2}\right)^{-m} M_{I_{\mathrm{agg}}}\left(-\frac{\eta}{\sigma_n^2}\mathrm{s}\right), \quad (5.26)$$

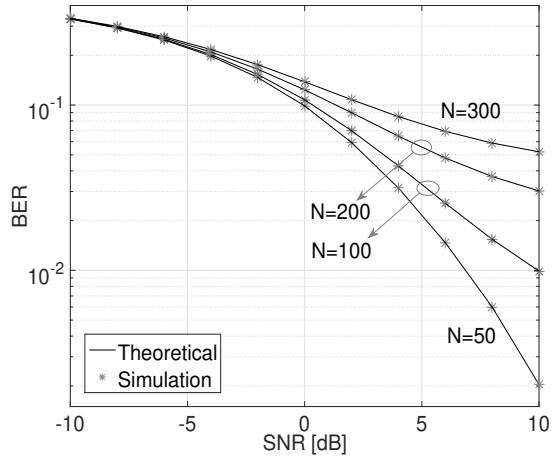

Fig. 5.6: Bit error rate vs. SNR for different N values, ρ=10^{-2}.

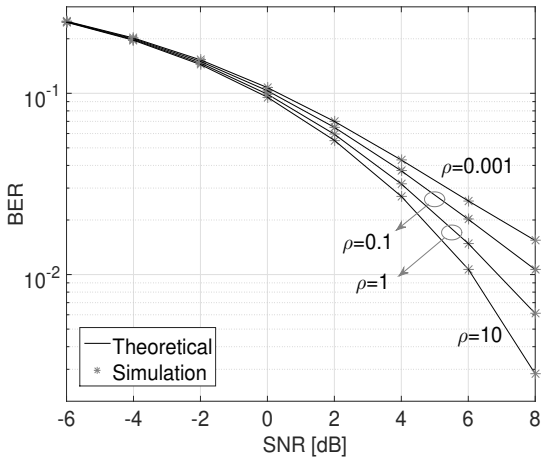

Fig. 5.7: Bit error rate vs. SNR for different ρ values, N=100.

the outage probability can be simplified and written as follows

$$P_{outage} = \frac{1}{2} - \frac{1}{\pi}\int_0^{\infty} \mathrm{Im}\left\{\left(1 - \frac{jq_0\ell_0^{-\alpha}s}{m\sigma_n^2}\right)^{-m} M_{I_{\mathrm{agg}}}\left(-\frac{j\eta}{\sigma_n^2}\mathrm{s}\right) e^{-js\eta}\right\}\frac{\mathrm{ds}}{\mathrm{s}}. \tag{5.27}$$

5.5 Numerical Results

In this section, we present numerical results to characterize the spatial-spectral interference model as a function of network parameters. A circular area of radius $R = 25$m is considered. The reference receiver is located at $\|v_0\| = 10$m and $f_0 = 62$ GHz. Moreover, f_s and f_e are set to 58 GHz and 64 GHz, respectively. We assume the pathloss exponent, α, and the shape factor of Nakagami distribution, m, are set to 2.5 and 5, respectively. Here, the transmitted power of all interfering APs are assumed to be the same and set to 30 dBm. The beamwidth of the mmWave signals, i.e., 2θ, is set to 20 degrees. We assume Gaussian power spectral density (PSD) for interfering APs (it can be any PSD shape) and a raised-cosine (RC) matched filter at the reference receiver side. It is worth mentioning that the proposed model is not limited to these assumptions on specific power spectral densities of the desired and interferers' signals.

In Fig. 5.6 and 5.7 , BER versus SNR is shown for different N and ρ values, respectively.

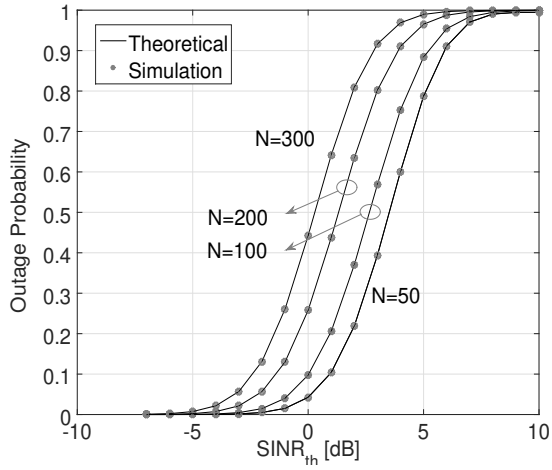

Fig. 5.8: Outage probability vs. SINR_{th} for different N values, ρ=10^{-2}.

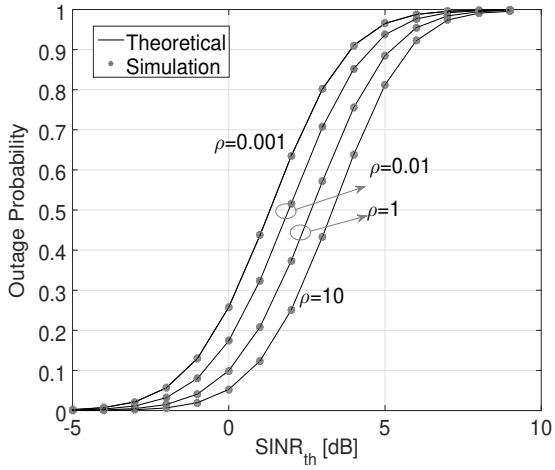

Fig. 5.9: Outage probability vs. SINR_{th} for different ρ values, N=150.

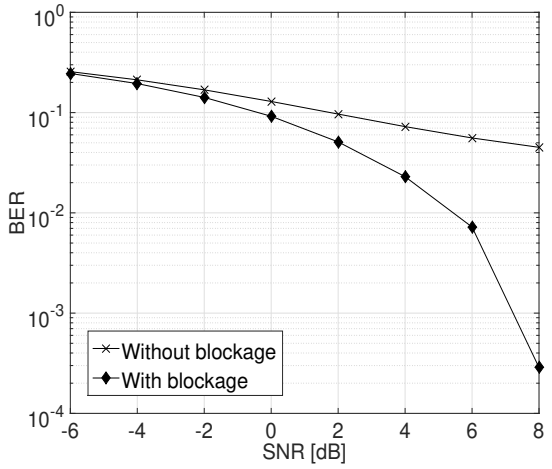

Fig. 5.10: Bit error rate versus SNR for N=200.

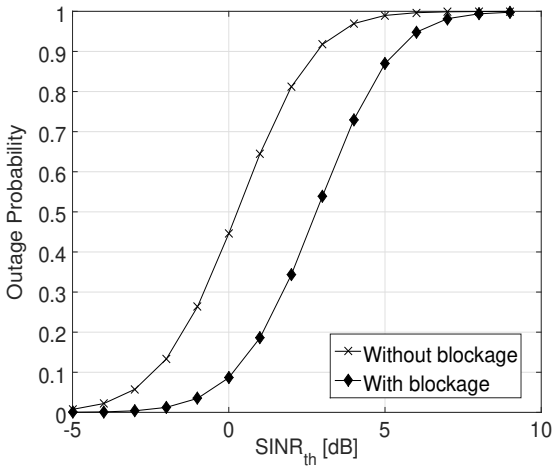

Fig. 5.11: Outage probability versus SINR_{th} for N=300.

As expected, the performance of the system degrades as N increases. The same trend can be observed in Fig. 5.7 where by increasing the density of the blockages, larger number of interfering APs are blocked. Therefore, the accumulated interference signal decreases and results in a better performance. This is an important result that indicates mmWave signals' sensitivity to blockages can be advantageous; in fact, objects and users that serve as obstacles reduce the level of interference.

In Fig. 5.8 and 5.9, the performance of the desired communication link is shown in

terms of outage probability. Here, the performance increases when there is lower number of active interfering APs (i.e., increase in the density of blockage, ρ, and decreasing the total number of interfering APs, N). It is important to note that in all Fig. 5.6, 5.7, 5.8 and 5.9, the simulated average BER and outage probability plots align well with the result from the theoretically derived interference model. Moreover, the performance of the desired communication link with and without consideration of the effect of the blockages sensitivity of the interfering links are illustrated in terms of both metrics, i.e., BER and outage probability, in Fig. 5.10 and 5.11, respectively. As illustrated, unlike traditional interference model, where the impact of the blockages is not considered, directionality of mmWave signals leads to a noticeably different interference profile which is effectively captured by the proposed model. It is worth reiterating, the proposed model considers the uncertainty of the interfering node configuration in both spatial and spectral domains, simultaneously.

5.6 Summary and Conclusion

In this chapter, we propose a spatial-spectral interference model for dense finite-area 5G mmWave network considering the effect of blockages on mmWave signals. The proposed model accounts for randomness in both spectral and spatial network configurations as well as blockage effects. The interference model builds off a new blockage model which captures the average number of obstacles that cause a complete link blockage. Using numerical simulations, we validate the theoretical results and demonstrate how beam directionality and randomness in node configuration impact the accumulated interference at arbitrary locations of a mmWave network.

Chapter 6

Network Regime: Noise-limited or Interference-limited?

With the unique propagation characteristics at mmWave frequencies, one of the fundamental questions to address is whether mmWave networks are noise or interference-limited. The regime in which the network operates significantly impacts the MAC layer design, resource allocation procedure and also interference management techniques. In this chapter, we first derive the statistical characteristic of the cumulative interference in finite-sized mmWave networks considering configuration randomness across spatial and spectral domains while including the effect of blockages. Subsequently, using the derived interference model we set up a likelihood ratio test (LRT) (that is dependent on various network parameters) in order to detect the regime of the network from an arbitrarily located user standpoint. Unlike traditional networks, in mmWave networks, different likelihood of experiencing an interference-limited regime can be observed at different locations.

6.1 Introduction

Highly narrow beams, large available bandwidth and high signal attenuation in mmWave spectrum may lead us to the conclusion that mmWave network performance is limited only

by thermal noise (noise-limited regime). However, depending on the density of APs, density of the obstacles, transmission probability, and operating beamwidth, mmWave network performance may degrade due to interference (interference-limited regime). Unlike traditional wireless networks, mmWave networks may transit from a noise-limited regime to an interference-limited regime or exhibit intermediate behavior in which both regimes can be observed[77]. The regime in which the network is operating highly affects the MAC layer design and resource allocation strategies[78–82]. Moreover, determining the network regime is critical in terms of identifying the most appropriate interference coordination technique that is effective in an interference-limited regime. However, when the network is in a noise-limited regime, we may not need any interference management mechanism or only a simple one may suffice. Therefore, one of the fundamental questions of interest in mmWave dense networks is whether the performance is limited by the interference or just by thermal noise.

There have been a few prior efforts focused on determining network regimes.[83;84] have proposed conditions under which the network is noise or interference-limited. However, the density of the interfering APs are assumed to be fixed which may not be suitable for 5G mmWave networks that may exhibit uncertain spatial configurations due to factors like unplanned user-installed APs[85] and sensitivity to obstacles. In[77], the network regime is determined, modeling the transmitter location as a PPP. However, mmWave specifications such as severe pathloss and beam sensitivity to small-sized obstacles are not taken into consideration. The fact that interference power can change due to the presence of obstacles[9] limits the applicability of[77]. In[80], the transition probability from a noise-limited to an interference-limited regime is calculated in a PPP mmWave network with random blockages. However, considering the spatial locations of the interfering APs as a PPP is not an appropriate choice for modeling finite-sized networks with fixed number of APs where performance becomes location dependent, as shown in[59]. Moreover, the blockage model used in[80] is based on the unrealistic assumption of having a complete link outage with only one obstacle. However, in many practical mmWave applications such as indoor mmWave environments, outdoor mmWave small cells where coverage range is limited or even cases where terminals are equipped with larger number of antennas with wider beamwidths, more

than one obstacle is needed to impact the power level, causing link blockage[86].

6.1.1 Contributions

In this chapter, we take a systematic approach to determine the network regime in mmWave networks. In order to overcome the limitation of prior efforts, we consider a more realistic and appropriate network and blockage models upon which the regime identification is formulated as a hypothesis testing problem. Specifically, we detect whether an arbitrarily located user experiences a noise or interference-limited regime based on the received signal power distribution in the presence of arbitrary-sized blockages. We calculate the distributions of the signal-plus-noise and signal-plus-interference powers which serve as the null and alternate hypotheses, respectively. In order to calculate the interference power, a 2D BPP[10] is assumed to account for the randomness of interfering APs configuration in both spatial and spectral domains in a finite area[1]. In fact, we consider a grid structure of space-frequency locations where interfering APs are placed randomly based on a BPP. We also account for beam directionality by including the effect of presence of arbitrary-sized blockages in the environment using a more realistic blockage model. It is notable that, unlike[80] and other works on blockage modeling[49;63;64;66;70], in this blockage model the net effect of partial blockage caused by each individual obstacle is calculated. Since, more than only one obstacle may cause complete link blockage. Moreover, due to the inherent complexity in evaluating the exact distribution, an approximation of the distribution under the alternate hypothesis (signal-plus-interference power) is calculated using the maximum entropy (ME) technique [2]. Subsequently, using the standard likelihood ratio test (LRT) based on a Neyman-Pearson (NP) framework, we determine the regime of the network. It is important to note that determining the regime of the network is highly impacted by the interference model that appropriately reflects the network specifications. Therefore, the purpose of this chapter is to

[1]BPP is an appropriate choice in order to model the node locations in finite-sized networks with a given number of nodes[48].

[2]Based on the principle of ME[87], ME distribution is the least informative distribution subject to specified properties or measures. Intuitively speaking, it has the minimum amount of prior information built into the distribution.

leverage the detailed statistical interference model and its relation to various key deployment parameters including access point density, blockage density, transmit power, bandwidth and antenna pattern to provide an accurate assessment of the regime of the mmWave networks. It is also shown that the likelihood of experiencing an interference-limited regime depends on the interferer and blockage densities and varies at different spatial locations.

6.2 System Model

We consider a circular area of radius R in 2D plane ($\mathbb{R}^2$) centered at the origin, with N number of interfering APs operating in frequency band $[f_s, f_e]$. We also assume that a reference receiver, located at an arbitrary location $v_0 \in B(O;R) = \left\{ x \in \mathbb{R}^2 \middle| \ \|x\|_2 < R \right\}$ with arbitrary frequency $f_0 \in [f_s, f_e]$, is communicating with a reference transmitter over an intended communication link. This assumption gives the freedom of evaluating the network regime for users at different locations enabling more efficient resource management (e.g., interference coordination/cancellation only for those users whose performances are limited by interference). Interfering APs are distributed based on BPP in the space-frequency domain with success probability p. In other words, we consider a grid structure where the total N interferers are randomly located at space-frequency locations based on a BPP[3]. The overall received interference signal is the sum of the received signal from each interferer at a random space-frequency location. We also assume a random number of arbitrary-sized blockages in the environment distributed based on a PPP [49;64;66;70] with parameter ρ. Due to the presence of the arbitrary blockages in the environment, the transmitted signal of interfering APs may be blocked and not all of the interfering APs contribute to the total received interference signal. Therefore, we are primarily concerned with the interferers that are in the LoS of the reference receiver.

In order to calculate the distribution of the number of active (non-blocked) interfering APs, we consider the blockage model presented in our prior work [10]. In [10], the blockage effect is modeled by considering the net effect of partial blockage that each individual obstacle

[3]Reference transmitter-receiver pair is not a part of the point process.

causes by intersecting the interferers' beam. In this model, obstacles are assumed to be modeled as circles with uniformly distributed radius d in $[d_s, d_e]$. Assuming a radiation cone for the $i^{\text{th}} \in \{1, 2, ..., N\}$ interfering AP (where the edges are determined by the beamwidth of the signal, 2θ) we show that the average probability of each interfering AP being blocked corresponds to

$$p_{\text{b}} = \frac{1}{\frac{\mathbb{E}[d]}{2\tan(\theta)}} p_{\text{b1}} + \frac{1}{\mathbb{E}\left[\ell\right] - \frac{\mathbb{E}[d]}{2\tan(\theta)}} p_{\text{b2}}. \tag{6.1}$$

Here, p_{b1} and p_{b2} are obtained using

$$p_{\text{b1}} = 1 - \frac{\sqrt{\frac{\pi\tan(\theta)}{\rho}}}{(d_e - d_s)} \left[\text{erf}(d_e \sqrt{\frac{\rho}{4\tan(\theta)}}) - \text{erf}(d_s \sqrt{\frac{\rho}{4\tan(\theta)}}) \right], \tag{6.2}$$

and

$$p_{\text{b2}} = \frac{(1+\Delta)^{\left\lceil \frac{\Delta}{e^{\rho\mathbb{E}[S]}-1} \right\rceil} e^{-(1+\Delta)}}{\left\lceil \frac{\Delta}{e^{\rho\mathbb{E}[S]}-1} \right\rceil !}, \tag{6.3}$$

where $\Delta = 2\rho\mathbb{E}\left[\ell\right]\tan\left(\theta\right)$. Here, $\mathbb{E}[\ell]$ and $\mathbb{E}[S]$ denote the average distance from the interfering APs to the reference receiver and the average partial blockage caused by individual interfering APs, respectively. Given the BPP assumption of interfering nodes, the distribution of ℓ corresponds to

$$f_L\left(\ell\right) = \begin{cases} \frac{2\ell}{R^2} & 0 < \ell \leq R - \|v_0\| \\ \frac{2\ell\cos^{-1}\left(\frac{\|v_0\|^2 - R^2 + \ell^2}{2\ell\|v_0\|}\right)}{\pi R^2} & R - \|v_0\| < \ell \leq R + \|v_0\|. \end{cases} \tag{6.4}$$

In addition, the average partial blockage can be expressed as

$$\begin{aligned}\mathbb{E}\left[S\right] &= \mathbb{E}\left[\frac{2d\ell}{r}\left|d,r,\ell\right.\right] \\ &= \int_{d_s}^{d_e}\int_{\frac{d}{2\tan(\theta)}}^{R+\|v_0\|}\int_{\frac{d}{2\tan(\theta)}}^{\ell}\frac{2d\ell}{r}f_D\left(d\right)f\left(r,\ell\right)\mathrm{d}d\,\mathrm{d}r\,\mathrm{d}\ell. \end{aligned} \tag{6.5}$$

Detailed derivation of the blockage model is provided in our prior work [10].

Given the blockage probability in (6.1), the distribution of the total number of non-blocked interfering APs is calculated using the following lemma:

Lemma 6. *The total number of non-blocked interfering APs, denoted as K, is a Binomial random variable with success probability $p\left(1-p_{\mathrm{b}}\right)$.*

Proof. Let $K = K_1 + K_2 + ... + K_N$, where K_i is a Bernoulli random variable and equals 1, if the i^{th} interfering AP is not blocked, and 0, otherwise. Therefore, the PGF of K is given by

$$G_K = (1-p_{\mathrm{b}})\mathrm{z} + p_{\mathrm{b}}. \tag{6.6}$$

Subsequently, we have

$$\begin{aligned} G_K\left(\mathrm{z}\right) &= \mathbb{E}\left[\mathrm{z}^{\sum_{i=1}^{N}K_i}\right] = \sum_{k\geq 0}\left(\mathbb{E}\left[\mathrm{z}^K\right]\right)^k p\left(N=k\right) \\ &= G_N\left(G_{K_i}(\mathrm{z})\right) = \left[(1-p)+p\left((1-p_{\mathrm{b}})\mathrm{z}+p_{\mathrm{b}}\right)\right]^N \\ &= \left[1-p\left(1-p_{\mathrm{b}}\right)+p\left(1-p_{\mathrm{b}}\right)\mathrm{z}\right]^N, \end{aligned} \tag{6.7}$$

which is the PGF of a Binomial random variable with success probability $p\left(1-p_{\mathrm{b}}\right)$. ■

Now, having the distribution of the number of active interferers, in lemma 6, we set up a hypothesis test in order to determine the regime of the network.

6.3 Regime Classification

In this section, we formulate a binary hypothesis test where regime detection decision is based on the received power at an arbitrary located receiver. This hypothesis test is formally defined as:

$$\begin{aligned} H_0: &\quad Y = \varphi + \mathcal{N} \qquad \text{(Noise-limited regime)} \\ H_1: &\quad Y = \varphi + I \qquad \text{(Interference-limited regime)}, \end{aligned} \tag{6.8}$$

where φ, I and $\mathcal{N}$ denote the average received power of the desired signal, aggregated interference and noise powers, respectively. We assume that the signal power is known and noise is characterized by a Gaussian random variable with mean 0 and variance ${\sigma_n}^2$. Here, under H_0 hypothesis, the reference receiver experiences a noise-limited environment. This case may happen when most of the interfering APs are blocked by the blockages in the environment and the received interference power is low enough that the thermal noise is dominant. Alternately, under hypothesis H_1, the performance is limited by the received interference power. The distributions of the received power under both hypotheses need to be identified in order to derive the test.

6.3.1 Distribution under H_0

In this subsection, given the average received power of the desired signal, φ, we calculate the PDF of the received power under the null hypothesis.

Lemma 7. *The statistical distribution of the received power under H_0 is*

$$H_0: \quad Y \sim \frac{\mathrm{e}^{-\frac{y-\varphi}{2\sigma^2}}}{2\sigma^2 \Gamma\left(\frac{1}{2}\right)\sqrt{\frac{y-\varphi}{2\sigma^2}}} \tag{6.9}$$

Proof. Since noise is assumed to be Gaussian with mean 0 and variance ${\sigma_n}^2$, the distribution of the noise power is $\mathcal{N} \sim {\sigma_n}^2 \chi_1^2$, where χ_1^2 denotes a chi-squared distribution with 1 degree

of freedom. Consequently, the CDF of the power is given by

$$F_Y\left(Y \leq y\right) = F_Y\left(\mathcal{N} \leq y-\varphi\right) = \frac{1}{\Gamma\left(\frac{1}{2}\right)}\gamma\left(\frac{1}{2}, \frac{y-\varphi}{2\sigma^2}\right). \tag{6.10}$$

Then, by taking derivative of the CDF, the PDF of the power under the null hypothesis is determined as

$$\begin{aligned} f_Y(y)|\, H_0 &= \frac{\mathrm{d}}{\mathrm{d}y}\left\{\frac{1}{\Gamma\left(\frac{1}{2}\right)}\gamma\left(\frac{1}{2}, \frac{y-\varphi}{2\sigma^2}\right)\right\} \\ &= \frac{\mathrm{d}}{\mathrm{d}y}\left\{\frac{1}{\Gamma\left(\frac{1}{2}\right)}\int_0^{\frac{y-\varphi}{2\sigma^2}} t^{\frac{1}{2}-1}\mathrm{e}^{-t}\mathrm{d}t\right\} \\ &= \frac{\mathrm{e}^{-\frac{y-\varphi}{2\sigma^2}}}{2\sigma^2\Gamma\left(\frac{1}{2}\right)\sqrt{\frac{y-\varphi}{2\sigma^2}}}. \end{aligned} \tag{6.11}$$

■

6.3.2 Distribution under H_1

In this subsection, we calculate the distribution of the received power in the interference-limited regime where the power of the noise is negligible. Therefore, the power received by an arbitrarily-located reference receiver is

$$Y = \varphi + \sum_{i=1}^{K} \mathcal{P}_{I_i}, \tag{6.12}$$

where $\mathcal{P}_{I_i}$ is the effective received interference power from the i^{th} interfering AP at the output of the matched filter which corresponds to[47],

$$\mathcal{P}_{I_i} = q_i h_i \|\ell_i\|^{-\alpha} \Upsilon\left(\omega_i\right). \tag{6.13}$$

Here, h_i and $\|.\|^{-\alpha}$ model the Nakagami-m small scale fading and pathloss effects, respectively. $\ell_i = v_0 - v_i$ and $\omega_i = f_i - f_0$ denote the spatial and spectral distance between the i^{th} interfering AP and the reference receiver, respectively. q_i is the transmitted power of the i^{th} interfering AP. Moreover, $\Upsilon(\omega_i)$ is defined as

$$\Upsilon(\omega_i) = \int_{f_0-\frac{W}{2}}^{f_0+\frac{W}{2}} \Phi(f - f_i) \left|H(f - f_0)\right|^2 \mathrm{d}f, \tag{6.14}$$

where $H(f - f_0)$ is the transfer function of the matched filter at the reference receiver with arbitrary frequency f_0, and $\Phi(f - f_i)$ is the power spectral density of the baseband equivalent of the interferers signals. Considering (6.13), as $\|\ell_i\|^{-\alpha}$ captures the impact of spatial distances (and thereby random spatial configuration), $\Upsilon(\omega_i)$ accounts for the effect of frequency separation (and thereby random spectral configuration) in the interference power. The statistical distribution of the received signal power in the alternate hypothesis H_1, in terms of MGF, is obtained using the following theorem:

Theorem 3. *The MGF of Y, under alternate hypothesis H_1, is given by*

$$M_Y(\mathrm{s}) = \mathrm{e}^{\varphi \mathrm{s}} \Big[1 - p(1 - p_{\mathrm{b}}) + p(1 - p_{\mathrm{b}}) M_{\mathcal{P}_{I_i}}(\mathrm{s})\Big]^N, \tag{6.15}$$

where,

$$M_{\mathcal{P}_{I_i}}(\mathrm{s}) = \sum_{n=0}^{\infty} \frac{(q\,\mathrm{s})^n}{n!} \frac{m^{-n}\Gamma(n+m)}{\Gamma(m)} \frac{2\gamma_n(f_s, f_e)\,\kappa_n(R, v_0)}{R^2(f_e - f_s)}. \tag{6.16}$$

Here, $M_{\mathcal{P}_{I_i}}(\mathrm{s})$ is the MGF of the i^{th} interferer's power and

$$\gamma_n(f_s, f_e) = \int_0^{\min(|\omega_e|,|\omega_s|)} \Upsilon(\omega)^n \mathrm{d}\omega + \int_0^{\max(|\omega_e|,|\omega_s|)} \Upsilon(\omega)^n \mathrm{d}\omega, \tag{6.17}$$

and

$$\kappa_n\left(R, v_0\right) = \int_0^{R-\|v_0\|} \ell^{-n\alpha+1}\,\mathrm{d}\ell \;+ \int_{R-\|v_0\|}^{R+\|v_0\|} \frac{\ell^{-n\alpha+1}}{\pi}\cos^{-1}\left(\frac{\|v_0\|^2 - R^2 + \ell^2}{2\ell\,\|v_0\|}\right)\mathrm{d}\ell. \tag{6.18}$$

Proof. In order to calculate the MGF of the received signal power under alternate hypothesis, we have

$$\begin{aligned} M_Y(\mathrm{s}) &= \mathbb{E}\left[\mathrm{e}^{\mathrm{s}\left(\varphi+\sum_{i=1}^{K}\mathcal{P}_{I_i}\right)}\right] = \mathbb{E}\left[\mathrm{e}^{\mathrm{s}\varphi+\mathrm{s}\sum_{i=1}^{K}\mathcal{P}_{I_i}}\right] \\ &= \mathrm{e}^{\varphi\mathrm{s}}\mathbb{E}\left[\mathrm{e}^{\mathrm{s}\sum_{i=1}^{K}\mathcal{P}_{I_i}}\right] = \mathrm{e}^{\varphi\mathrm{s}}\sum_{k\geq 0}\left(\mathbb{E}\left[\mathrm{e}^{\mathrm{s}\mathcal{P}_{I_i}}\right]\right)^k p\left(K=k\right) \\ &= \mathrm{e}^{\varphi\mathrm{s}} G_K\left(M_{\mathcal{P}_{I_i}}(\mathrm{s})\right) \\ &= \mathrm{e}^{\varphi\mathrm{s}}\left[1 - p\left(1-p_{\mathrm{b}}\right) + p\left(1-p_{\mathrm{b}}\right) M_{\mathcal{P}_{I_i}}(\mathrm{s})\right]^N. \end{aligned} \tag{6.19}$$

where $M_{\mathcal{P}_{I_i}}(\mathrm{s})$ is the MGF of the i^{th} interferer's power. The MGF of the power of the individual interfere is calculated as

$$\begin{aligned} M_{\mathcal{P}_{I_i}}(\mathrm{s}) &= \mathbb{E}\left[\mathrm{e}^{\mathrm{s}\,q\,h\,\ell^{-\alpha}\Upsilon(\omega)}\right] \\ &= \int_0^{\infty}\int_0^{R+\|v_0\|\max(|\omega_e|,|\omega_s|)}\int_0^{} \mathrm{e}^{\mathrm{s}\,q\,h\,\ell^{-\alpha}\Upsilon(\omega)} f_\Omega(\omega)\, f_L(\ell)\, f(h)\,\mathrm{d}\omega\,\mathrm{d}\ell\,\mathrm{d}h. \end{aligned} \tag{6.20}$$

Given the BPP assumption of the location of interferer in space-frequency domain, the distributions of spectral distance is given by[10]

$$f_\Omega(\omega) = \begin{cases} \frac{2}{f_e - f_s} & 0 < \omega \leq \min\left(|\omega_e|, |\omega_s|\right) \\ \frac{1}{f_e - f_s} & \min\left(|\omega_e|, |\omega_s|\right) < \omega \leq \max\left(|\omega_s|, |\omega_s|\right), \end{cases} \tag{6.21}$$

where $\omega_e = f_e - f_0$ and $\omega_s = f_s - f_0$. Having the spatial and spectral distance distributions given in (6.4) and (6.21), Nakagami-m assumption of the small scale fading, i.e., h and using

the polynomial expansion of the exponential function, the integral in (6.19) is derived as in (6.16). Subsequently, by substituting (6.16) in (6.19), the result in (6.15) is obtained. ■

Calculating the inverse Laplace transform of the MGF in (6.15) to find the distribution is a tedious task and computationally complex. A more straightforward method might be to approximate the given distribution with known distributions. Therefore, in order to make the problem tractable, we use the ME method. Specifically, the ME technique[87] is used to approximate the distribution of the received power under the alternate hypothesis with a tractable and simpler form. Basically, ME estimate is an estimate with maximal information entropy (least-informative) subject to the given moments. All the information about the interference power distribution is provided by the MGF in (6.15). Therefore, we can use as many moments as needed (as the prior information or constraints) to make the estimation more precise. However, considering higher number of moments leads to the calculation of sets of non-linear equations which itself adds complexity to the problem. Here, for simplicity, we use the first moment of the received power (mean received power) as the constraint while maximizing the entropy of the distribution. We believe that this is a reasonable and logical starting point as the difference in mean power of interference and noise should offer the greatest discriminatory effect between H_0 and H_1. Later, Section 6.4, we show the performance of the resulting test using receiver operating characteristic (ROC) curve and it can been considered as the lower bound on the performance of the ideal test with the true distribution under H_1. In fact, the test performance can be improved by including the higher order moments as part of the ME estimation constraints at the cost of increasing model complexity. This will be explored as part of our future work.

Lemma 8. *The approximated PDF of the received signal power under alternate hypothesis H_1 is given by*

$$H_1 : \; Y \sim \lambda \mathrm{e}^{-\lambda(y-\varphi)}, \tag{6.22}$$

where λ is derived by solving $(\lambda\varphi + 1)\,\mathrm{e}^{-\lambda\varphi} - \mathbb{E}[y]\,\lambda^2 = 0$ and $\mathbb{E}[y]$ is the first moment of

the received signal power under the alternate hypothesis.

Proof. Considering the first moment as the constraint in the ME method, the PDF of the received signal power can be calculated by solving

$$\begin{aligned} \max \quad & -f_Y(y)\ln\left(f_Y(y)\right) \\ \text{s.t.} \quad & \int_{\varphi}^{\infty} y\, f_Y(y) = \mathbb{E}[y]. \end{aligned} \tag{6.23}$$

Here, $\mathbb{E}[y] = \frac{\partial}{\partial \mathrm{s}} \mathrm{M}_Y(\mathrm{s})\big|_{\mathrm{s}=0}$. The ME probability is found using the dual Lagrangian method [87],

$$\frac{\partial}{\partial f_Y(y)} L\left(f_Y(y), \lambda\right) = 0, \tag{6.24}$$

where,

$$L\left(f_Y(y), \lambda\right) = -f_Y(y)\ln\left(f_Y(y)\right) + \lambda\left(\int_{\varphi}^{\infty} y\, f_Y(y) - \mathbb{E}[y]\right), \tag{6.25}$$

is the Lagrangian of the optimization problem (6.23). By solving (6.24) using the KKT conditions, the distribution $f_Y(y)$ is derived as in (6.22), where λ is calculated by solving $(\lambda\varphi + 1)\,\mathrm{e}^{-\lambda\varphi} - \mathbb{E}[y]\,\lambda^2 = 0$. ■

6.3.3 Likelihood Ratio Test

With the knowledge of distribution of Y under both H_0 and H_1, we can write down the likelihood ratio as

$$\begin{aligned} \mathrm{LRT}(y) &= \frac{f_Y(y)|\,H_1}{f_Y(y)|\,H_0} = \frac{\lambda \mathrm{e}^{-\lambda(y-\varphi)}}{\frac{\mathrm{e}^{-\frac{y-\varphi}{2\sigma^2}}}{2\sigma^2\Gamma\left(\frac{1}{2}\right)\sqrt{\frac{y-\varphi}{2\sigma^2}}}} \\ &= 2\Gamma\left(\frac{1}{2}\right)\sigma^2\lambda \mathrm{e}^{\left(-\lambda+\frac{1}{2\sigma^2}\right)y+\lambda\varphi-\frac{\varphi}{2\sigma^2}}\sqrt{\frac{y-\varphi}{2\sigma^2}}. \end{aligned} \tag{6.26}$$

Considering the well-known *Neyman-Pearson* (NP) criterion, the decision rule, i.e., δ_{NP} is

$$\delta_{\text{NP}} = \begin{cases} 1 & \text{LRT}\,(y) \geq \eta \Rightarrow \;\; y \geq \text{LRT}^{-1}(\eta) = \eta' \\ 0 & \text{LRT}\,(y) < \eta \Rightarrow \;\; y < \text{LRT}^{-1}(\eta) = \eta'. \end{cases} \tag{6.27}$$

It is notable that, the NP framework is chosen in order to prevent the imposition of a specific cost to the decision made and priors on the hypotheses. In order to calculate the threshold η', we have

$$\begin{aligned} P_F\left(\delta_{NP}\right) = \beta_{\text{th}} \Rightarrow \int_{\eta'}^{\infty} \frac{\mathrm{e}^{-\frac{y-\varphi}{2\sigma^2}}}{2\sigma^2\Gamma\left(\frac{1}{2}\right)\sqrt{\frac{y-\varphi}{2\sigma^2}}}\,\mathrm{d}y = \beta_{\text{th}} \\ \Rightarrow \eta' = 2\sigma^2\big(\text{erf}^{-1}\left(1-\beta_{\text{th}}\right)\big)^2 + \varphi, \end{aligned} \tag{6.28}$$

where β_{th} denotes the *significance level* of the test. Having the threshold η' in (6.28), the detection probability is obtained as

$$P_D\left(\delta_{NP}\right) = \int_{\eta'}^{\infty} \lambda \mathrm{e}^{-\lambda(y-\varphi)}\,\mathrm{d}y = e^{-\lambda(\eta'-\varphi)}. \tag{6.29}$$

6.4 Numerical Results

In this section, we present numerical results to determine the performance of the test given the various key deployment parameters. A circular area of radius $R = 10$ m is considered. The reference receiver is located at spectral location $f_0 = 62$ GHz. Moreover, f_s and f_e are set to 58 GHz and 64 GHz, respectively. The pathloss exponent, α, and the shape factor of Nakagami distribution, m, are set to 2.5 and 3, respectively. Here, the transmitted power of all interfering APs are assumed to be the same and set to 27 dBm. The beamwidth of the mmWave signals, 2θ, is set to 20 degrees. We assume Gaussian PSD for interfering APs and an RC-0 for the matched filter at the reference receiver side. It is worth mentioning that the proposed model and the hypothesis test are not limited to specific power spectral densities

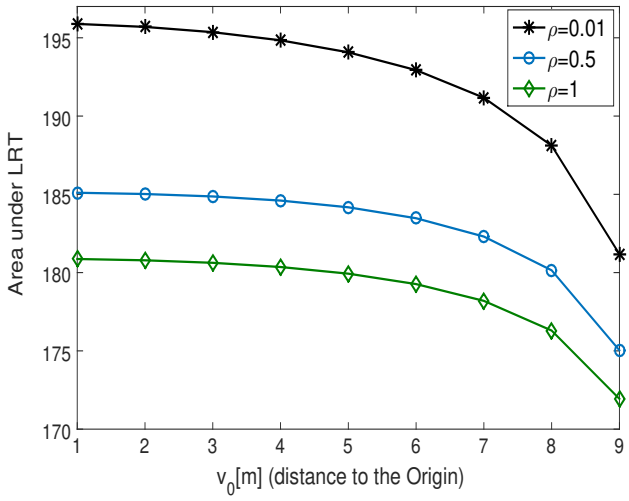

Fig. 6.1: LRT versus reference receiver location for different ρ, N=200.

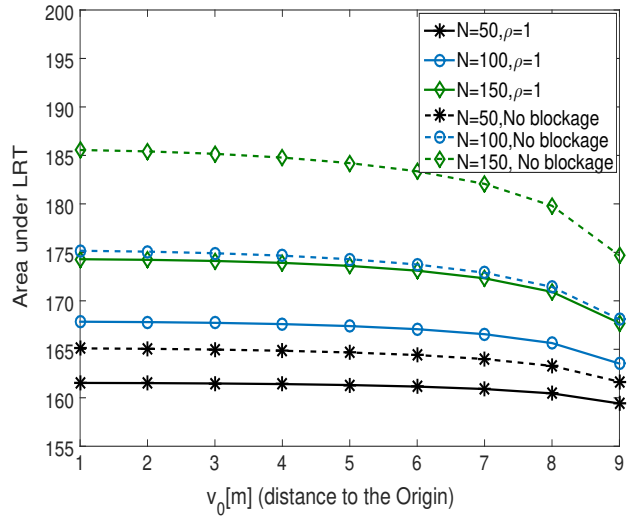

Fig. 6.2: LRT versus reference receiver location for different N values.

or pulse shape choices of the desired and interferers' signals.

In Fig. 6.1, the area under the LRT curve is shown as a function of distance from the origin (for fixed number of interfering APs). Since, (6.9) is independent of the reference receiver's location; therefore, higher values in Fig. 6.1 represent the higher values in (6.22) which means the higher likelihood of being in the interference-limited regime. When the density of blockages increase, more interfering APs are blocked. Therefore, there is less number of

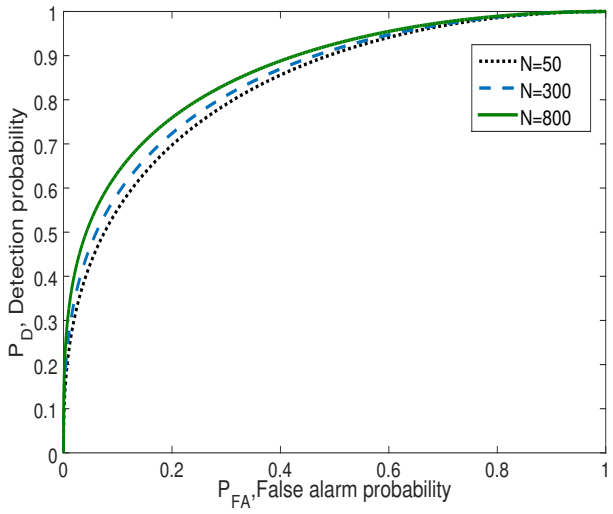

Fig. 6.3: ROC curve for different N values, ρ=1.

interfering APs that introduce interference to the reference receiver and the probability of being in the interference regime decreases. In addition, it can be seen that the probability of experiencing the interference-limited regime decreases as the reference receiver moves from the center of the area to its periphery. The same trend can be observed as the number of interfering APs changes (with the fixed blockage density), as shown in Fig. 6.2. The scenarios in which the effect of the presence of blockages is not considered is also provided in Fig. 6.2. Here, we can see how ignoring the blockage effect results in an overestimation in the likelihood of observing an interference-limited regime.

In Fig. 6.3, ROC curve is shown for different number of interfering APs and blockage density ρ set to 1. Here, the detection probability represents the probability of detecting an interference-limited regime for a specific set of deployment parameters.

As we can see in the results, the derived distributions are functions of various key deployment parameters including access point density, blockage density, transmit power, bandwidth and antenna beamwidth. Using the binary hypothesis test in (6.27) we can decide, given a specific set of deployment parameters for the network, which regime is more probable for receivers located at different locations in the finite-sized network.

6.5 Summary and Conclusion

In this chapter, we set up a binary hypothesis test based on the received signal power in order to detect the regime of the mmWave networks in the presence of the blockages. We derive the distributions of the signal-plus-noise and signal-plus-interference powers, i.e., the power distributions in the case of null and alternate hypotheses of the binary test, respectively. Due to the complexity of the derived distribution under alternate hypothesis and in order to make the problem tractable, we leverage the method of maximum entropy to approximate the distribution. Using the approximated distribution and deploying the Neyman-Pearson criterion, we calculate the probability of experiencing an interference-limited regime. It is worth reiterating that the detailed statistical interference model and its relation to various key deployment parameters including access point density, blockage density, transmit power, bandwidth and antenna pattern helps provide an accurate assessment of the network regimes at different locations in the network.

Chapter 7

Cross-layer Interference Model

In this chapter, we provide an interference model to evaluate the interference power received at the physical layer of the receiving terminal, considering antenna directivity, effect of obstacles and MAC layer constraints that control the number of terminals transmitting simultaneously. We first develop a blockage model and then derive the Laplace transform of the interference power received at a typical receiving node. Subsequently, using the derived Laplace transform, we evaluate the network error performance. Analytical results are validated via Monte-Carlo simulations.

7.1 Introduction

It has been well-established that using directional antennas poses multiple challenges in different aspects of 5G communication. In fact, mmWave signals are highly sensitive to blockages. The sensitivity to obstacles in turn impacts the interference behavior [9;10]. In addition, it is clear that the interference phenomenon happens at the physical layer of the receiving node. However, the interference signal and its undesired effects are impacted by features of the interfering nodes at different network layers. Network operation and traffic behavior that describe the transmitter activity and the interrelation among terminals are controlled by the MAC protocols. Therefore, an efficient and comprehensive interference

model for mmWave applications must capture both mmWave physical layer specifications and MAC layers constraints. Such cross-layer models can guide the design and development of interference coordination and management schemes[4;88].

There have been a couple of candidate MAC layer protocols for 5G mmWave applications. Among them, multisuer MAC protocol that are based on directional transmission have attracted attention[4]. Such protocols effectively increase the network capacity by exploiting the spatial features. In networks with carrier sensing mechanism, the spatial distribution of active (simultaneously transmitting) transmitters is typically modeled as MPP[59]. MPP can be viewed as a thinned version of PPP where it considers an exclusion area (circular area with radius proportional to the sensing threshold of the transmitter) around each node, and all nodes closer than a certain distance are excluded. In fact, in MPP networks, active nodes are separated by a specific range from each other. However, in real scenarios in mmWave networks with directional signals (that can be easily blocked by obstacles), two transmitters can be close to each other and transmit in two different directions without introducing interference to each other. In addition, they may not be interfering with each other due to the presence of obstacles in between. Therefore, considering antenna directionality and blockage effect, not all the nodes in the circular exclusion area should be eliminated from the point process. There have been several prior works on modeling CSMA/CA networks using MPP[89;90] or modified versions of MPP[91–94]. However, none of these prior efforts consider the directionality of the antennas which makes them unsuitable for mmWave applications. Although majority of work on the performance evaluation of D-CSMA/CA networks rely on simulations, authors in[95–98] have conducted an analytical evaluation of networks with directional MAC protocol. However, blockage effect resulting from high directionality of mmWave signals are not taken into account. Moreover, spatial distribution of APs and random orientation of the antennas are not considered in[97;98].

7.1.1 Contributions

In this chapter, we propose a cross-layer interference model that considers both directionality of mmWave signals with random antenna orientation and blockage effect from both physical and MAC layer perspective. Using tools from stochastic geometry, we model the spatial distribution of APs and blockages as Poisson processes. Transmitting nodes are equipped with directional antennas that are directed towards their intended receivers. We also assume that APs employ sensing mechanism-enabled MAC protocol to access the shared channel. Considering random orientation of antennas, presence of blockages and MAC layer protocol, we derive the intensity of APs that actively introduce interference and contribute to the interference power level. However, the Laplace transform of the interference power introduced by this set of APs is not known in closed form and it requires the probability of joint medium access for arbitrary number of APs. The approach that is usually followed[89] is to ignore the correlation accross multiple APs in the probability of joint access and only accounting for the pairwise impact of the APs. Following the same approach, to characterize the set of simultaneously transmitting APs, we approximate the set by an inhomogeneous PPP (IH-PPP) whose intensity depends on the distance to the origin. In addition, we also approximate the distribution of the active APs by a homogeneous PPP (H-PPP). Later, it is shown that the intensity of the IH-PPP is lower bounded by the intensity of the H-PPP. Subsequently, we evaluate the network performance and validate it using Monte-Carlo simulations of the network.

7.2 System Model

As shown in Fig. 7.1, we assume a network of APs, distributed over $\mathbb{R}^2$ plane, based on Poisson point process Φ_{P} with intensity λ. It has also been assumed that all APs are equipped with directional antennas, steered towards their intended receiver, in uniformly random directions. We approximate the radiation pattern of the antenna by a 2D conic

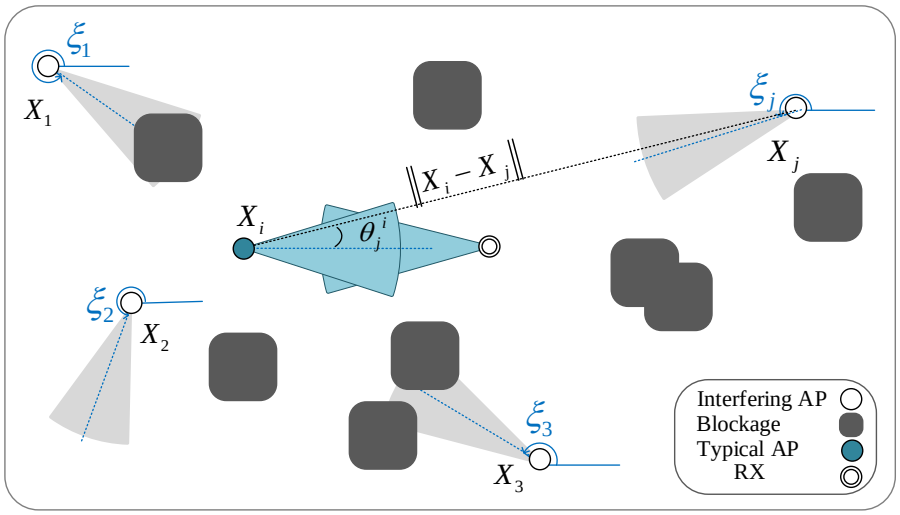

Fig. 7.1: Representation of the system setup in the presence of obstacles (objects such as humans, trees and so on).

pattern [1] $G(\theta, \xi) = \frac{\mathbb{1}(|\theta - \xi| \leq \varphi)}{2\varphi}$, where 2φ is the half-power beamwidth of the antenna arrays and ξ, uniformly distributed in $(-\pi, \pi]$, denotes the boresight of the AP antenna pattern in its local orientation (See Fig. 7.2 for $\xi = 0$). In addition, θ is the azimuthal angle and $-\pi < \theta \leq \pi$. Maintaining a reasonable accuracy, this approximation provides mathematical simplicity and tractability and has been used extensively in the literature[72;99].

7.2.1 Blockage Model

We model the spatial distribution of the blockages as PPP with parameter ρ[49]. Due to the presence of blockages in the environment, not all the surrounding APs are sensed by a given AP. In other words, some of them are considered as blocked APs, as their signal is blocked by the obstacles that lies within their LoS path. To calculate the LoS probability for two arbitrary APs, as mentioned previously, we approximate the radiation pattern of the antennas by a 2D conic pattern, where its edges are determined by the signal beamwidth 2φ (see Fig. 7.3). Considering the APs with average antenna length ℓ, smaller than blockage

[1] Radiation pattern of the directional antennas (ignoring small side-lobes and back-lobes for mathematical tractability) can be modeled as $g(\theta, \phi) = \cos^n(\phi)$; with polar angle $\phi \in [0, \frac{\pi}{2}]$ and azimuthal angle $\theta \in (-\pi, \pi]$ (see Fig. 7.2a), where n is a positive number corresponding to the antenna pattern directivity[71]. Larger n corresponds to a more directional radiation pattern.

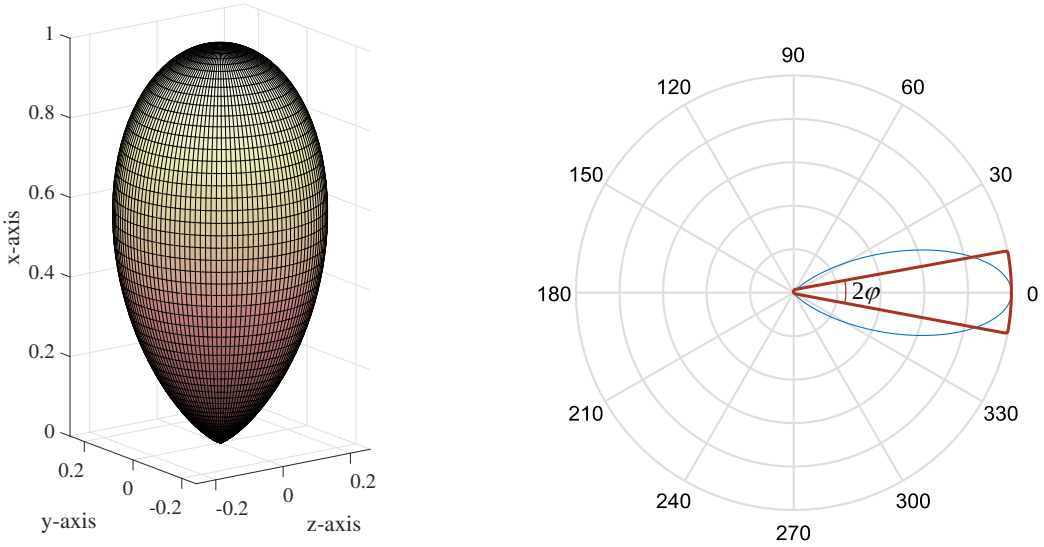

(a) 3D pattern (b) 2D pattern

Fig. 7.2: Antenna radiation pattern, ignoring the side and backlobes, in 3D (7.2a) and representation of the approximated half-power beamwidth in 2D (7.2b).

dimension, we assume there is no LoS path between the two APs when at least one blockage lies in their LoS path. Given the PPP assumption of the location of the blockages, two APs separated with random distance r, have non-blocked LoS path towards each other with probability $\mathtt{P}_{\mathtt{LoS}}(r)$, given by (see Fig. 7.3)

$$\mathtt{P}_{\mathtt{LoS}}(r)=\begin{cases} \mathrm{e}^{-\rho r^2 \tan(\varphi)} & 0 \leq r < \frac{\ell}{2\tan(\varphi)} \\ \mathrm{e}^{-\rho \frac{r\ell}{2}} & r \geq \frac{\ell}{2\tan(\varphi)}. \end{cases} \tag{7.1}$$

Based on the described blockage model, if the distance between the two arbitrary APs is less than a certain value which is a function of the AP antenna size and the beamwidth of its radiation pattern, the LoS probability depends on the beamwidth, as well as the distance separating the APs and the blockage density. However, beyond that distance it depends on the antenna size rather than the radiation beamwidth. We utilize this simple yet fairly reasonable blockage model to make the analysis tractable. More detailed but complicated blockage models can be found [10;100].

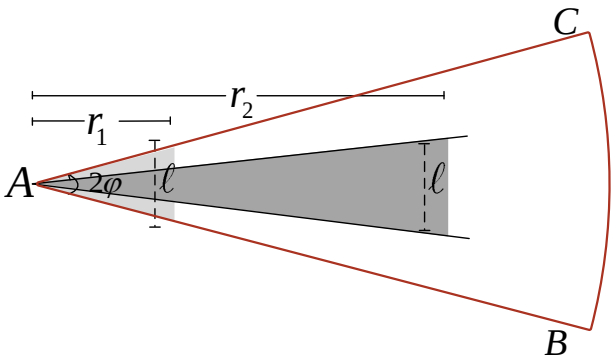

Fig. 7.3: Terminal 1 (resp. terminal 2) with distance r_1 (resp. r_2) to the transmitting AP. terminal 1 (resp. terminal 2) is blocked if at least one blockage intersect the triangle with area ${r_1}^2 \tan(\varphi)$ (resp. $\frac{r_2 \ell}{2}$), respectively. The region ABC represents the conic radiation pattern of the transmitting AP.

7.2.2 MAC Protocol Mechanism

We assume that D-CSMA/CA protocol is employed as the MAC strategy for APs to access the shared medium/channel. Based on CSMA/CA protocol, each AP senses the channel continuously, if the channel is busy (other APs are transmitting) it defers its transmission until the end of the current transmissions and generates a random *back-off* delay. As long as the medium is sensed as idle, the back-off delay timer starts decreasing and when it reaches zero, the AP transmits its packet. The purpose of the back-off timer is to avoid collision among APs. Roughly speaking, this MAC protocol determines which APs are allowed to transmit simultaneously given the fact that they are not sensed by each other. Therefore, not all the APs transmit at the same time and simultaneously transmitting APs have a certain separation between them. In networks with sensing mechanism, the spatial distribution of active transmitters is typically modeled as Matern point process (MPP type I or type II) [59]. MPP is a thinned version of PPP where points are retained in the point process if they are located beyond a specific distance (also known as hard-core distance proportional to the carrier sensing threshold of the transmitters in CSMA/CA networks) away from all other points (type I). In type II, a uniformly distributed random mark (corresponding to the back-off timer in CSMA/CA protocol) is associated with each point, and a point of the parent

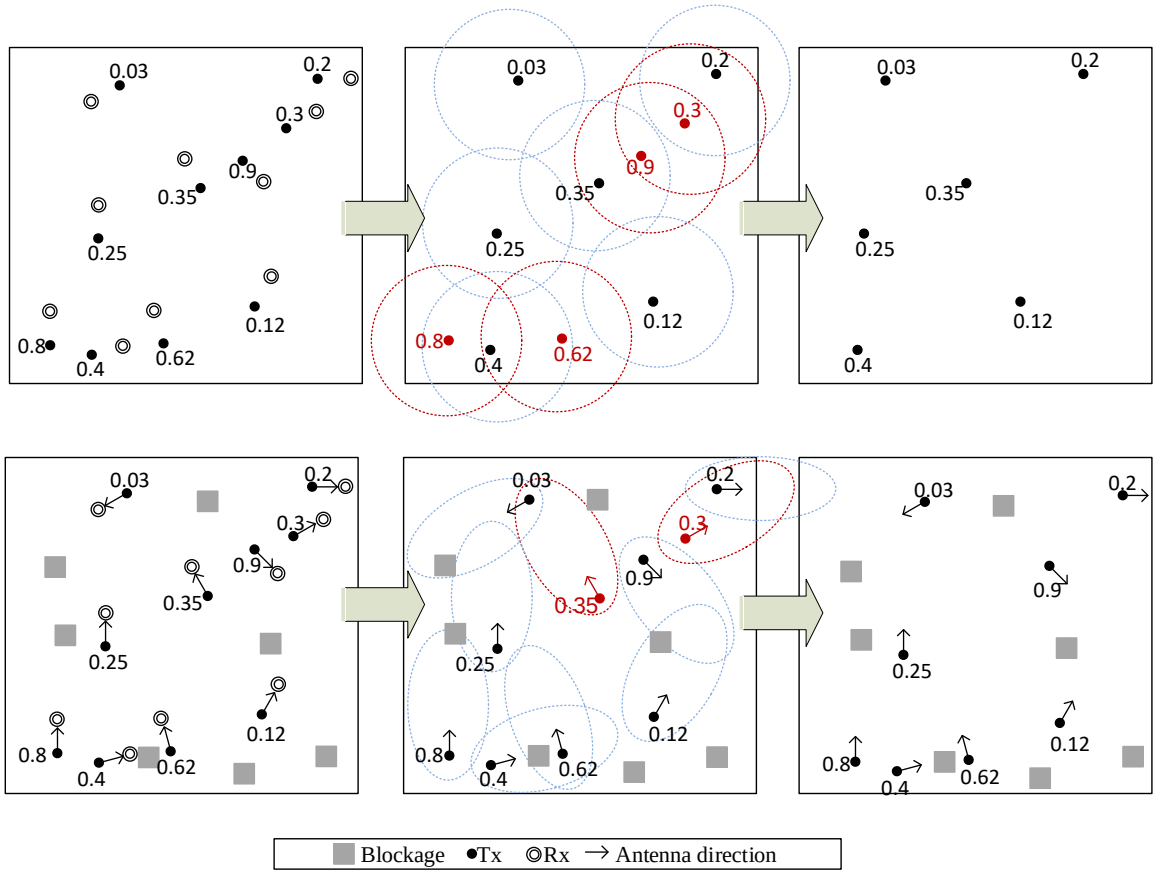

Fig. 7.4: Generating MPP points from the parent PPP without (with) considering antennas directionality and effect of blockage in the upper (lower) panels).

PPP is excluded [2] if there exists another point, with a smaller mark, within its hard-core distance (type II-see Fig. 7.4 upper panels). Those nodes that reside within the hard-core distance of a given node represents the set of APs that are sensed by it and contend for accessing the medium. Therefore, the hard-core region is a demonstration of the contention area of a given AP. We refer to the nodes in the contention area/hard-core region of a given node as its neighbors. In any set of neighbors, only the node with the smallest mark (smallest back-off timer) wins the contention and, in fact, accesses the medium and transmits. It is

[2]When a node is excluded from the primary point process, it means that it stops transmission and will try retransmission at another time slot. This way, the packet collision due to simultaneous transmissions of various terminals can be avoided to some extent. In fact, due to the inevitable phenomena such as transmission delay, collision will nevertheless occur. However, we do not consider such cases to allow the readers to follow the analysis with ease.

notable that due to the effect of random channel fading, the contention area may deviate from the regular circular perimeter of radius equal to the hard-core distance (sensing threshold) centered at each node. Utilizing these types of MPP to model the CSMA/CA networks are based on the underlying assumption of omni-directional transmission. However, in case of mmWave networks with very directional signals, two APs can be close to each other and transmit in two different directions without being sensed by each other. In addition, they may not be heard by one another due to the presence of obstacles in between (See Fig. 7.4 lower panels). Therefore, considering antenna directions and blockage effect, the set of the neighbors of a given AP may change considerably, which in turn affects the set of simultaneously transmitting APs and hence interference power level. In fact, considering the blockages sensitivity and also high directionality of mmWave signals, two different APs, namely AP A and AP B, may not sense each other (the received power level from AP A at AP B is less than the carrier sensing threshold) if either of the following conditions hold:

- The LoS path from AP A to AP B is blocked, due to the presence of obstacles,
- AP A and AP B transmit in different direction and basically have different boresight orientations,
- AP A and AP B have a clear LoS and they have non-zero antenna gains toward each other; however, due to the small channel gain they fall out of each other's sensing range.

Definition 7.2.1 (**Neighbor set**). *In order to formally define the set of the neighbors of a given AP, we define the set* $\tilde{\Phi}_{\mathrm{P}} \equiv \{(X_i, n_i, \mathcal{P}_i)\}$, *where* $X_i \in \Phi_{\mathrm{P}}$. *In addition,* $\{n_i\}$ *is the set of i.i.d marks, uniformly distributed in* $[0, 1]$, *that captures the effect of back-off timer in CSMA/CA protocol. Moreover,* $\{\mathcal{P}_i = (P_i^j, j)\}$ *where* P_i^j *denotes the power of* i^{th} *AP received at* j^{th} *AP. The set of neighbors of an arbitrary* i^{th} *AP located at* X_i *is defined as*

$$\mathcal{N}_{X_i} = \left\{ (X_j, n_j, \mathcal{P}_j) \in \tilde{\Phi}_{\mathrm{P}} : \frac{P_j^i}{\|X_i - X_j\|^{\alpha}} \geq \sigma, j \neq i \right\}. \tag{7.2}$$

Here, σ denotes the carrier sensing threshold. Moreover, $\|X_i - X_j\|^{\alpha}$ captures the path loss effect between the two APs, where $\|\cdot\|$ represents the Euclidean distance and α is the pathloss exponent. In addition,

$$P_j^i = H_j^i G(\theta_j^i, \xi_i)\bar{G}(\theta_j^i + \pi - \xi_j, \xi_j)Z_j^i, \tag{7.3}$$

For the sake of simplicity, we assume all APs transmit with unit power. Here, H_j^i represents the Nakagami-m channel fading gain. Moreover, $G(\cdot, \xi_i)$ and $\bar{G}(\cdot, \xi_j)$ denote the antenna gains of i^{th} and j^{th} APs in their relative directions towards each other. It is worth mentioning that the input angle to the $G(\cdot, \xi_i)$ and $\bar{G}(\cdot, \xi_j)$ is relative to the antenna boresight. The parameters θ_j^i is the orientation of the i^{th} AP with respect to the j^{th} AP. Furthermore, ξ_i and ξ_j denote the boresight of the i^{th} and j^{th} APs antenna in their local orientation (See Fig. 7.1). Given the fact that j^{th} AP can be at any random location in the network with a random direction, we assume that θ_j^i and ξ_j are uniform random variables in $[-\pi, \pi]$. Therefore, assuming the 2D conic radiation pattern,

$$G(\theta_j^i, \xi_i)\bar{G}(\theta_j^i + \pi - \xi_j, \xi_j) = \begin{cases} \frac{1}{4\varphi^2} & \text{with probability } \frac{\varphi^2}{\pi^2} \\ 0 & \text{with probability } 1 - \frac{\varphi^2}{\pi^2} \end{cases} \tag{7.4}$$

Furthermore, Z_j^i is a binary random factor which is 1 with probability P_{LoS} in (7.1), when j^{th} AP has LoS path toward i^{th} AP, and 0 with probability $1 - P_{LoS}$, otherwise.

Now, given the definition of the neighbor set, we can define the set of APs that, based on the D-CSMA/CA protocol are allowed to transmit concurrently (retained in the point process) and basically form the potential interfering APs. The point process of the retained nodes is formally defined as

$$\Phi_{\mathrm{S}} \equiv \{X_i \in \Phi_{\mathrm{P}} : e_i = 1\} \tag{7.5}$$

where e_i represents the medium access indicator of i^{th} AP given by $e_i = \mathbb{1}\left(n_i < n_j \quad \forall X_j \in \mathcal{N}_{X_i}\right)$.

7.3 Cross-layer Interference Analysis

In this section, our goal is to characterize the interference power level by determining its Laplace transform. To this end, we first derive the density of the APs that are authorized to transmit simultaneously, based on the MAC protocol, and contribute to the interference power level. As formally defined in (7.5), Φ_{S} is the point process that describes the set of these simultaneously transmitting APs. The Laplace transform of the interference power introduce by this set of APs is not known in closed form and it requires the probability of joint medium access for arbitrary number of APs. The approach that is usually followed [89] is to ignore the correlated effect of multiple APs in the probability of joint access and only accounting for the pairwise impact of the APs. Following the same path, to characterize the set of simultaneously transmitting APs, we also account for the pairwise effect on a randomly selected AP (referred to as the typical AP). Without loss of generality and given the stationarity property of PPP, we assume the typical AP is located at the origin and hence, denoted as X_0.

Lemma 9. *The expected number of neighbors of the typical AP is obtained as*

$$\bar{\mathcal{N}} = \frac{2\lambda\varphi^2}{\pi} \sum_{k=0}^{m-1} \frac{(4m\sigma\varphi^2)^k}{k!} \int_0^{\infty} \mathtt{P}_{\mathtt{LoS}}(r)\, r^{1+\alpha k} \mathrm{e}^{-4m\sigma\varphi^2 r^{\alpha}} \mathrm{d}r \tag{7.6}$$

Here, $\mathtt{P}_{\mathtt{LoS}}(r)$ is given in (7.1).

Proof. Proof is provided in Appendix B. ■

Ignoring the correlated effect of multiple APs in the the probability of joint access and only account for the pairwise correlation, as discussed earlier at the beginning of this section, leads to the approximation of the law of $\{\Phi_{\mathrm{S}} \backslash X_0 \mid X_0 \in \Phi_{\mathrm{S}}\}$ by an inhomogeneous PPP of intensity $\lambda'(d) = \lambda\vartheta(d)$, where λ is the intensity of the primary PPP and $\vartheta(d)$ is an intermediate function given by

$$\vartheta(d) = \mathbb{P}\{e_y = 1 \,|e_0 = 1\} = \frac{\mathbb{P}\{e_0 = 1, e_y = 1\}}{\mathbb{P}\{e_0 = 1\}}. \tag{7.7}$$

In other words, the intensity of the inhomogeneous PPP is the intensity of the primary PPP thinned with $\vartheta(d)$ which is the probability of retaining a generic AP, located at X_y, given that the typical AP is retained in the point process. Here, d is the distance between them. In the next following lemmas, we derive the probabilities in the numerator and denominator of (7.7), i.e., the *probability of joint access* and *probability of access*, respectively.

Lemma 10 (**Probability of Joint Access**). *The probability of joint access, which is defined as the probability of a generic AP located at an arbitrary location X_y (at distance d from the typical AP) and the typical AP to be granted transmission, is given by*

$$\mathbb{P}\{e_0 = 1, e_y = 1\} = \frac{2\mathcal{A}(d)}{\bar{\mathcal{N}}}\left(\frac{\mathrm{e}^{\omega(d)} - 1}{\omega(d)} - \frac{\mathrm{e}^{\omega(d)-\bar{\mathcal{N}}} - 1}{\omega(d) - \bar{\mathcal{N}}}\right), \tag{7.8}$$

where $\mathcal{A}(d)$, $\omega(d)$ and κ are given as

$$\mathcal{A}(d) = 1 - \frac{\varphi^2 \Gamma(m, 4m\varphi^2\sigma d^{\alpha})}{\pi^2 \Gamma(m)} \mathsf{P}_{\mathsf{LoS}}(d), \tag{7.9}$$

$$\omega(d) = -\kappa + \lambda \frac{\varphi^4}{\pi^4} \sum_{k=0}^{m-1} \sum_{t=0}^{m-1} \frac{(4m\sigma\varphi^2)^{k+t}}{t!k!} \int_{\mathbb{R}^2} \frac{\|x\|^{\alpha k}}{\|x - X_y\|^{-\alpha t}} \mathsf{P}_{\mathsf{LoS}}(\|x\|)\, \mathsf{P}_{\mathsf{LoS}}(\|x - X_y\|) \times \mathrm{e}^{-4m\sigma\varphi^2(\|x\|^{\alpha} + \|x - X_y\|^{\alpha})} \mathrm{d}x, \tag{7.10}$$

and

$$\kappa = \frac{\lambda}{\Gamma(m)} \int_{\mathbb{R}^2} \mathbb{E}_{g_j^y \bar{g}_j^y, z}\left[\Gamma\left(m, m\frac{\sigma\|x - X_y\|^{-\alpha}}{g_j^y \bar{g}_j^y z}\right)\right] \mathrm{d}x, \tag{7.11}$$

Here, κ is the average number of neighbors of the AP located at X_y.

Proof. Proof is provided in Appendix B. ■

Lemma 11 (**Probability of Access**). *The probability of the typical AP to be granted*

transmission is given by

$$\mathbb{P}\{e_0 = 1\} = \frac{\mathrm{e}^{-\bar{\mathcal{N}}} + \bar{\mathcal{N}} - 1}{\bar{\mathcal{N}}^2} + \left(1 - \frac{\varphi^2 \Gamma\left(m, 4m\varphi^2 \sigma d^\alpha\right)}{\pi^2 \Gamma\left(m\right)} \mathcal{P}_{\mathcal{LoS}}\left(d\right)\right) \frac{1 - \left(1 + \bar{\mathcal{N}}\right) \mathrm{e}^{-\bar{\mathcal{N}}}}{\bar{\mathcal{N}}^2}. \tag{7.12}$$

Proof. Proof is given in Appendix B. ■

Lemma 12. *The intensity of the inhomogeneous PPP that describes the simultaneous transmissions of the D-MAC mmWave network with blockage considerations is given by*

$$\lambda^{'}\left(d\right) = \lambda \frac{2\bar{\mathcal{N}} \mathcal{A}\left(d\right) \left(\frac{\mathrm{e}^{\omega(d)} - 1}{\omega(d)} - \frac{\mathrm{e}^{\omega(d) - \bar{\mathcal{N}}} - 1}{\omega(d) - \bar{\mathcal{N}}}\right)}{\mathcal{A}\left(d\right)\left(1 - \mathrm{e}^{-\bar{\mathcal{N}}} - \bar{\mathcal{N}}\mathrm{e}^{-\bar{\mathcal{N}}}\right) + \mathrm{e}^{-\bar{\mathcal{N}}} + \bar{\mathcal{N}} - 1}, \tag{7.13}$$

where $\mathcal{A}(d)$ and $\omega(d)$ is given in (7.9) and (7.10), respectively.

Proof. Using (7.7), the proof simply follows based on the ratio of the two probabilities derived in (7.8) and (7.12). ■

Therefore, having the intensity of the inhomogeneous PPP, we can derive the Laplace transform of the aggregated interference.

Lemma 13. *The Laplace transform of the aggregated interference power, denoted by $\mathcal{L}_{I_{\mathrm{agg}}}(\mathrm{s})$, from the non-blocked active interfering APs to a receiver located at U is given by*

$$\mathcal{L}_{I_{\mathrm{agg}}}(\mathrm{s}) = \exp\left\{\int_{\mathbb{R}^2} -\frac{\varphi^2}{\pi^2} \mathcal{P}_{\mathcal{LoS}}\left(\|x - U\|\right) \left(1 - \left(1 + \frac{\|x - U\|^{-\alpha}}{4m\varphi^2}\mathrm{s}\right)^{-m}\right) \lambda'\left(\|x\|\right) \mathrm{d}x\right\} \tag{7.14}$$

Proof. Proof is given in B. ■

7.3.1 Probability of Successful Reception

Now, armed with the Laplace transform of the aggregated interference power level, we calculate the probability of successfully receiving a signal from the typical AP at its associated

receiving terminal at distance u. As mentioned previously, a signal from the typical AP is received successfully, when both of the following conditions hold:

- The LoS path from the typical AP towards the arbitrary located receiver is not blocked.
- Considering the antennas direction/alignment and the channel gain, the received signal strength is greater than the interference plus noise power level at the receiving terminal, with a threshold based on the system requirement.

Since, these two events are independent, we see the successful reception probability, obtained in the following theorem, will manifest itself as the multiplication of these two events.

Theorem 4. *The probability of having a successful signal reception from the typical AP at its dedicated receiving terminal is given by*

$$P_{recept} = P_{LoS}(u) \sum_{k=0}^{m-1} \frac{(-m\beta u^{\alpha})^k}{k!} \left(\frac{\partial^k}{\partial \mathrm{s}^k} \mathrm{e}^{-\mathrm{s}\sigma_n^2} \mathcal{L}_{I_{\mathrm{agg}}}(\mathrm{s}) \right) |_{\mathrm{s}=m\beta u^{\alpha}} \tag{7.15}$$

where, $\mathcal{L}_{I_{agg}}$ is given in (7.14).

Proof. Proof is provided in B. ■

7.3.2 Probability of Successful Transmission

The previous calculation of the probability of successful reception is based on the underlying assumption that the typical AP is retained in the point process and hence is transmitting. However, the typical AP postpones the transmission if it senses another AP transmitting with smaller back-off timer. Therefore, the transmission will take place with certain probability, derived in the following theorem.

Theorem 5. *The probability of successful transmission of the typical AP is given by*

$$P_{Trans} = \frac{1 - \mathrm{e}^{-\bar{\mathcal{N}}}}{\bar{\mathcal{N}}} \tag{7.16}$$

Proof. Proof is given in B. ■

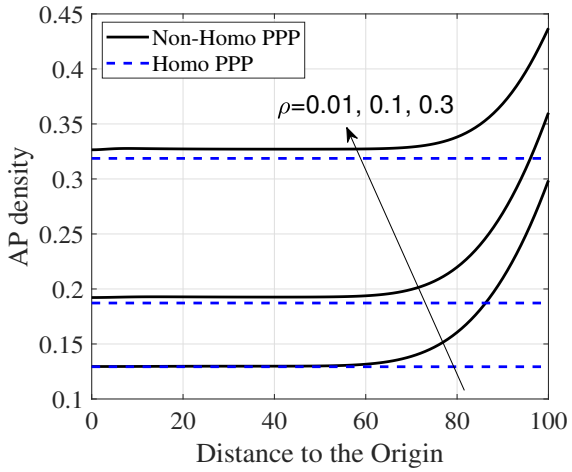

Fig. 7.5: Comparison of the intensity of IH-PPP and H-PPP in different blockage density. Here, $\lambda = 0.5$, $\sigma = 0.01$ and $\varphi = 10^{\circ}$.

Therefore, the probability of having a successful communication link between the typical AP and its dedicated receiving terminal, at distance u apart, is defined as $\mathtt{P}(u) = \mathtt{P}_{\mathtt{Trans}}.\mathtt{P}_{\mathtt{Recept}}(u)$.

7.4 Approximation by Homogeneous PPP

As discussed in previous section, the neighbors of the typical AP reside within an arbitrary shape area around it. We can bound the area by a disc of radius r_{cont}, where $\mathbb{P}\{hg(\theta,\xi)\bar{g}(\theta+\pi-\xi,\xi)r_{\text{cont}}^{-\alpha}, \geq \sigma\,|h, g\bar{g}\} \leq \varepsilon$. Here, ε is a small value. In fact, r_{cont} is a sufficiently large distance beyond which the probability of an AP becoming a neighbor for the typical AP is very negligible (smaller than ε).

$$
\begin{aligned}
&\mathbb{P}\{hg(\theta,\xi)\bar{g}(\theta+\pi-\xi,\xi)r_{\text{cont}}^{-\alpha},\geq\sigma\,|h,g\bar{g}\}\leq\varepsilon\\
&\quad=\mathbb{E}\left[\mathbb{P}\{hg(\theta,\xi)\bar{g}(\theta+\pi-\xi,\xi)r_{\text{cont}}^{-\alpha},\geq\sigma\,|h,g\bar{g}\}\right]\leq\varepsilon\\
&\quad=\mathbb{E}\left[\mathbb{P}\{h\geq\frac{\sigma r_{\text{cont}}^{\alpha}}{g(\theta,\xi)\bar{g}(\theta+\pi-\xi,\xi)}\,|h,g\bar{g}\}\right]\leq\varepsilon\\
&\quad=\mathbb{E}\left[1-F_h\left(\frac{\sigma r_{\text{cont}}^{\alpha}}{g(\theta,\xi)\bar{g}(\theta+\pi-\xi,\xi)}\right)\right]\leq\varepsilon\\
&\quad=\frac{\varphi^2}{\pi^2}\left(1-F_h\left(\frac{\sigma r_{\text{cont}}^{\alpha}}{g(\theta,\xi)\bar{g}(\theta+\pi-\xi,\xi)}\right)\right)\leq\varepsilon
\end{aligned}
\tag{7.17}
$$

Therefore,

$$
r_{\text{cont}}\geq\left(\frac{F_h^{-1}\left(1-\frac{\varepsilon\pi^2}{\varphi^2}\right)}{4\sigma\varphi^2}\right)^{\frac{1}{\alpha}}
\tag{7.18}
$$

Here, ${F_h}^{-1}(.)$ is the inverse CDF of the squared fading gain of the channel. In order to calculate the intensity of the H-PPP, we first define the neighborhood success probability, denoted by η, that is average probability that an AP stays in the neighborhood of the typical AP.

$$
\begin{aligned}
\eta&=\int_0^{r_{\text{cont}}}\mathbb{P}\{hg(\theta,\xi)\bar{g}(\theta+\pi-\xi,\xi)zr^{-\alpha}\geq\sigma\,|h,g\bar{g}\}f\,(r)\,\mathrm{d}r\\
&=\int_0^{r_{\text{cont}}}\mathbb{E}\left[\mathbb{P}\{hg(\theta,\xi)\bar{g}(\theta+\pi-\xi,\xi)zr^{-\alpha}\geq\sigma\,|h,g\bar{g}\}\right]f\,(r)\,\mathrm{d}r\\
&=\int_0^{r_{\text{cont}}}\mathbb{E}\left[\mathbb{P}\{h\geq\frac{\sigma r^{\alpha}}{g(\theta,\xi)\bar{g}(\theta+\pi-\xi,\xi)z}\,|h,g\bar{g}\}\right]f\,(r)\,\mathrm{d}r\\
&=\int_0^{r_{\text{cont}}}\mathtt{P}_{\mathtt{LoS}}\,(r)\,\frac{\varphi^2}{\pi^2\Gamma(m)}\Gamma\left(m,4m\sigma\varphi^2r^{\alpha}\right)f\,(r)\,\mathrm{d}r
\end{aligned}
\tag{7.19}
$$

where $f\,(r)$ is the distance distribution in PPP network model.

Now given the neighborhood success probability as determined by the MAC protocol, the average number of APs that concurrently transmit can be obtained by the following lemma.

Lemma 14. *Considering D-MAC protocol with sensing threshold σ, the average number of APs that concurrently transmit is given by $\frac{1-e^{-\lambda A\eta}}{\eta A}$, where $A = \pi r_{\text{cont}}^2$ is the contention area, and η denotes the neighborhood success probability.*

Proof. Proof is provided in B. ■

Fig. 7.5 represents the intensity of the H-PPP and IH-PPP in different blockage density ρ. As we can see, the density of the IH-PPP is lower bounded by H-PPP. In fact, in areas close to the typical AP, the intensity can be approximated by H-PPP. However, as we move to the perimeter of the network, this approximation is no longer valid.

7.5 Numerical Results

This section provides numerical results to characterize the interference model. Monte-Carlo simulation validates the proposed model. We consider Nakagami-m channel with shape factor $m = 2$. Pathloss exponent α is set to 2. The beamwidth of the mmWave signals, i.e., 2φ, is assumed to be 20 degrees. The distance between the typical AP and its intended receiver (denoted by u) and the average AP antenna length ℓ are 10m and 0.5m, respectively.

Fig. 7.6 shows the probabilities of transmission and reception and also the probability of having a successful communication link in our setup. As we can see, the probability of transmission increases as blockage density increases. This is due to the fact that as ρ increases the number of APs that can be sensed by the typical AP decreases. Therefore, the chance of the typical AP to access the channel increases. However, the probability of reception decreases. In fact, as ρ increases, in one hand the higher number of interfering APs are blocked; however, on the other hand the probability of the desired signal from the typical AP getting blocked decreases as well, and the overall effect is decrease in probability of transmission. Here we can see, considering beam directionality and hence sensitivity to blockages at mmWave frequencies, we might be able to design and operate a denser network of APs as captured by our model.

In Fig. 7.7, we can see that all three probabilities decrease with the increase in primary

AP density. In fact, having higher number of APs in the network decreases the chance of the typical AP to be granted transmission. In addition, the interference power level received at the corresponding receiving terminal increases, as well. In fact, even with high directionality of mmWave signals and sensitivity to the obstacles, the density of the APs can not be arbitrarily increased to achieve higher data rate. The efficient number of APs, beyond which the network performance is less than the desirable threshold, is captured in our model

Fig. 7.8 represents the system performance versus carrier sensing threshold. As we can see, the probability of transmission increases as sensing threshold increases. As σ increases the probability of the typical AP senses the other APs decreases, as well. This gives a higher chance to the typical AP to access the channel. However, on the other hand the probability of reception decreases which is due to the fact that with the increase in σ, the APs have lower chance of hearing each other. Therefore higher number of simultaneous transmissions happen in the network and increases the interference power level. Here, we can see, although by increasing the sensing threshold ($\sigma \to \infty$ represents the ALOHA protocol, where every AP accesses the medium randomly without sensing the channel), we might increase the probability of having a successful transmission. However, it decreases the probability of receiving the signal properly. Therefore, a proper sensing threshold needs to be determined to have an acceptable link success level. Clearly, our proposed model captures the effective sensing threshold.

In Fig. 7.9, the probability of transmission decreases as the beamwidth increases. In fact, as φ increases, in one hand, the antenna gains decrease, but on the other hand the probability of two antennas having non-zero gains towards one another increases. Therefore, the chance of both sensing each other increases. In addition, the probability that the desired link (between the typical AP and its dedicated receiving terminal) is blocked increases. However, the overall effect represents a decrease in the transmission probability. Moreover, the probability of reception also decreases, due to multiple reasons. In fact, the antenna gain of the interfering APs towards the receiver decreases. However, the probability of these APs having non-zero antenna gain at the receiver increases. In addition, the probability of having a blockage in the LoS path from the typical AP to the receiving terminal increases, as

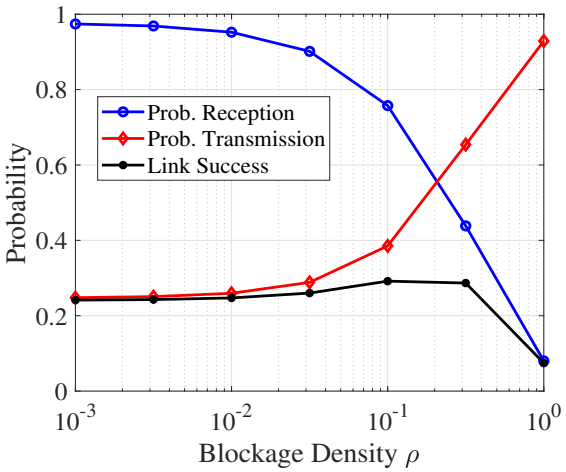

Fig. 7.6: $\mathtt{P}$, $\mathtt{P}_{\mathtt{Trans}}$ and $\mathtt{P}_{\mathtt{Recept}}$ versus blockage density ρ.

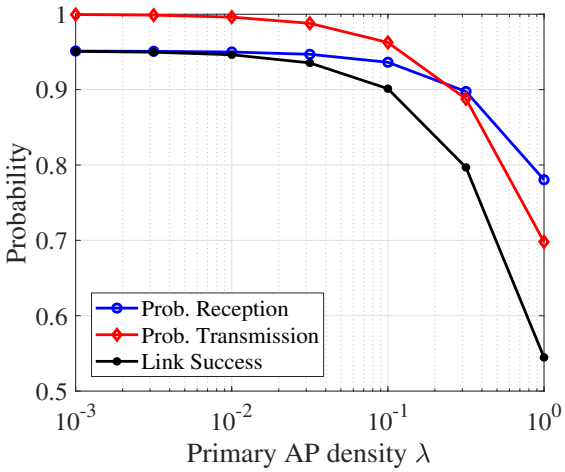

Fig. 7.7: $\mathtt{P}$, $\mathtt{P}_{\mathtt{Trans}}$ and $\mathtt{P}_{\mathtt{Recept}}$ versus primary AP density λ.

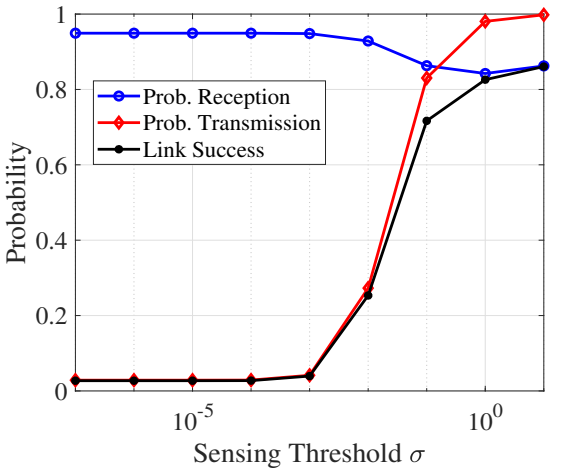

Fig. 7.8: $\mathtt{P}$, $\mathtt{P}_{\mathtt{Trans}}$ and $\mathtt{P}_{\mathtt{Recept}}$ versus carrier sensing threshold σ.

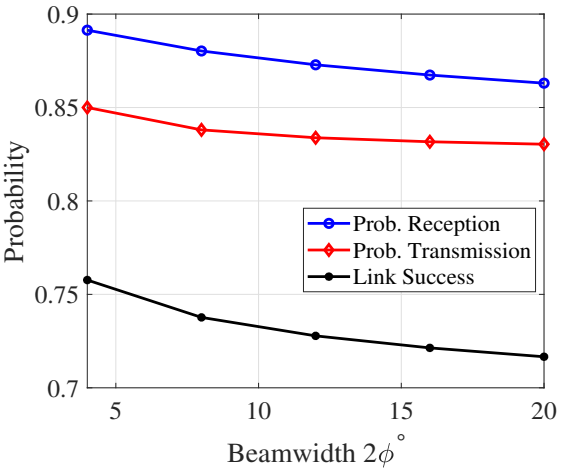

Fig. 7.9: $\mathtt{P}$, $\mathtt{P}_{\mathtt{Trans}}$ and $\mathtt{P}_{\mathtt{Recept}}$ versus antenna beamwidth 2φ.

well. As it is seen, in an overall sense, the probability of reception decrease with the increase in the beamwidth. It is worth mentioning that, although having a narrower beamwidth results in higher successful link probability, we can not arbitrarily decrease the beamwidth. In fact, beam alignment error and beam searching overheads increase with the decrease in the beamwidth. Analysing the trade-off in successful link probability and beam alignment error/searching overhead is an interesting topic that can be considered as part of future work.

7.6 Summary and Conclusion

In this chapter, we propose a cross-layer interference model for 5G mmWave networks. The derived model captures mmWave beam directionality, sensitivity to blockages and also MAC layer constraints. We propose a blockage model to account for the effect of obstacles in the environment. In addition, the MAC protocol is considered in deriving the number of simultaneously transmitting APs. We approximate this set of APs by IH-PPP and H-PPP. As we have seen, the intensity of the IH-PPP can be lower bounded by the intensity of the H-PPP. Subsequently, the Laplace transform of the power of the received interference at an arbitrarily located user is derived and the network performance is evaluated and validated using simulations.

Chapter 8

Conclusion and Future work

In this chapter, we provide concluding remarks of the present dissertation with summary of the results and future research directions.

8.1 Summary and Conclusion

In this dissertation, two main challenges associated with the utilization of mmWave spectrum for next-generation wireless systems are studied: (i)The first concern is how mmWave-enabled radio base stations can be integrated in the current LTE cellular setup, providing a unified HetNet structure, that results in higher data rate and cellular coverage? and (ii) given the challenging propagation characteristics of this band, including strong atmospheric absorption and vulnerability to obstacles, what network performance does a typical user experience?

To this end, in chapter 3, we proposed a novel framework of how to effectively incorporate the mmWave-enabled small cells into the area of larger LTE base stations and improve the data rate. By allowing the users to adaptively switch between different frequency bands, the the model enables the combination of dual air interfaces, leading to increased throughput. We also incorporated relay stations into our model and consider a two-hop transmission scheme to overcome the severe pathloss and shadowing issue in the mmWave band. In

addition, the corresponding resource allocation problem for the proposed network model has been proposed and solved. Our results show that this approach increases the overall sum rate of the network.

In chapters 4 and 5, we have suggested two interference models that consider the effect of obstacles in the environment and evaluate the performance of 5G mmWave networks. The proposed interference models account for the effect of small to medium sized blockages such as human body, car, foliage, etc. To include the effect of obstacles, a new blockage model has been proposed and used as a random scaling factor to the interference power level. The suggested interference model in chapters 4 and 5 are suitable for large scale and finite-sized mmWave-enabled wireless networks. It is notable that, our proposed model accounts for randomness in both node locations and their operating frequencies. This can be quite beneficial given the notions of adaptive frequency selection and dynamic channel allocation strategies instead of static assignments for 5G networks. Therefore, considering the uncertainty in spectral domain while modeling the accumulated interference provides a more accurate model. Simulation results have shown that considering the effect of blockages leads to a different interference profile.

In chapter 6, a systematic approach has been proposed to determine the network regime in mmWave networks. The regime identification is formulated as a hypothesis testing problem. Specifically, we detect whether an arbitrarily located user experiences a noise or interference-limited regime based on the received signal power distribution in the presence of arbitrary-sized blockages. Based on our finding, mmWave networks can exhibit either interference-limited regime or noise-limited regime, depending on various factors such as access point density, blockage density, signal beamwidth, and so on.

Finally, in chapter 8, a joint PHY/MAC interference analysis framework has been proposed. This interference model considers both directionality of mmWave signals with random antenna orientation and blockage effect from both physical and MAC layer perspective. In addition, it has been assumed that APs employ sensing mechanism-enabled MAC protocol to access the shared channel. Under such assumptions, we derive the intensity of APs that actively introduce interference and contribute to the interference power level at a receiving

node. Subsequently, using the derived intensity, we obtain the Laplace transform of the interference power. The results show that although mmWave signals can be easily blocked and attenuated, some level of carrier sensing is still needed in mmWave networks. In fact, in a dense network of APs, the interference power level can still be considerable. In addition, the efficient number of APs, beyond which the network performance is lower than the desirable threshold, is captured in our model. Furthermore, we see that considering beam directionality and hence sensitivity to blockages at mmWave frequencies, we might be able to design and operate a denser network of APs as captured by our model.

8.2 Future work

Research accomplished in this dissertation can lead to multiple follow-on efforts and future research directions that are highlighted in the following:

- In chapter 3, the macro base station is equipped with a single transmit-receive antenna. In future work, it would be interesting to consider base stations equipped with multiple transceiver antennas and evaluate the effect of MIMO technique on the presented model. In addition, as we discussed, considering high pathloss and shadowing effects in mmWave frequency bands and therefore the need for highly directional beam antennas to have an acceptable link quality, obstacles and blockages in the environment have a considerable effect on the strength and quality of the received signal. Therefore, it would be important to consider the impact of the beamwidth of the antennas and the density of the obstacles on the presented multi-band HetNet. Such analysis of HetNets can be also done using tools from stochastic geometry[101–103]. Finally, backhaul configurations that can support the proposed scheme would also be of particular interest[104].

- In chapters 4 and 5, we assume all interfering APs have equal transmit power. In future work, we can consider heterogeneous interferers where each interferer transmits at different power level. In addition considering the mobility of the nodes would also

be of particular interest. In addition, we consider the correlated obstacle, in the sense that obstacle may overlap and hence more than one obstacle cause the outage in the LoS path. Correlated blockage can be also considered in a sense that one obstacle may block more than one communication link. Moreover, obstacles movement introduces temporal correlation in the probability of link blockage. It would be interesting to study such temporal correlation in the presence of moving blockage. In chapter 5, specifically and complementary to the present approach, a general polygon-shaped network area and cosine elliptical radiation area for interfering APs. In addition, the case where the center of blockages are outside of the radiation area but close to the edges where part of the mass of the blockages resides in the radiation area can also be included.

- In chapter 6, we consider a binary hypothesis where network operates under two interference-limited and noise-limited regimes. However, there might be a case where network exhibits intermediate behavior in which none of the interference or noise powers are negligible compared to the other one. Therefore, it would be complementary to this setup to consider the regime classification problem as a hypothesis testing where all three network regimes are included.

- As mentioned in chapter 7, the correlated effect of multiple APs is ignored for the sake of simplicity and tractability. In fact, we only account for the pairwise impacts of the APs. It would be interesting to study the correlated effect of the arbitrary number of APs in such setup. In addition, to allow the readers to follow the analysis with ease, we ignore the issues of D-MAC protocols. In fact, directional antennas may lead to directional hidden/exposed terminal problem, deafness, head-of-line blocking problem and etc. In the future works, we can evaluate the network performance considering such cases in the problem setup.

Bibliography

[1] readingrat.com, "Evolution of mobile phone communications," May 2017. [Online]. Available: http://readingrat.net

[2] T. S. Rappaport *et al.*, *Wireless communications: principles and practice*. prentice hall PTR New Jersey, 1996, vol. 2.

[3] T. S. Rappaport, R. W. Heath, R. C. Daniels, and N. Murdock, *Millimeter-Wave Wireless Communications*. Prentice Hall, 2014.

[4] M. Agiwal, A. Roy, and N. Saxena, "Next generation 5G wireless networks: A comprehensive survey," *IEEE Commun. Surveys Tuts.*, vol. 18, no. 3, pp. 1617–1655, Feb. 2016.

[5] J. G. Andrews, S. Buzzi, W. Choi, S. V. Hanly, A. Lozano, A. C. K. Soong, and J. C. Zhang, "What will 5G be?" vol. 32, no. 6, Jun. 2014.

[6] Wikipedia, "Internet of things — wikipedia, the free encyclopedia," May 2017. [Online]. Available: https://en.wikipedia.org/w/index.php?title=Internet_of_things&oldid=800274246

[7] T. S. Rappaport, S. Sun, R. Mayzus, H. Zhao, Y. Azar, K. Wang, G. N. Wong, J. K. Schulz, M. Samimi, and F. Gutierrez, "Millimeter wave mobile communications for 5g cellular: It will work!" *IEEE Access*, vol. 1, pp. 335–349, 2013.

[8] S. Niknam, A. A. Nasir, H. Mehrpouyan, and B. Natarajan, "A multiband OFDMA heterogeneous network for millimeter wave 5G wireless applications," *IEEE Access*, vol. 4, pp. 5640–5648, Sep. 2016.

[9] S. Niknam, B. Natarajan, and H. Mehrpouyan, "A spatial-spectral interference model for millimeter wave 5G applications," in *Proc. IEEE Veh. Tech. Conf.*, Sep. 2017, pp. 1–5.

[10] S. Niknam, B. Natarajan, and R. Barazideh, "Interference analysis for finite-area 5g mmwave networks considering blockage effect," *IEEE Access*, vol. 6, pp. 23 470–23 479, Apr. 2018.

[11] S. Niknam and B. Natarajan, "On the regimes in millimeter wave networks: Noise-limited or interference-limited?" in *IEEE Int. Conf. on Commun. Workshops*, 2018.

[12] S. Niknam, R. Barazideh, and B. Natarajan, "Cross-layer interference modeling for 5G mmwave networks in the presence of blockage," in *IEEE Veh. Tech. Conf.*, Aug. 2018, pp. 1–5.

[13] S. Niknam, H. Dhillon, and B. Natarajan, "A joint phy/mac interference analysis with blockage effect for 5g mmwave networks," *to be submitted to*, 2018.

[14] F. Baccelli *et al.*, "Stochastic geometry and wireless networks: Volume I applications," *Foundations and Trends® in Networking*, vol. 4, no. 1–2, pp. 1–150, 2010.

[15] ——, "Stochastic geometry and wireless networks: Volume II applications," *Foundations and Trends® in Networking*, vol. 4, no. 1–2, pp. 249–449, 2010.

[16] B. Blaszczyszyn, M. Haenggi, P. Keeler, and S. Mukherjee, *Stochastic geometry analysis of cellular networks*. Cambridge University Press, 2018.

[17] M. Haenggi, *Stochastic geometry for wireless networks*. Cambridge University Press, 2012.

[18] V. Schmidt, *Stochastic geometry, spatial statistics and random fields*. Springer, 2014.

[19] M. Patzold, *Mobile fading channels: Modelling, analysis and simulation*. John Wiley & Sons, Inc., 2001.

[20] A. Goldsmith, *Wireless communications*. Cambridge university press, 2005.

[21] R. Barazideh *et al.*, "Performance of analog nonlinear filtering for impulsive noise mitigation in OFDM-based PLC systems," in *IEEE Latin-American Conf. on Commun.*, Nov 2017, pp. 1–6.

[22] R. Barazideh, A. V. Nikitin, and B. Natarajan, "Practical implementation of adaptive analog nonlinear filtering for impulsive noise mitigation," in *IEEE Int. Conf. on Commun.*, May 2018, pp. 1–7.

[23] M. Afshang, M. S. Tavallali, H. Y. Shwe, and P. H. J. Chong, "Effect of time frame duration and collision on the performance of OFDMA-based cognitive radio network," in *IEEE/CIC Int. Conf. on Commun. in China*, Oct 2014, pp. 861–866.

[24] R. Barazideh, S. Niknam, B. Natarajan, and A. V. Nikitin, "Intermittently nonlinear impulsive noise mitigation and doppler shift compensation in UWA-OFDM systems," *Submitted to IEEE J. Ocean. Eng.*, 2018.

[25] R. Barazideh, B. Natarajan, A. V. Nikitin, and S. Niknam, "Performance analysis of analog intermittently nonlinear filter in the presence of impulsive noise," *arXiv preprint arXiv:1811.08940*, 2018.

[26] J. Andrews, "Seven ways that HetNets are a cellular paradigm shift," vol. 51, no. 3, pp. 136–144, Mar. 2013.

[27] N. Corporation, "Ten key rules of 5G deployment," *Nokia Networks white paper*, 2015.

[28] H. Mehrpouyan, M. Matthaiou, R. Wang, and G. Karagiannidis, "Hybrid millimeter-wave systems: A novel paradigm for HetNets," vol. 53, no. 1, Jan. 2015.

[29] X. Han, H. Chen, L. Xie, and K. Wang, "A resource allocation scheme for the heterogeneous OFDMA system with ad hoc relay," in *Proc. IEEE Int. Conf. Commun. Tech.*, Sep. 2011, pp. 637–641.

[30] D. Fooladivanda and C. Rosenberg, "Joint resource allocation and user association for heterogeneous wireless cellular networks," vol. 12, no. 1, pp. 248–257, Jan. 2013.

[31] A. Abdelnasser and E. Hossain, "Subchannel and power allocation schemes for clustered femtocells in two-tier OFDMA hetnets," in *Proc. IEEE Int. Conf. Commun. Workshops*, Jun. 2013, pp. 1129–1133.

[32] L. Liang and G. Feng, "A game-theoretic framework for interference coordination in OFDMA relay systems," vol. 61, no. 1, pp. 321–332, 2012.

[33] C. Hsu, H. Su, and P. Lin, "Joint subcarrier pairing and power allocation for OFDM transmission with decode- and-forward relaying," vol. 59, no. 1, pp. 399–414, Jan. 2011.

[34] Z. Hasan, E. Hossain, and V. K. Bhargava, "Resource allocation for multiuser OFDMA-based amplify-and-forward relay networks with selective relaying," in *Proc. IEEE Int. Conf. Commun.*, 2011, pp. 1–6.

[35] G. A. S. Sidhu, F. Gao, and A. Nallanathan, "A joint resource allocation scheme for multi-relay aided uplink multi-user OFDMA system," in *Proc. Int. Conf. Wireless Commun. and Signal Process.*, 2010, pp. 1–6.

[36] T. Bai and R. W. Heath., "Coverage and rate analysis for millimeter-wave cellular networks," vol. 14, no. 2, Oct. 2015.

[37] A. Osseiran *et al.*, "Scenarios for 5G mobile and wireless communications: The vision of the METIS project," vol. 52, no. 5, May 2014.

[38] M. Herdin, "A chunk based OFDM amplify-and-forward relaying scheme for 4G mobile radio systems," in *Proc. IEEE Int. Conf. Commun.*, vol. 10, Jun. 2006, pp. 4507–4512.

[39] Y. Wang, X. Qu, T. Wu, and B. Liu, "Power allocation and subcarrier pairing algorithm for regenerative OFDM relay system," in *Proc. IEEE Veh. Tech. Conf.*, Apr. 2007, pp. 2727–2731.

[40] S. Boyd and L. Vandenberghe, *Convex optimization*. Cambridge university press, 2009.

[41] W. Yu and R. Lui, "Dual methods for nonconvex spectrum optimization of multicarrier systems," vol. 54, no. 7, pp. 1310–1322, Jul. 2006.

[42] C. E. R. R. L. . S. C. Thomas H.. Cormen, Leiserson, *Introduction to algorithms*. Cambridge: MIT press, 2001.

[43] F. Khan, *LTE for 4G mobile broadband: air interface technologies and performance*. Cambridge University Press, 2009.

[44] Y. Dong, Z. Chen, P. Fan, and K. B. Letaief, "Mobility-aware uplink interference model for 5G heterogeneous networks," vol. 15, no. 3, pp. 2231–2244, Mar. 2016.

[45] K. Venugopal, M. C. Valenti, and R. W. Heath, "Interference in finite-sized highly dense millimeter wave networks," in *Inform. Theory and Applicat. Workshop*, Feb. 2015, pp. 175–180.

[46] R. W. Heath and M. Kountouris, "Modeling heterogeneous network interference," in *Inform. Theory and Applicat. Workshop*, Feb. 2012, pp. 17–22.

[47] Y. M. Shobowale and K. A. Hamdi, "A unified model for interference analysis in unlicensed frequency bands," vol. 8, no. 8, pp. 4004–4013, Aug. 2009.

[48] M. Haenggi and R. Ganti, *Interference in large wireless networks*. Now Publishers Inc, 2009.

[49] T. Bai, R. Vaze, and R. W. Heath, "Analysis of blockage effects on urban cellular networks," vol. 13, no. 9, pp. 5070–5083, Sep. 2014.

[50] M. Taranetz and M. Rupp, "A circular interference model for heterogeneous cellular networks," vol. 15, no. 2, pp. 1432–1444, Feb. 2016.

[51] Z. Gong and M. Haenggi, "Interference and outage in mobile random networks: Expectation, distribution, and correlation," vol. 13, no. 2, pp. 337–349, Feb. 2014.

[52] A. K. Gupta, J. G. Andrews, and R. Heath, "Macro diversity in cellular networks with random blockages," *arXiv preprint arXiv:1701.02044v1*, 2017.

[53] G. R. MacCartney, S. Deng, S. Sun, and T. S. Rappaport, "Millimeter-wave human blockage at 73 GHz with a simple double knife-edge diffraction model and extension for directional antennas," in *Proc. IEEE Veh. Tech. Conf.*, Sep. 2016, pp. 1–6.

[54] 3rd Generation Partnership Project, "Further advancements for E-UTRA physical layer aspects," Sophia Antipolis Valbonne, France, TR 36.814, Mar. 2010.

[55] K. Haneda *et al.*, "Indoor 5G 3GPP-like channel models for office and shopping mall environments," *arXiv preprint arXiv:1603.04079v1*, 2016.

[56] T. H. Chan, S. Hranilovic, and F. R. Kschischang, "Capacity-achieving probability measure for conditionally gaussian channels with bounded inputs," vol. 51, no. 6, pp. 2073–2088, Jun. 2005.

[57] K. A. Hamdi, "A useful technique for interference analysis in nakagami fading," vol. 55, no. 6, pp. 1120–1124, Jun. 2007.

[58] M. Abramowitz and I. A. Stegun, *Handbook of mathematical functions: with formulas, graphs, and mathematical tables*. Courier Corporation, 1954, vol. 55.

[59] M. Haenggi, *Stochastic Geometry for Wireless Networks*. Cambridge, U.K: Cambridge Univ. Press, 2012.

[60] J. G. Andrews, R. K. Ganti, M. Haenggi, N. Jindal, and S. Weber, "A primer on spatial modeling and analysis in wireless networks," vol. 48, no. 11, pp. 156–163, Nov. 2010.

[61] E. Dahlman, G. Mildh, S. Parkvall, J. Peisa, J. Sachs, and Y. Selén, "5G radio access," *Ericsson review*, vol. 91, no. 6, pp. 42–48, 2014.

[62] J. Liu, M. Sheng, L. Liu, and J. Li, "Interference management in ultra-dense networks: Challenges and approaches," *IEEE Network*, vol. PP, no. 99, pp. 1–8, Aug. 2017.

[63] A. K. Gupta, J. G. Andrews, and R. W. Heath Jr, "Macro diversity in cellular networks with random blockages," *arXiv preprint arXiv:1701.02044*, 2017.

[64] M. K. Muller, M. Taranetz, and M. Rupp, "Analyzing wireless indoor communications by blockage models," *IEEE Access*, vol. 5, pp. 2172–2186, 2017.

[65] K. Venugopal, M. C. Valenti, and R. W. Heath, "Device-to-device millimeter wave communications: Interference, coverage, rate, and finite topologies," vol. 15, no. 9, pp. 6175–6188, Sep. 2016.

[66] A. Thornburg, T. Bai, and R. W. Heath, "Performance analysis of outdoor mmwave ad hoc networks," *IEEE Trans. Signal Process.*, vol. 64, no. 15, pp. 4065–4079, 2016.

[67] S. Collonge, G. Zaharia, and G. E. Zein, "Influence of the human activity on wide-band characteristics of the 60 GHz indoor radio channel," vol. 3, no. 6, pp. 2396–2406, Nov. 2004.

[68] M. Gapeyenko *et al.*, "Analysis of human-body blockage in urban millimeter-wave cellular communications," in *Proc. IEEE Int. Conf. Commun.*, 2016, pp. 1–7.

[69] Z. Khalid and S. Durrani, "Distance distributions in regular polygons," vol. 62, no. 5, pp. 2363–2368, Jun. 2013.

[70] K. Venugopal and R. W. Heath, "Millimeter wave networked wearables in dense indoor environments," *IEEE Access*, vol. 4, pp. 1205–1221, 2016.

[71] C. A. Balanis, *Antenna Theory :Analysis and Design*. John Wiley & Sons, Inc, 2005.

[72] J. Kokkoniemi, J. Lehtomaki, and M. Juntti, "Stochastic geometry analysis for mean interference power and outage probability in THz networks," vol. 16, no. 5, pp. 3017–3028, May 2017.

[73] M. Afshang and H. S. Dhillon, "Fundamentals of modeling finite wireless networks using binomial point process," vol. 16, no. 5, pp. 3355–3370, May 2017.

[74] N. L. Garcia and T. G. Kurtz, "Spatial point processes and the projection method," in *In and Out of Equilibrium 2*. Springer, 2008, pp. 271–298.

[75] J. Filipe *et al.*, "Infinite servers queue systems busy period-a practical case on logistics problems solving," *Appl. Math. Sci.*, no. 25, pp. 1221–1228, 2015.

[76] 3rd Generation Partnership Project, "Further advancements for E-UTRA physical layer aspects," Sophia Antipolis Valbonne, France, TR 36.814, Mar. 2010.

[77] M. Rebato, M. Mezzavilla, S. Rangan, F. Boccardi, and M. Zorzi, "Understanding noise and interference regimes in 5G millimeter-wave cellular networks," in *European Wireless Conf.*, May 2016, pp. 1–5.

[78] R. Amiri *et al.*, "A machine learning approach for power allocation in hetnets considering qos," *arXiv preprint arXiv:1803.06760*, 2018.

[79] M. Yousefvand, S. Khorsandi, and A. Mohammadi, "Interference-constraint spectrum allocation model for cognitive radio networks," in *IEEE Int. Conf. Intelligent Sys.*, Sept 2012, pp. 357–362.

[80] H. Shokri-Ghadikolaei and C. Fischione, "Millimeter wave ad hoc networks: Noise-limited or interference-limited?" in *Proc. IEEE Globecom Workshops*, Dec. 2015, pp. 1–7.

[81] R. Amiri, H. Mehrpouyan, D. Matolak, and M. Elkashlan, "Joint power allocation in interference-limited networks via distributed coordinated learning," *arXiv preprint arXiv:1806.02449*, 2018.

[82] M. Afshang, Z. Yazdanshenasan, S. Mukherjee, and P. H. J. Chong, "Hybrid division duplex for hetnets: Coordinated interference management with uplink power control," in *IEEE Int. Conf. on Commun. Workshop*, June 2015, pp. 106–112.

[83] M. Ebrahimi, M. Maddah-Ali, and A. Khandani, "Interference-limited versus noise-limited communication over dense wireless networks," in *Canadian Workshop on Inform. Theory*, Jun. 2007, pp. 172–175.

[84] N. Jindal, J. G. Andrews, and S. Weber, "Energy-limited vs. interference-limited ad hoc network capacity," in *Proc. Asilomar Conf. on Signals, Syst. and Comput.*, Nov 2007, pp. 148–152.

[85] J. G. Andrews *et al.*, "A primer on spatial modeling and analysis in wireless networks," *IEEE Communications Magazine*, vol. 48, no. 11, pp. 156–163, November 2010.

[86] Y. Niu *et al.*, "A survey of millimeter wave communications (mmwave) for 5G: opportunities and challenges," *Wireless Networks*, vol. 21, no. 8, pp. 2657–2676, Nov 2015.

[87] T. M. Cover and J. A. Thomas, *Elements of information theory*. John Wiley & Sons, 2012.

[88] R. Amiri and H. Mehrpouyan, "Self-organizing mmwave networks: A power allocation scheme based on machine learning," *arXiv preprint arXiv:1804.05757*, 2018.

[89] H. Q. Nguyen, F. Baccelli, and D. Kofman, "A stochastic geometry analysis of dense ieee 802.11 networks," in *IEEE Int. Conf. on Comput. Commun.*, May 2007, pp. 1199–1207.

[90] G. Alfano, M. Garetto, and E. Leonardi, "New directions into the stochastic geometry analysis of dense csma networks," *IEEE Trans. on Mobile Comput.*, vol. 13, no. 2, pp. 324–336, Feb. 2014.

[91] A. Busson and G. Chelius, "Capacity and interference modeling of CSMA/CA networks using SSI point processes," *Telecommun. Syst.*, vol. 57, no. 1, pp. 25–39, 2014.

[92] T. Lei *et al.*, "A modified matern hard core point process for modeling and analysis of

dense IEEE 802.11 networks," in *Int. Sympo. on Wireless Commun. Syst.*, 2016, pp. 608–612.

[93] Z. Tong, H. Lu, M. Haenggi, and C. Poellabauer, "A stochastic geometry approach to the modeling of IEEE 802.11p for vehicular ad hoc networks," *Submitted to IEEE Trans. on Veh. Tech.*, 2015.

[94] H. ElSawy and E. Hossain, "A modified hard core point process for analysis of random csma wireless networks in general fading environments," *IEEE Trans. on Commun.*, vol. 61, no. 4, pp. 1520–1534, Apr. 2013.

[95] O. Bazan and M. Jaseemuddin, "Performance analysis of directional CSMA/CA in the presence of deafness," *IET Commun.*, vol. 4, no. 18, pp. 2252–2261, Dec. 2010.

[96] Y. Wang and J. J. Garcia-Luna-Aceves, "Collision avoidance in single-channel ad hoc networks using directional antennas," in *Int. Conf. on Distrib. Comput. Syst., 2003. Proceedings.*, May 2003, pp. 640–649.

[97] J. l. Hsu and I. Rubin, "Performance analysis of directional CSMA/CA MAC protocol in mobile ad hoc networks," in *IEEE Int. Conf. on Commun.*, vol. 8, Jun. 2006, pp. 3657–3662.

[98] M. M. Carvalho and J. J. Garcia-Luna-Aceves, "Modeling wireless ad hoc networks with directional antennas," in *IEEE Int. Conf. on Comput. Commun.*, Apr. 2006, pp. 1–12.

[99] J. Wildman, P. H. J. Nardelli, M. Latva-aho, and S. Weber, "On the joint impact of beamwidth and orientation error on throughput in directional wireless poisson networks," vol. 13, no. 12, pp. 7072–7085, Dec 2014.

[100] S. Aditya, H. S. Dhillon, A. F. Molisch, and H. Behairy, "A tractable analysis of the blind spot probability in localization networks under correlated blocking," *IEEE Transactions on Wireless Communications*, pp. 1–1, Oct 2018.

[101] M. Afshang and H. S. Dhillon, "Poisson cluster process based analysis of hetnets with correlated user and base station locations," *IEEE Trans. on Wireless Commun.*, vol. 17, no. 4, pp. 2417–2431, April 2018.

[102] Z. Yazdanshenasan, M. Afshang, and P. H. J. Chong, "Dynamic interference mitigation in two tier hetnets: Modeling and analysis," in *IEEE Veh. Techn. Conf.*, Sept 2014, pp. 1–6.

[103] M. Afshang and H. S. Dhillon, "A new clustered hetnet model to accurately characterize user-centric small cell deployments," in *IEEE Wireless Commun. and Net. Conf.*, March 2017, pp. 1–6.

[104] C. Saha, M. Afshang, and H. S. Dhillon, "Integrated mmwave access and backhaul in 5g: Bandwidth partitioning and downlink analysis," in *IEEE Int. Conf. on Commun.*, May 2018, pp. 1–6.

Appendix A

Proofs of Chapter 5

We assume that the sequence of frequencies used by interfering APs, i.e., f_i, are uncorrelated. However, the sequence of the frequency distance between the frequency of the victim receiver, f_0, and frequency of the i^{th} interfering AP, f_i, i.e., $w_i = f_i - f_0$, are correlated due to the common factor f_0. The conditional probability density function (PDF) of $w_i = f_i - f_0$ is given by

$$f_\Omega(\omega) = \begin{cases} \frac{2}{f_e - f_s} & 0 < \omega \leq \min(|\omega_e|, |\omega_s|) \\ \frac{1}{f_e - f_s} & \min(|\omega_e|, |\omega_s|) < \omega \leq \max(|\omega_e|, |\omega_s|), \end{cases} \tag{A.1}$$

where, $\omega_e = f_e - f_0$ and $\omega_s = f_s - f_0$. We drop the subscript i for notational simplicity.

Proof. Considering the frequency axis given in Fig. A.1, the frequency distance between the reference receiver and an interfering AP is calculated,
1) When $\omega \leq \min(|\omega_e|, |\omega_s|)$, the CDF of ω, i.e., $F_\Omega(\omega)$, is the intersection of line segment $2|\omega|$ and $|f_e - f_s|$ divided by $|f_e - f_s|$.
2) When $\min(|\omega_e|, |\omega_s|) < \omega \leq \max(|\omega_s|, |\omega_s|)$, the CDF is $\frac{|\min(|\omega_e|, |\omega_s|)| + \omega}{|f_e - f_s|}$.

$$F_\Omega(\omega) = \begin{cases} \frac{2\omega}{|f_e - f_s|} & 0 < \omega \leq \min(|\omega_e|, |\omega_s|) \\ \frac{|\min(|\omega_e|, |\omega_s|)| + \omega}{|f_e - f_s|} & \min(|\omega_e|, |\omega_s|) < \omega \leq \max(|\omega_e|, |\omega_s|), \end{cases} \tag{A.2}$$

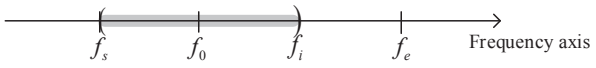

Fig. A.1: The frequency axis.

Subsequently, the PDF of the frequency distance is given by taking derivative of the CDF with respect to ω. ■

Appendix B

Proofs of Chapter 7

B.1 Proof of Lemma 9

By definition, the average number of neighbors of the typical node can be written as

$$
\begin{aligned}
\bar{\mathcal{N}} &= \mathbb{E}^0\left[\sum_{\left(X_j,n_j,P_j^0\right)\in\tilde{\Phi}_{\mathrm{P}}\setminus X_0}\mathbb{1}\left(\frac{P_j^0}{\|X_j-X_0\|^\alpha}\geq\sigma\right)\right]\\
&\overset{(a)}{=}\mathbb{E}\left[\sum_{\left(X_j,n_j,P_j^0\right)\in\tilde{\Phi}_{\mathrm{P}}}\mathbb{1}\left(\frac{P_j^0}{\|X_j\|^\alpha}\geq\sigma\right)\right]\\
&=\mathbb{E}\left[\sum_{\left(X_j,n_j,P_j^0\right)\in\tilde{\Phi}}\mathbb{1}\left(\frac{H_j^0G\left(\theta_j^0,\xi_0\right)\bar{G}\left(\theta_j^0+\pi-\xi_j,\xi_j\right)Z_j^0}{\|X_j-X_0\|^\alpha}\geq\sigma\right)\right]\\
&\overset{(b)}{=}\int_{\mathbb{R}^2}\mathbb{P}\left\{\frac{hg_j^0\bar{g}_j^0z}{\|x\|^\alpha}\geq\sigma\right\}\lambda\mathrm{d}x\\
&=\lambda\int_{\mathbb{R}^2}\mathbb{E}_{g_j^0\bar{g}_j^0,z}\left[\mathbb{P}\left\{\frac{hg_j^0\bar{g}_j^0z}{\|x\|^\alpha}\geq\sigma\left|g_j^0\bar{g}_j^0,z\right.\right\}\right]\mathrm{d}x\\
&=\lambda\int_{\mathbb{R}^2}\mathbb{E}_{g_j^0\bar{g}_j^0,z}\left[\frac{1}{\Gamma\left(m\right)}\Gamma\left(m,\frac{m\sigma\|x\|^\alpha}{g_j^0\bar{g}_j^0z}\right)\right]\mathrm{d}x
\end{aligned}
$$

$$\overset{(c)}{=} \lambda \frac{\varphi^2}{\pi^2} \int_0^{\infty} \int_0^{2\pi} \mathtt{P}_{\mathtt{LoS}}(r) \frac{\Gamma\left(m, 4m\sigma\varphi^2 r^{\alpha}\right)}{\Gamma(m)} r \mathrm{d}\theta \mathrm{d}r$$

$$\overset{(d)}{=} \frac{2\lambda\varphi^2}{\pi} \sum_{k=0}^{m-1} \frac{\left(4m\sigma\varphi^2\right)^k}{k!} \int_0^{\infty} \mathtt{P}_{\mathtt{LoS}}(r) r^{1+\alpha k} \mathrm{e}^{-4m\sigma\varphi^2 r^{\alpha}} \mathrm{d}r \tag{B.1}$$

where $\mathbb{E}^0$ is the expectation with respect to the palm distribution. Here, (a) and (b) follow from Slivnyak's and Campbell's theorems, respectively. In addition, (c) follows from taking the expectation and converting to polar coordinates. Finally, using series expansion of the upper incomplete Gamma function for integer m, step (d) follows.

B.2 Proof of Lemma 10

In order to prove the result in (7.8), we have

$$\mathbb{P}\left\{e_0 = 1, e_y = 1\right\} = \mathbb{E}_{n_0, n_y}\Big[\mathbb{P}\{\, e_0 = 1, e_y = 1 |\, n_0, n_y\}\Big]. \tag{B.2}$$

Therefore, we first need to calculate the conditional probability $\mathbb{P}\left\{e_0 = 1, e_y = 1 |\, n_0, n_y\right\}$ and then decondition on the back-off marks n_0 and n_y. It is notable that, since the back-off timer of the typical AP, i.e. n_0 can be either smaller or larger than n_y, we consider one of the cases

and then multiply the result by a factor of 2.

$$
\begin{aligned}
&\mathbb{P}\left\{e_0 = 1, e_y = 1 \middle| n_0, n_y\right\} \\
&\overset{(a)}{=} \exp\left\{ -\lambda n_y \int_{\mathbb{R}^2} \left[1 - \mathbb{E}_{g_j^0 \bar{g}_j^0, z} \left[\mathbb{P}\left\{ h \leq \frac{\sigma \|x - 0\|^\alpha}{g_j^0 \bar{g}_j^0 z} \middle| g_j^0 \bar{g}_j^0, z \right\} \right] \right.\right. \\
&\qquad\qquad \left.\left. \times \mathbb{E}_{g_j^y \bar{g}_j^y, z} \left[\mathbb{P}\left\{ h \leq \frac{\sigma \|x - X_y\|^\alpha}{g_j^y \bar{g}_j^y z} \middle| g_j^y \bar{g}_j^y, z \right\} \right] \right] \mathrm{d}x \right\} \\
&\quad \times \exp\left\{ -\lambda \left(n_0 - n_y\right) \left(1 - \int_{\mathbb{R}^2} \mathbb{E}_{g_j^0 \bar{g}_j^0, z} \left[\mathbb{P}\left\{ h \leq \frac{\sigma \|x - 0\|^\alpha}{g_j^0 \bar{g}_j^0 z} \middle| g_j^0, \bar{g}_j^0, z \right\} \right] \mathrm{d}x \right) \right\} \\
&\quad \times \left(1 - \frac{\varphi^2 \Gamma\left(m, 4m\varphi^2 \sigma d^\alpha\right)}{\pi^2 \Gamma\left(m\right)} \mathtt{P}_{\mathtt{LoS}}\left(d\right) \right) \\
&\overset{(b)}{=} \exp\left\{ -\lambda n_y \frac{1}{\Gamma\left(m\right)} \int_{\mathbb{R}^2} \mathbb{E}_{g_j^y \bar{g}_j^y, z} \left[\Gamma\left(m, m \frac{\sigma \|x - X_y\|^\alpha}{g_j^y \bar{g}_j^y z} \right) \right] + \mathbb{E}_{g_j^0 \bar{g}_j^0, z} \left[\Gamma\left(m, m \frac{\sigma \|x - 0\|^\alpha}{g_j^0 \bar{g}_j^0 z} \right) \right] \mathrm{d}x \right\} \\
&\quad \times \exp\left\{ \lambda n_y \frac{1}{\Gamma(m)^2} \int_{\mathbb{R}^2} \mathbb{E}_{g_j^y \bar{g}_j^y, z} \left[\Gamma\left(m, m \frac{\sigma \|x - X_y\|^\alpha}{g_j^y \bar{g}_j^y z} \right) \right] \mathbb{E}_{g_j^0 \bar{g}_j^0, z} \left[\Gamma\left(m, m \frac{\sigma \|x - 0\|^\alpha}{g_j^0 \bar{g}_j^0 z} \right) \right] \mathrm{d}x \right\} \\
&\quad \times \exp\left\{ -\left(n_0 - n_y\right) \bar{\mathcal{N}} \right\} \left(1 - \frac{\varphi^2 \Gamma\left(m, 4m\varphi^2 \sigma d^\alpha\right)}{\pi^2 \Gamma\left(m\right)} \mathtt{P}_{\mathtt{LoS}}\left(d\right) \right) \\
&= \exp\left\{ -n_y \bar{\mathcal{N}} - n_y \kappa \right\} \\
&\quad \times \exp\left\{ n_y \left(\lambda \frac{\varphi^4}{\pi^4} \sum_{k=0}^{m-1} \sum_{t=0}^{m-1} \frac{\left(4m\sigma\varphi^2\right)^{k+t}}{t! k!} \int_{\mathbb{R}^2} \frac{\|x\|^{\alpha k}}{\|x - X_y\|^{-\alpha t}} \right.\right. \\
&\qquad\qquad \left.\left. \times \mathtt{P}_{\mathtt{LoS}}\left(\|x\|\right) \mathtt{P}_{\mathtt{LoS}}\left(\|x - X_y\|\right) \mathrm{e}^{-4m\sigma\varphi^2 \left(\|x\|^\alpha + \|x - X_y\|^\alpha\right)} \mathrm{d}x \right) \right\} \\
&\quad \times \exp\left\{ -\left(n_0 - n_y\right) \bar{\mathcal{N}} \right\} \left(1 - \frac{\varphi^2 \Gamma\left(m, 4m\varphi^2 \sigma d^\alpha\right)}{\pi^2 \Gamma\left(m\right)} \mathtt{P}_{\mathtt{LoS}}\left(d\right) \right). \qquad \text{(B.3)}
\end{aligned}
$$

Assuming n_y smaller than n_0, then the typical AP and the AP y will jointly access the medium if both do not sense any other AP with mark smaller than n_y and the typical AP does not sense any AP with mark in the interval $[n_y, n_0)$ including y. Since, the sets of APs with mark smaller than n_y and with mark in the interval $[n_y, n_0)$ are independent, the two conditions are independent and step (a) follows. In fact, in (B.3), step (a), the first exponential expression is the probability that the typical AP and AP y will jointly access

the medium if both do not sense any other AP with mark smaller than n_y; and the rest is the probability that the typical AP does not sense any AP with mark in the interval $[n_y, n_0)$ including y. In addition, (b) follows from applying the integration by parts formula on the first integral. Subsequently, upon some algebraic manipulation, we arrive at the expression in (B.3). Finally, by substituting (B.3) in (B.2) and taking the expectation, the result in (7.8) is obtained.

B.3 Proof of Lemma 11

$$
\begin{aligned}
&\mathbb{P}\left\{e_0 = 1\right\} \\
&= \int_0^1 (1-n_0)\,\mathrm{e}^{-n_0\bar{\mathcal{N}}} + n_0 \mathbb{E}_{g_y^0 \bar{g}_y^0, z}\left[\mathbb{P}\left\{h \leq \frac{\sigma d^\alpha}{G_y^0 \bar{G}_y^0 Z}\,\middle|\, g_y^0 \bar{g}_y^0, z\right\}\right] \mathrm{e}^{-n_0\bar{\mathcal{N}}} \mathrm{d}n_0 \\
&= \int_0^1 (1-n_0)\,\mathrm{e}^{-n_0\bar{\mathcal{N}}} + n_0 \left(1 - \frac{\varphi^2 \Gamma\left(m, 4m\varphi^2\sigma d^\alpha\right)}{\pi^2 \Gamma\left(m\right)} \mathtt{P}_{\mathtt{LoS}}\left(d\right)\right) \mathrm{e}^{-n_0\bar{\mathcal{N}}} \mathrm{d}n_0 \\
&= \frac{\mathrm{e}^{-\bar{\mathcal{N}}} + \bar{\mathcal{N}} - 1}{\bar{\mathcal{N}}^2} + \left(1 - \frac{\varphi^2 \Gamma\left(m, 4m\varphi^2\sigma d^\alpha\right)}{\pi^2 \Gamma\left(m\right)} \mathtt{P}_{\mathtt{LoS}}\left(d\right)\right) \frac{1 - \left(1+\bar{\mathcal{N}}\right)\mathrm{e}^{-\bar{\mathcal{N}}}}{\bar{\mathcal{N}}^2}.
\end{aligned} \tag{B.4}
$$

It is notable that, in the above probability the AP y located at distance d from the typical AP is not necessarily transmitting.

B.4 Proof of Lemma 13

$$
\begin{aligned}
\mathcal{L}_{I_{\text{agg}}}(\mathrm{s}) &= \mathbb{E}\left[\mathrm{e}^{-\mathrm{s}I_{\text{agg}}}\right] \\
&= \mathbb{E}_{\Phi_{\mathrm{S}},h,g\bar{g},z}\left[\exp\left\{-\mathrm{s}\sum_{X_i\in\Phi_{\mathrm{S}}\setminus X_0} H_i^u G\left(\theta_i^u,\xi_u\right)\bar{G}\left(\theta_i^u+\pi-\xi_u,\xi_u\right)Z_i^u\|X_i-U\|^{-\alpha}\right\}\right] \\
&= \mathbb{E}_{\Phi_{\mathrm{S}},h,g\bar{g},z}\left[\prod_{X_i\in\Phi_{\mathrm{S}}\setminus X_0}\exp\left\{-\mathrm{s}H_i^u G\left(\theta_i^u,\xi_u\right)\bar{G}\left(\theta_i^u+\pi-\xi_u,\xi_u\right)Z_i^u\|X_i-U\|^{-\alpha}\right\}\right] \\
&= \mathbb{E}_{\Phi_{\mathrm{S}}}\left[\prod_{X_i\in\Phi_{\mathrm{S}}\setminus X_0}\mathbb{E}_{h,g\bar{g},z}\left[\exp\left\{-\mathrm{s}H_i^u G\left(\theta_i^u,\xi_u\right)\bar{G}\left(\theta_i^u+\pi-\xi_u,\xi_u\right)Z_i^u\|X_i-U\|^{-\alpha}\right\}\right]\right] \\
&\overset{(a)}{=} \exp\left\{\int_{\mathbb{R}^2} -\left(1-\mathbb{E}_{h,g\bar{g},z}\left[\exp\left\{-\mathrm{s}hg_i^u\bar{g}_i^u z\|x-U\|^{-\alpha}\right\}\right]\right)\lambda'\left(\|x\|\right)\mathrm{d}x\right\} \\
&= \exp\left\{\int_{\mathbb{R}^2}\int_0^\infty -\frac{\varphi^2}{\pi^2}\ \mathtt{P}_{\mathtt{LoS}}\left(\|x-U\|\right)\left(1-\exp\left\{\frac{-\mathrm{s}h\|x-U\|^{-\alpha}}{4\varphi^2}\right\}\right)f_H\left(h\right)\mathrm{d}h\lambda'\left(\|x\|\right)\mathrm{d}x\right\} \\
&= \exp\left\{\int_{\mathbb{R}^2} -\frac{\varphi^2}{\pi^2}\mathtt{P}_{\mathtt{LoS}}\left(\|x-U\|\right)\left(1-\left(1+\frac{\|x-U\|^{-\alpha}}{4m\varphi^2}\mathrm{s}\right)^{-m}\right)\lambda'\left(\|x\|\right)\mathrm{d}x\right\} \qquad \text{(B.5)}
\end{aligned}
$$

Here, (a) follows from the probability generating functional (PGFL) of the PPP.

B.5 Proof of Theorem 4

Formally defining, the probability of successful reception in the complementary cumulative distribution function (CCDF) of the signal to interference plus noise power at a given threshold β. As mentioned previously, this threshold is set based on the system requirement.

Therefore,

$$\begin{aligned}
\mathtt{P}_{\mathtt{recept}} &= \mathbb{E}_{I_{\mathrm{agg}},z}\left[\mathbb{P}\left\{\frac{H_0^u G\left(\theta_0^u,\xi_0\right)\bar{G}\left(\theta_0^u+\pi-\xi_u,\xi_u\right)Z_0^u\|X_0-U\|^{-\alpha}}{\underbrace{\sum_{X_i\in\Phi_{\mathrm{S}}\setminus X_0}H_i^u G\left(\theta_i^u,\xi_i\right)\bar{G}\left(\theta_i^u+\pi-\xi_u,\xi_u\right)Z_i^u\|X_i-U\|^{-\alpha}}_{I_{\mathrm{agg}}}+\sigma_n^2}>\beta\,|z,I_{\mathrm{agg}}\right\}\right]\\
&= \mathbb{E}_{I_{\mathrm{agg}},z}\left[\mathbb{P}\left\{\frac{hu^{-\alpha}z}{I_{\mathrm{agg}}+\sigma_n^2}>\beta\,|z,I_{\mathrm{agg}}\right\}\right]\\
&= \mathbb{E}_{I_{\mathrm{agg}},z}\left[\frac{1}{\Gamma\left(m\right)}\Gamma\left(m,m\frac{\beta\left(I_{\mathrm{agg}}+\sigma_n^2\right)}{u^{-\alpha}z}\right)\right]\\
&= \mathtt{P}_{\mathtt{LoS}}\left(u\right)\mathbb{E}_{I_{\mathrm{agg}}}\left[\sum_{k=0}^{m-1}\frac{\left(m\beta u^{\alpha}\right)^k}{k!}I^k\mathrm{e}^{-m\beta u^{\alpha}I}\right]
\end{aligned}$$

where, $I=I_{agg}+\sigma_n^2$ and $I\in[\sigma_n^2,\infty)$. In addition, σ_n^2 is the additive white Gaussian noise (AWGN) power. Therefore,

$$\begin{aligned}
\mathtt{P}_{\mathtt{recept}} &= \mathtt{P}_{\mathtt{LoS}}\left(u\right)\sum_{k=0}^{m-1}\frac{\left(m\beta u^{\alpha}\right)^k}{k!}\mathbb{E}_I\left[I^k\mathrm{e}^{-m\beta u^{\alpha}I}\right]\\
&= \mathtt{P}_{\mathtt{LoS}}\left(u\right)\sum_{k=0}^{m-1}\frac{\left(-m\beta u^{\alpha}\right)^k}{k!}\left(\frac{\partial^k}{\partial \mathrm{s}^k}\mathcal{L}_I\left(\mathrm{s}\right)\right)|_{\mathrm{s}=m\beta u^{\alpha}}\\
&= \mathtt{P}_{\mathtt{LoS}}\left(u\right)\sum_{k=0}^{m-1}\frac{\left(-m\beta u^{\alpha}\right)^k}{k!}\left(\frac{\partial^k}{\partial \mathrm{s}^k}\mathrm{e}^{-\mathrm{s}\sigma_n^2}\mathcal{L}_{I_{\mathrm{agg}}}\left(\mathrm{s}\right)\right)|_{\mathrm{s}=m\beta u^{\alpha}} \qquad \text{(B.6)}
\end{aligned}$$

B.6 Proof of Theorem 5

The proof can be simply carried out, where

$$\begin{aligned}
\mathtt{P}_{\mathtt{Trans}} &= \mathbb{E}_{n_0}\left[\mathrm{e}^{-\lambda n_0 \int\limits_{\mathbb{R}^2} \mathbb{P}\left\{\frac{h g_j^0 \bar{g}_j^0 z}{\|x\|^\alpha} \geq \sigma\right\} \mathrm{d}x}\right] \\
&= \mathbb{E}_{n_0}\left[\mathrm{e}^{-\lambda n_0 \int\limits_{\mathbb{R}^2} \mathbb{E}_{g_j^0 \bar{g}_j^0, z}\left[\mathbb{P}\left\{\frac{h g_j^0 \bar{g}_j^0 z}{\|x\|^\alpha} \geq \sigma \middle| g_j^0 \bar{g}_j^0, z\right\}\right] \mathrm{d}x}\right] \\
&= \mathbb{E}_{n_0}\left[\mathrm{e}^{-\lambda n_0 \int\limits_{\mathbb{R}^2} \mathbb{E}_{g_j^0 \bar{g}_j^0, z}\left[\frac{1}{\Gamma(m)} \Gamma\left(m, \frac{m\sigma\|x\|^\alpha}{g_j^0 \bar{g}_j^0 z}\right)\right] \mathrm{d}x}\right] \\
&= \mathbb{E}_{n_0}\left[\mathrm{e}^{-n_0 \bar{\mathcal{N}}}\right] = \frac{1 - \mathrm{e}^{-\bar{\mathcal{N}}}}{\bar{\mathcal{N}}}
\end{aligned} \tag{B.7}$$

B.7 Proof of Lemma 14

The density of concurrently transmitting APs, is the density of the primary Φ_{P} thinned by the probability of retaining a generic AP in Φ_{S}. Moreover,

$$\begin{aligned}
&\mathbb{P}\left\{\text{retaining a generic AP in } \Phi_{\mathrm{S}}\right\} \\
&= \mathbb{P}\left\{\text{retaining a generic AP in } \Phi_{\mathrm{S}} \,|\, |\mathcal{N}| = i\right\} \Pr\left\{|\mathcal{N}| = i\right\},
\end{aligned} \tag{B.8}$$

where $\mathbb{P}\left\{|\mathcal{N}| = i\right\}$ is probability of having i neighbors; and

$$\begin{aligned}
\mathbb{P}\left\{|\mathcal{N}| = i\right\} &= \sum_n \mathbb{P}\left\{|\mathcal{N}| = i\,,\ |\mathcal{K}| = n\right\} \\
&= \sum_{n=0}^{\infty} \frac{(\lambda A)^n \mathrm{e}^{-\lambda A}}{n!} \binom{n}{i} \eta^i (1-\eta)^{n-i}.
\end{aligned} \tag{B.9}$$

Here, $|\mathcal{K}|$ denotes the number of AP in the contention area of the typical AP. In fact, considering the PPP assumption of the distribution of APs, the probability of having n APs in contention area A around the typical AP is given by $\frac{(\lambda A)^n \mathrm{e}^{-\lambda A}}{n!}$. However, given the

pathloss, small scale fading, blockage effect and antenna directions, only i out of n APs are actually counted as neighbors, each of them with the average success probability η. In addition, with probability $\frac{1}{i+1}$ only one of them has the lowest mark and proceeds to transmit. Therefore,

$$\begin{aligned}
&\mathbb{P}\left\{\text{retaining a generic AP in } \Phi_{\mathrm{S}}\right\} \\
&= \sum_{i=0}^{n} \frac{1}{i+1} \sum_{n=0}^{\infty} \frac{(\lambda A)^n \mathrm{e}^{-\lambda A}}{n!} \binom{n}{i} \eta^i (1-\eta)^{n-i} \\
&= \sum_{i=0}^{\infty} \sum_{n=i}^{\infty} \frac{\mathrm{e}^{-\lambda A} \eta^i}{(i+1)!} (1-\eta)^{-i} \frac{(\lambda A)^n}{n!} \frac{n!}{(n-i)!} (1-\eta)^n \\
&= \frac{1-\mathrm{e}^{-\lambda A \eta}}{\eta \lambda A}.
\end{aligned}$$